UNIVERSITY OF INSUBRIA

VARESE

DEPARTMENT OF EXPERIMENTAL AND CLINICAL BIOMEDICAL SCIENCES

- FACULTY OF MEDICINE -

Mechanics and fluid-dynamics of the initial lymphatic system

CANDITATE:

FRANCESCA BIANCHIN

Matr. N. 608530

XXIII CYCLE OF Ph.D. PROGRAM IN EXPERIMENTAL MEDICINE AND ONCOLOGY

SCHOOL OF MEDICINE

TUTOR: Prof. Daniela Negrini

DIRECTOR OF DOCTORAL SCHOOL: Prof. Roberto Accolla

ACADEMIC YEAR 2009-2010

INDEX

Abstract

The diaphragmatic lymphatic system drains fluid and solutes from the pleural and peritoneal cavities by exploiting pressure gradients ($\Delta P_{TM} = P_{lymph}-P_{int}$) between the vessel lumen and the interstitium; while lymph progression is sustained by pressure gradients ($\Delta P_l = P_{lymph2}–P_{lymph1}$) between adjacent lymphatic segments. The aim of the study is to examine the pattern of fluid fluxes in the lymphatics, determining the role of tissue and vessel wall in the transmission of tissue forces to the lymphatic lumen and clarifying whether the organization of the diaphragmatic network might be a tool to optimize lymphatic absorption and/or progression. Experiments were performed in anesthetized, paralysed and mechanically ventilated rats. Lymph hydraulic pressure and flux were recorded by the micropuncture technique combined with fluorescent dextrans injection to visualise lymph flow. Flow velocity and direction were calculated by measuring the fluorescence progression and vessel diameter on acquired videos. Mechanical compliance of the vessel wall was measured by sequential injections of saline solution into the vessel, while recording P_{lymph}. The presence of muscular fibers around the lymphatic vessel wall was investigated by immunofluorescence assay.

Two populations of vessels were identified with different mechanical properties: compliant vessels work as reservoirs of drained lymph, stiffer vessels propel fluid along the network. Flow direction and amplitude vary with time and, with respect to the P_{lymph} pressure gradient, flow direction in some vessels reverts multiple times independently from both cardiac and ventilatory action.

1 Introduction

Hippocrates was one of the first authors to mention the lymphatic system in 460-360 BC in one sentence of his work "On Joints" where he briefly described the lymph nodes and the existence of "white blood" in some vessels. Herophilus, a Greek anatomist living in Alexandria in 3rd century BC, described the vessels as "absorbitive veins of the lymphatics". Ruphus of Ephesus, a Roman physician, identified the axillary, inguinal and mesenteric lymph nodes during the first century AD. Findings of Ruphus and Herophilus were propagated by the Greek physician Galen, who described the mesenteric lymph nodes observed in apes and pigs in the second century AD.

The lymphatic system of the diaphragm has been an object of anatomical and physiological research for more than a century, since Recklinghausen in 1863 suggested the presence of small openings, or *stomata*, that connect the lymphatic lumen with the peritoneal cavity. In 1903 MacCallum found that tracers injected into the peritoneal cavity consistently migrated into the peritoneal lymphatic vessels of the diaphragm through ample lymphatic spaces called *lacunae*. Moreover it was evident that lymphatic vessels were tubular structures (Shinohara, 1997).

1.1 The lymphatic system

The lymphatic system is a complex network of vessels that carries a transparent fluid called *lympha* (from latin "water"). It includes the lymphoid tissue, lymphatic vessels through which the lymph travels and all the structures dedicated to the circulation and production of lymphocytes (spleen, thymus, bone marrow and the lymphoid tissue

associated with the digestive system). The blood does not directly come in contact with the parenchymal cells and tissues in the body, but constituents of the blood first exit the microvascular exchange blood vessels to become interstitial fluid, which comes in contact with the parenchymal cells of the body. Lymph is the fluid that is formed when interstitial fluid enters the initial lymphatic vessels of the lymphatic system. The lymph is then moved along the lymphatic vessel network.

The lymphatic system can be divided into the conducting system and the lymphoid tissue. The conducting system carries the lymph and consists of tubular vessels that include the lymph capillaries, the lymph vessels and the thoracic ducts. The lymphoid tissue is primarily involved in immune responses and consists of lymphocytes and other white blood cells enveloped in connective tissue through which the lymph passes. The regions of the lymphoid tissue that are densely packed with lymphocytes are known as lymphoid follicles. Lymphoid tissue may either consist of loosely organized lymphoid follicles known as the mucosa-associated lymphoid tissue (MALT) or can be structurally well organized as lymph nodes. A lymph node is an organized collection of lymphoid tissue, through which the lymph passes on its way to returning to the blood. Lymph nodes are located at intervals along the lymphatic system and are particularly numerous in the chest, neck, pelvis, inguinal region and in association with the blood vessels of the intestines.

1.2 Lymphatic system functional role

The lymphatic system is constituted of a vast network of thin-walled lymphatic vessels (lymphatics), which extends throughout most of the body and drains fluid and particles

from the interstitial spaces. This one-way transport system is a key component in the maintenance of normal interstitial fluid volume and protein concentration. In fact, an important role of the lymphatic system is to maintain tissue fluid homeostasis. Both a interstitial volume reduction (dehydration) and a liquid accumulation in the tissue (oedema) can determine tissutal suffering. In both situations, the fluid homeostasis alteration from the physiological value seriously compromises the tissutal activity. Therefore, the role of the lymphatic system to maintain tissue fluid homeostasis is very important to assure activity of the tissue and organ, in particular in the interstitial space, for example pulmonary, and in the serous cavity, that are more frequently exposed to the damage connected to increased liquid volume.

Lymphatics transport fluid and solutes of different dimensions, as proteins, leukocytes and cells from the body tissues to the central venous system. Moreover, the lymphatic system also sub-serves specific regional roles: 1) it is responsible for the removal of interstitial fluid from tissues, 2) it absorbs and transports fatty acids and cholesterol across the mucosa of the small intestine to the circulatory system (Casley-Smith, 1962), 3) the lymphatics play many important roles in immune defence mechanisms. If pathogens invade the body, they are taken up together with the interstitial fluid by the lymphatics. The lymph passes through one or several lymph nodes, where an immune response may be initiated if any foreign substance is detected, before it enters the venous system. In collaboration with the antigen-presenting cells (as dendritic cells) of the lymph nodes, T and B cells recognize non-self epitopes and mount an immune response. The activated immune cells proliferate in the lymph nodes and produce antibodies. Both cells and antibodies are delivered into the general circulation via

lymphatics and then return to the blood stream (Von der Weid and Zawieja, 2004), 4) the lymph carries lymphocytes from the efferent lymphatics exiting the lymph nodes.

In the vessels lumen a transparent fluid called lymph is carried along the lymphatic system. The ionic lymph and plasma compositions are similar, but lymph presents a minor protein concentration and a greater fatty concentration. Moreover, in the lymph there are mainly plasmatic proteins and proteins with hormonal and enzymatic function (as lipase, maltase, amylase). The lymph composition changes along the same vessel: because all molecules in the interstitial liquid, even proteins and cells, might enter into the lymphatic vessels, *pre-nodal lymph* composition is the same of the interstitial liquid and it will be modified after the progression through the lymph nodes (*post-nodal lymph*). The pre-nodal lymph flows in the vessels of lymph formation, the post-nodal lymph flows in greater vessels exiting the lymph nodes, and has a major protein concentration.

Unlike blood vessels, lymphatics do not form a closed circulatory system. The unidirectional flow of lymph returns fluid to the cardiovascular system. Lymphatic flow begins in the initial lymphatics, then the lymph progresses in the collecting and terminal lymphatic and the flow ends in the veins networks (Jeltsch et al., 2003). Lymphatic capillaries consist of a single layer of non-fenestrated endothelial cells resting on an incomplete basal lamina. Pre-nodal collectors drain the capillary networks and transport lymph to the regional lymph nodes. Lymphatic capillaries do not present musculature although collectors possess a smooth muscle cell layer (Schmid-Schonbein, 1990). Post-nodal lymphatic trunks carry lymph to collecting lymph nodes or directly into lymphatic ducts. Lymph from the gastrointestinal and lumbar regions drains into the cisterna chyli at the inferior end of the thoracic duct. The thoracic duct ascends upward behind the

aorta to the left jugulo-subclavian junction and receives lymph from the body wall, except from its upper right quadrant from which the lymph is collected into the right lymphatic duct, and returned to the veins at the right jugulo-subclavian junction (Foster 1996 and Swartz, 2001).

1.3 Interstitial liquid and microvascular filtration processes

In the lymphatic system the lymph is drained initially from the interstitial space to the initial lymphatic vessels. The interstitial space is constituted by insoluble macromolecules such as collagen, elastin, proteoglycans and hyaluronic acid, which create a three-dimensional structure, in which the interstitial liquid fills the porosities.

The interstitial liquid is filtrated passively through the vascular capillary walls by the combined pressure gradient (ΔP_{TM}) developing between the vessel lumen and the interstitium, as described by the Starling equation:

$$J_v = L_p \cdot S \cdot \Delta P_{TM} = L_p \cdot S \cdot [(P_c - P_{int}) - \sigma_d (\pi_p - \pi_{int})] = L_p \cdot S \, (\Delta P - \sigma_d \Delta \pi) \qquad \text{(Eq.1.1)}$$

where J_l (mL/min) is the lymphatic filtration flow, P_c and P_{int} are the hydrostatic pressure respectively in the haematic capillary and in the interstitial tissue, π_p and π_{int} the colloidosmotic pressures that can be generated inside the plasma and in the interstitial liquid, respectively.

L_p is the hydraulic permeability coefficient of the capillary endothelium and S the endothelial surface interested. The coefficient σ_d assumes values between 0 and 1 depending upon the endothelium and solute characteristics. In fact, σ_d is proportional to

the ratio between the molecular radius of the solute and the radius of the endothelial pores. If the solute dimensions are smaller than the endothelial pores, so $\sigma_d = 0$ and thus $\Delta\pi = 0$. In the pulmonary and brain endothelium pores are very small, so that the endothelium is virtually impermeable to the plasmatic proteins. These endothelia are protected by the filtration processes, indeed $\sigma_d \sim 1$. The P_c or π_{in} increase favours the liquid movement from the vessel to the interstitial space, while a P_{int} or π_p increase favours the liquid movement from the interstitial space to the plasma. As the Eq. 1.1 suggests, Jv depends upon $\Delta P_{TM,}$ L_p and S parameters, which are very variable in different tissues or in the same tissue but in different functional conditions.

1.4 Lymphatic flow

It has been experimentally demonstrated that lymphatics are able to drain fluid from compartments at subatmospheric pressure (Miserocchi and Negrini, 1986; Miserocchi et al., 1989) in physiological conditions. Also lymphatic flow can be modelled according to the Starling equation:

$$J_l = K_l \cdot \Delta P_{lymph} = K_l \cdot [(P_{int} - P_{lymph}) - \sigma_d (\pi_{int} - \pi_{lymph})] \quad \text{(Eq. 1.2)}$$

where J_l (mL/min) is the lymphatic flow from the tissue, K_l is the hydraulic conductance of the initial lymphatics, P_{lymph} and π_{lymph} are the hydrostatic and colloidosmotic pressures that can be generated inside the lumen of the initial lymphatic. However, the dimensions of the lymphatic endothelium openings allow the passage of proteins,

macromolecules and cells, as erythrocytes, lymphocytes and tumoral cells. In the initial lymphatic endothelium $\sigma_d = 0$ and $\pi_{int} = \pi_{lymph}$, therefore:

$$J_l = K_l \cdot \Delta P_{lymph} = K_l \cdot (P_{int} - P_{lymph}) \qquad \text{(Eq. 1.3)}$$

where K_l is the hydraulic conductance of the initial lymphatics, P_{int} is interstitial fluid pressure and P_{lymph} is the fluid pressure that can be generated inside the lumen of the initial lymphatics. K_l depends upon initial lymphatic size and density. This equation provides a functional description of lymphatic flow, while little is known about the exact mechanism responsible for lymphatic filling and subsequent lymph propulsion, due to pressure oscillations depending upon an intrinsic and extrinsic mechanism (Roddie, 1990). The intrinsic mechanism is based on the rhythmic contractile activity of the smooth muscles of the lymphatic walls, whereas the extrinsic mechanism depend upon intraluminal pressure oscillations induced by forces applied to the lymphatic walls by the surrounding tissues (Courtice and Simmonds, 1954).

1.5 Lymphatic safety factors

For many years physiologists have known that lymph flow increases as a result of an increased filtration across the microvascular or capillary wall due to elevated microvascular pressure or endothelial permeability. However, the mechanisms responsible for signalling to the lymphatic system to increase its ability to accommodate the increased fluid entering the tissues are poorly understood. Several mechanisms have been proposed to explain the lymph flow response that occurs following changes in

microvascular fluid filtration: 1) fluid entering the tissue increases interstitial fluid pressure, which elevates the pressure gradient acting between the interstitium and the small lymphatic capillaries, resulting in greater lymphatic filling (Taylor et al. 1973), 2) the larger lymphatic ducts are known to have an intrinsic ability to contract and many factors can affect both their rate of contraction and magnitude of the force generated. The increased intralymphatic pressure caused by the greater lymphatic filling could trigger a myogenic response exerted by the smooth muscle cells in larger lymphatics, causing them to contract more forcefully to propel lymph in a forward direction, opening the lymphatic valves and decreasing the intralymphatic pressure in small tissue lymphatics which increases their filling pressure (Hall et al. 1965, Ohhashi et al., 1980), 3) tissue motion can also accelerate lymph flow and it's an important means of increasing lymph flow in organs such as muscle and lungs (White et al., 1933, Morris, 1953), 4) when fluid enters the interstitium, the tissue spaces expand and fluid can more easily moved through the tissues to enter the lymphatics (Chen et al., 1991).

In the early 1960s Guyton and co-workers discovered that interstitial pressure was subatmospheric and it increased by 5-10 mmHg during oedema formation (Guyton and al., 1975). Guyton used the new concept of a dynamic tissue pressure to define an "oedema safety factor". This parameter defines all factors in an organ that could respond to increased transvascular filtration by changing direction to oppose the formation of oedema. These factors are a) the interstitial fluid pressure (P_{int}), b) the protein osmotic gradient acting across the microvascular wall ($\sigma_d \Delta\pi$) and c) local lymph flow (Guyton and Coleman, 1968).

Figure 1.1 shows the plot of tissue weight (representing the interstitial volume) as a function of microvascular pressure (corresponding to the P_c value of Eq. 1.1).

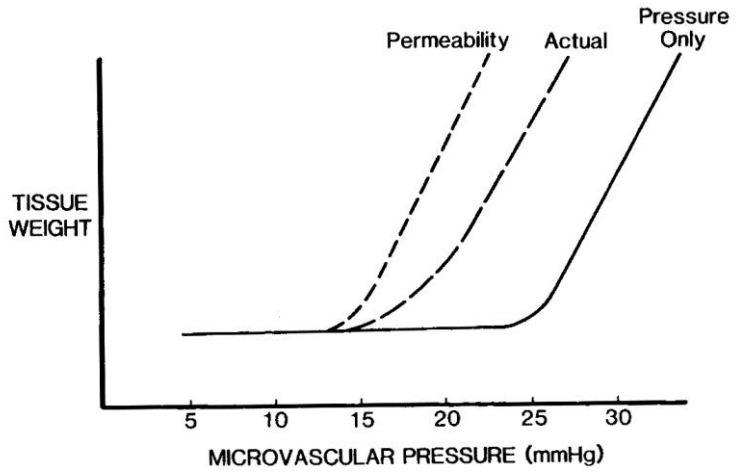

Fig. 1.1 Plot of *Tissue weight (oedema formation)* as function of microvascular hydraulic pressure for normal tissues (*Pressure Only*), or in conditions of decreased plasma proteins or increased vascular permeability (*Permeability*). *Actual* is lymph flow when tissues are damaged and lymph flow becomes large despite the action of oedema safety factors.

For a normal tissue, the plot of the tissue weight as a function of P_c is depicted as "pressure only": the interstitial volume is constant up to values of 25-30 mmHg until oedema develops, because the oedema safety factors can change up to these values. In these conditions, the oedema safety factor consists in a low endothelial L_p, in a high ($\sigma_d\Delta\pi$) and in the ability of the lymphatic system to adapt its flow in function of the endothelial filtration (J_l) so that all the filtered liquid across the microvascular wall is drained by the initial lymphatic vessels and the tissue weight is maintained constant.

Above 25-30 mmHg the filtration flow across the endothelium increases exceeding the drainage ability of the lymphatic system. Despite the action of oedema safety factor like L_p, ($\sigma_d\Delta\pi$) and high lymph flow, the liquid accumulates in the tissue, causing oedema development. If πp decreases or L_p increases in damaged microvessel wall, the tissue develops oedema at low P_c values (Eq. 1.1). In these conditions the lymphatic flow increases in relation to the increasing filtration flow and produces a curve similar to that

shown as "Actual" (Fig. 1.1). Therefore, in conditions associated with damage to microvessels, oedema does begin to rise at lower pressures, but the high lymph flow removes greater amounts of transmicrovascular filtration and less oedema develops for a given microvascular pressure (Guyton and Coleman, 1968). When the plasma proteins decrease or vascular permeability increases in damaged vessels there is a progressive accumulation of tissutal fluid as shown in "Permeability" plot (Fig. 1.1).

Another important oedema safety factor is P_{int}. The increase of the filtration between the capillary and the interstitium induces a P_{int} increase from subatmospheric to positive values. This phenomenon progressively reduces ΔP (Eq. 1.1) and avoids a further liquid filtration; moreover, the P_{int} increase promotes the lymphatic flow increase (Eq. 1.3).

Table 1.1 shows the percentage change in each safety factor as microvascular pressure was changed by 20 mmHg in several different tissues (Aukland and Nicolaysen, 1981).

Tissue	Increased $\sigma_d \Delta\pi$ (%)	Increased lymph flow (%)	Increased P_{int} (%)
Lung	50	17	33
Small Intestine	45	20	35
Colon	52	4	44
Liver	0	42	58
Heart	7	12	81

Tab. 1.1 Safety factors in various tissues. ($\sigma_d\Delta\pi$) is the colloidosmotic gradient and P_{int} is the tissue fluid pressure. The values are shown as percentages of the total safety factor measured when capillary pressure was increased 20 mmHg above control values.

The transvascular protein colloidosmotic pressure ($\sigma_d\Delta\pi$) is the major factor opposing oedema formation in organs with low permeability to plasma proteins, such as lung, small intestine and colon; but this factor is unimportant in the tissues that are very

permeable to plasma proteins such as heart and liver. The oedema safety factor explains how an excessive build up of tissue fluid is prevented under conditions that occur in normally functioning tissues, so different forces are responsible for opposing oedema formation in different tissues (Aukland and Nicolaysen, 1981).

1.6 Unidirectional lymph flow and valvular lymphatic system

An important issue in lymphatic function is the mechanism that provides the unidirectional transport of fluid from the interstitium into the initial lymphatics. Reversal of lymph fluid inside the initial or the collecting lymphatics is prevented by a set of intralymphatic valves (Casley, 1977; Mazzoni et al., 1987). They form a barrier to reflow inside a lymphatic lumen. But these valves are not at the proper anatomical position to prevent fluid escape into the interstitium. Inside initial lymphatics, high pressures can be generated with minimal fluid loss, indicating that both the intralymphatic valves as well as the wall of the collecting lymphatics have low permeability (Ikomi et al., 1997). To prevent fluid escape from the initial lymphatics into the interstitial space another barrier is required: the primary valve system. In fact, the endothelium of the initial lymphatics must permit fluid to enter from the interstitium into the lumen of the lymphatic and, on the other hand, must prevent fluid escape back into the interstitium.

Lymphatics have two valve systems: a set of primary valves in the wall of the endothelial cells of initial lymphatics and a secondary valve system in the lumen of the lymphatics (Mendoza and Schmid-Schonbein, 2003). The primary and the secondary

valves provide a mechanism that facilitates the unidirectional flow during periodic compression and expansion of initial lymphatics (Schmid-Schonbein, 2003).

1.6.1 The primary or endothelial valve system

Lymphatic endothelium does not show uniform attachments to its substrate but appears to be limited to local points of attachment, "anchoring filaments": fine fibers between the basal lamina and adjacent collagen and elastin fibers (Leak and Burke, 1966). The endothelial cells are strongly attached with these filaments to the connective tissue fibers. Moreover, lymphatic endothelial cells have points where they lack evidence of attachment to their substrate, notably near the junctions. Endothelial cells have border regions with a discontinuous overlapping pattern. Thus both overlapping junctions and open junctions may be present. Cell borders are only partially fused with neighboring cells, while other portions form flaps without direct cell attachment. This mechanism, called endothelial or primary valve system, allows fluid motion from the interstitium into the lymphatic lumen: the unattached borders of the lymphatic endothelial cells may function as valves or inlet valves to the lymphatic lumen (Kalima, 1973). The endothelial or primary valves may be opened during expansion of the initial lymphatics by means of a positive fluid pressure drop from the interstitium to the lumen ($P_{linf} < P_{int}$), but may fall back and be compressed against the lymph wall during compression of the initial lymphatics, and thereby they partially or completely close the endothelial barrier ($P_{linf} > P_{int}$). They can open and close rapidly, possibly by a mechanical flap action of overlapping cell extensions at the endothelial junctions (Mendoza and Schmid-Schonbein, 2003). These partially attached endothelial cells thus effectively serve as valves in the wall to prevent the return of lymph flow from the initial lymphatics back

into the interstitium (Casley-Smith, 1972). The primary valves could also be forced open by expansion of the interstitium or the initial lymphatics, as seen in fact during lymph oedema (Castenholz, 1984). A functional implication of these valves is that fluid permeability is quite different during the expansion phase of the initial lymphatics (when the valves are open) and during compression (when valves are close). The permeability of lymphatic endothelium with open valves may be unselective with respect to the molecular species. In addition, there may be an intermediate state when the valves are partially open (Casley-Smith, 1983). When a collecting lymphatic is occluded, tissue oedema develops. The primary valves may initially be compressed in a closed position by the lymph pressure but, with progression of the oedema, eventually the entire initial lymph channel will be expanded to the point at which the endothelial cells become stretched, the primary valves are pulled apart, and open fenestrae are formed. This feature, and the fact that the lymphatic endothelium basement membrane has large openings, sets up the possibility for unrestricted fluid exchange with interstitium without molecular species selectivity (Schmid-Schonbein, 1990).

1.6.2 The intraluminal or secondary valve system

Lymphatics have a system of intraluminal or secondary valves that prevents reflow along the length of the lymphatic channels. To prevent retrograde flow, these valves have to operate at very low flow rates and in channels that may be of highly irregular geometry. The valves have bi-leaflet morphology, with the individual valves made up of a thin collagen sheet covered on both sides by endothelium, and they are filled with numerous filaments. Each leaflet is attached at opposite sides to the lymph channel wall, and toward their down stream end they fuse together to form a buttress. The buttress is

attached to the wall so that its free ends form the opening for the passage of lymph fluid. The valve leaflets are relatively long (typically about twice the length of the lymph cross-sectional dimension), forming a funnel inside the lymphatic channels (Mazzoni et al., 1987). This feature facilitates the opening and closing of the secondary valves by fluid pressure drops across the leaflets generated by hydraulic pressure gradients inside the funnel. There are two fluid-filled sinuses between the leaflet and the wall and a centre funnel-shaped portion through which the lymph fluid can pass. The two buttresses prevent inversion of the leaflets, which in turn are quite flexible. There is no evidence for the presence of muscle in the valves to achieve active closure: all motion occurs in response to the lymph fluid forces or tension in the leaflets. The majority of lymphatic valves are bicuspid (Albertine et al., 1987). Monocuspid, tricuspid, or temporary valves that may slide back into the lymphatic wall have only rarely reported in selected organs (Daroczy, 1984). The secondary valves are used when fluid passes through them after entry into the lymphatic lumen. Thus fluid is transported along the lumen of the initial lymphatics in a proximal direction towards the contractile lymphatics and nodes. In general, collecting lymphatics have secondary valves, arranged in a ladder configuration, designated as lymphangions. Each lymphangion consists of a contractile compartment with an inlet and an outlet valve. Chains of lymphangions, as seen along the collecting lymphatics, serve as entry-valves and exit-valves from one compartment to the next (Schmid-Schonbein, 2003). This two valves system is required to prevent backflow and to guarantee the unidirectional transport in lymphatics: if only the entry valve is intact but the exit valve is compromised, fluid will flow in and out through the leaky exit valve with each compression cycle. Similarly, if the entry valve is compromised, fluid will leak in and out of the entry valve. When two

valves are present, one is open, while the other one is closed, so unidirectional transport is possible. Moreover, in the presence of two valves, the exact level of the pressure in the interstitial fluid compartment is less important. The only requirement is that the lymphatic pressure transiently falls below the interstitial fluid pressure, a process that is supported by local expansion of the initial lymphatics.

The mechanism of leaflet opening and closure can be depicted by considering the fluid pressure at different points around the leaflets: P_1 in front of the valve, P_2 downstream and P_3 in the sinuses (Fig. 1.2). In the funnel region the lymph fluid motion is accompanied by viscous dissipation, so that during a downstream motion $P_1 > P_2$. At the moment when the sinuses are closed, little or no motion occurs, and $P_2 = P_3$. Subsequently, the pressure drop across the leaflets, $P_1 - P_3$ is positive, and thus they are pushed open. The flow stoppage occurs when $P_1 = P_2 = P_3$ or when $P_3 > P_2 > P_1$ and the transleaflet pressure vanishes. Funnel-shaped valves can operate under extraordinarily low flow rates and without regard to the shape of the channel in which they are embedded. The effectiveness of the valve is easily improved by increasing the length of the funnel or decreasing its diameter, as seen particularly in those lymphangions that are close to the initial lymphatics and that have lower flow rates than the valves in the larger collecting lymphatics. Lymphatic valves are essential for the progression of lymph fluid flow, especially in long organs where the presence of gravitational forces can generate high hydrostatic pressures. The valves prevent the formation of a high fluid column, and they are equally effective in both initial and collecting lymphatics.

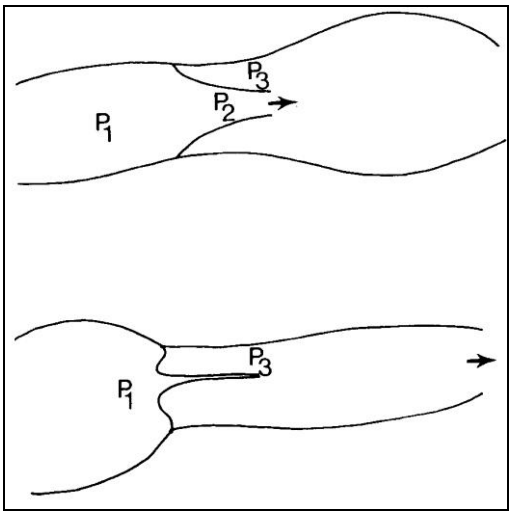

Fig. 1.2 Lymphatic pressure in vicinity of valve. P_1, upstream pressure, P_2, downstream pressure, P_3, abluminal pressure in outer pocket of valve leaflet. $P_2 – P_3$, is transleaflet pressure drop. $P_1 > P_2 > P_3$ in condition of flow; during closure $P_1 = P_2$ so that $P_2 – P_3 < 0$.

1.7 Structure, distribution and anatomy of lymph vessels

1.7.1 Cell origin

The development of the lymphatic vasculature, the origin of lymphatic endothelial cells and their growth into the nascent lymphatic vasculature is poorly understood. However, it is known that the lymphatic endothelium is crucial to the recruitment and differentiation of lymphatic muscle cells despite of the exact muscle cell origin (Von der Weid and Zawieja, 2004). Two theories of lymphatic development have been proposed: the first suggested that lymphatic endothelium derives from sprouting blood vascular (venous) endothelium, the so-called centrifugal theory. The second theory, the so-called centripetal theory, suggested that lymphatic endothelium differentiates in situ from primitive mesenchyma, and it subsequently acquires connections with the blood vascular system at a limited number of sites (Pepper, 2006). The most accredited is the first theory, which suggests that the main lymphatic trunks develop from the grand

veins, whereas all the other lymphatics arise independently from the venous system through canalization of connective tissues clefts. In support of this theory, lymphatics have been observed to sprout from the murine cardinal veins (Wigle and Oliver, 1999). These embryonic lymphatics are thought to develop as isolated lymphatic endothelial cell sacs, which then give rise to the lymphatic endothelial tubes (Wilting et al., 2001). Later, endothelium-derived signals will mediate the recruitment of lymphatic muscle cells to the developing vessel resulting in the maturation of the functional lymphatic.

1.7.2 Distribution and structure of lymphatic vessels

Lymphatic vessels are present in most tissues, with the exceptions of brain, retina, bone marrow, the umbilical cord and the inner renal medulla (Wenzel, 1972). In addition, both lymph and blood vessels are lacking in tissues like cartilage, cornea, the eye lens and the inner layer of large arteries. Compared with the high density of the blood microvasculature, the lymphatic network is sparse. Individual lymphatics originate in the tissue and form bifurcating trees and, in some organs, meshworks. Although in general lymphatics are wider than blood capillaries, their number is much smaller. Their detailed network morphology depends upon the tissue and organs involved.

The lymphatic system can be divided into two major structures known as initial lymphatics and collecting lymphatics. Interstitial tissue fluid and particulate matter enters the lymphatic system through the initial lymphatics: the latter drain into larger collecting lymphatics, which in turn carry fluid towards the lymph nodes and the central thoracic ducts.

1.7.2.1 The initial lymphatics

Initial lymphatics originate in the tissue parenchyma and consist of a continuous but highly attenuated endothelial wall devoid of smooth muscle cells. In contrast to the cylindrical geometry of most blood vessels, the cross section of initial lymphatics has an irregular shape in many tissues because the lumen may be completely collapsed, so that initial lymphatics rarely look like circular vessels. Yet in normal tissue, they can be readily identified thanks to their morphology and specific location in the tissue. The architecture of the initial lymphatics in different tissues varies considerably: from blind-ending ducts, sometimes with an expanded ampullary end or chains of bulbs, to a continuous network with only small projecting buds. They have few tight cell junctions and adhesion molecules, like VE-cadherins (Casley-Smith, 1972; Schmelz et al., 1994), and form overlapping cellular flaps between endothelial cells, so that the wall of these structures has a discontinuous single layer of flattened endothelial cells often with overlapping margins. Open gaps between the cells, up to 2-5 µm, are frequent in many tissues, often formed by overlapping cell leaflets that apparently might act as one-way valves (Aukland and Reed, 1993). Short interstitial fibers (anchoring filaments) connect the abluminal side of the lymphatic endothelium to the adjacent connective tissue. Initial lymphatics have two valve systems: a primary valve system at the level of the initial lymphatic endothelium, and a secondary valve system that is positioned in the lumen of the lymphatics (Trzewik et al., 2001; see chapters 1.6.1 and 1.6.2). Compared with collecting lymphatics, the initial lymphatics are considerably more numerous and form the major portion of the lymphatic network (Schmid-Schonbein, 2006). Moreover, initial lymphatics are frequently associated with structures that have smooth muscle (arterioles and respiratory bronchioles). They are located in the adventitia of arterioles

in close proximity to the smooth muscle cells, nerve fibers, adipocytes, and what is a continuous line of mast cells. In contrast, other parts of the tissue parenchyma may be relatively depleted of initial lymphatics. For example, the capillary space in skeletal muscle has no initial lymphatics. Instead, initial lymphatics form a meshwork that is tightly paired with the arcade arterioles and larger venules in this organ. Initial lymphatics and arterioles in skeletal muscle are in close apposition to one another. Expansion of the arterioles leads to compression of the adjacent lymphatic vessel, and active contraction of the arteriole serves to expand the lymphatic vessels. Thus, both vasomotion and pressure pulsation serve to promote lymph fluid transport (Intaglietta and Gross, 1982). Skeletal muscle contraction may expand and compress the initial lymphatics (Mazzoni et al., 1990). It is a carefully controlled process, closely linked to the physiological activity of the organ. Lymph flow is also enhanced by elevation of capillary fluid filtration and interstitial fluid pressure, especially if the interstitial fluid pressure reaches values much higher than those inside the initial lymphatics (Aukland and Reed, 1993; Swartz et al., 1999).

Moreover, initial lymphatics have the ability to collect and transport interstitial fluid, proteins, colloids, and cells (Ikomi et al., 1996). In organs such as the intestine or skeletal muscle, all lymphatics inside the tissue parenchyma are initial lymphatics.

1.7.2.2 The collecting lymphatics

In the majority of organs that have been investigated the collecting lymphatics are located downstream of the initial lymphatics. After lymph formation in the initial lymphatics, lymph enters into the collecting lymphatics and is then carried toward the

lymph nodes (interposed along the path of collecting lymphatics) to end into two large trunks, the thoracic duct and the right lymphatic duct, which converge into the large veins at the base of the neck (Fig. 1.3). Characteristic are their circular cross sections, so that a circumferential mechanical stress can be generated by the smooth muscle layer, a typical feature of these vessels (Schmid-Schonbein, 2006). In fact, in contrast to the initial lymphatics, a characteristic feature of the collecting lymphatic vessels is their smooth muscle tunica, clearly detectable in histological sections (Johnston, 1985) and because they exhibit spontaneous peristaltic contractions with periodic compressions and expansions of the lymphatic lumen, a phenomenon not seen in the initial lymphatics (Hargens and Zweifach, 1977). Smooth muscle cells (SMC) are strategically arranged into one to three layers, intermixed with collagen and elastic fibres, and surrounded by an adventitia made of fibroblasts and connective tissue elements. They are bordered on the luminal side by an intimal monolayer of endothelial cells (Yoffey and Courtice, 1970). In the smallest lymphatics the layers may not be easily distinguished, the intima being covered by connective tissue with elastic and muscular elements scattered throughout. Generally, as the vessels progress centrally, the amount of smooth muscle increases and the media becomes more ordered with distinguishable layers (Horstmann, 1952). Moreover, lymphatic ducts are reinforced by smooth muscle cells, and the adventitia of large lymphatic ducts contains vasa vasorum and a rich neural network. The smooth muscle layer may be occasionally interrupted where unidirectional valves (made of endothelium and matrix) divide the vessel into multiple *lymphangions* (see chapter 1.6.2) (Mislin, 1976). The smooth muscle exhibits spontaneous and phasic contractions that enable each chamber to act as a “primitive heart” in order to pump lymph. The contractions are fast and strong, leading in some vessels to the complete but

transient obstruction of the lymphangion lumen. Unlike the blood vascular system, in which flow is ensured by the rhythmic contractile activity of the heart, the flow of lymph within the lymphatic tree may be supported initially by external mechanical forces (contraction of surrounding skeletal muscle) and later by the contraction of smooth muscle cells in the walls of larger lymphatics (Pepper, 2006).

Collecting lymphatics can transport fluid in the absence of an external pressure drop along their length; in fact, they can pump against a pressure drop. They are usually quite large compared to vessels of the blood microcirculation. The development of active tension is similar to that seen in vascular smooth muscle. The lymphatic smooth muscle cells exhibit many of the characteristics of arteriolar smooth muscle, with smooth muscle myosin heavy chain isoforms as well as cardiac α-actin, vascular α-actin, enteric γ-actin, and skeletal α-actin. The contractile lymphatics exhibit a myogenic response accompanied by generation of membrane action potentials and calcium influx into the endothelial cytoplasm (Schmid-Schonbein, 2006; see chapter 1.8.1). They also show nitric oxide–dependent vasodilation (Schmid-Schonbein, 2006). The pacemaker activity appears to be located at the inlet valve of each lymphangion, and it is sensitive to the rate of distension. Reduction of external calcium ion concentration monotonically increases contraction frequency but reduces the force of spontaneous contraction (McHale and Allen, 1983). The contraction is propagated as a peristaltic wave along the collecting lymphatics at a velocity of ~ 5 mm/s (Ohhashi et al., 1980), a speed that allows the orderly compression of upstream lymphangions, filling the downstream segments, and the closure of the valves in between. Two adjacent valves never open at the same time, and lymph flow instantly ceases when the rhythmic contractions stop. The ducts require a finite transmural pressure to maintain fluid pumping (Hargens and

Zweifach, 1976). The magnitude of the lymphatic wall tension also appears to modulate contraction frequency (Hargens and Zweifach, 1977). Spontaneous activity is accompanied by the production of action potentials in the wall of the lymphangions (Azuma et al., 1977), which are potassium sensitive and probably depend upon a lymphatic smooth muscle sodium pump and calcium flux. Individual contractions are the result of a single action potential (Allen and McHale, 1986). Depletion of potassium causes membrane depolarization and sustained muscle tension. The frequency of the spontaneous contractions varies in different tissues (from < 1 to 30 cycles/min), although the frequency of the same lymphatic remains relatively constant (Hall et al., 1965).

In mammalian organs, like the intestine or skeletal muscle, all lymphatics inside the tissue parenchyma are initial lymphatics. Collecting lymphatics originate only at strategic transition points where the lymphatics exit the tissue parenchyma (Unthank and Bohlen, 1988).

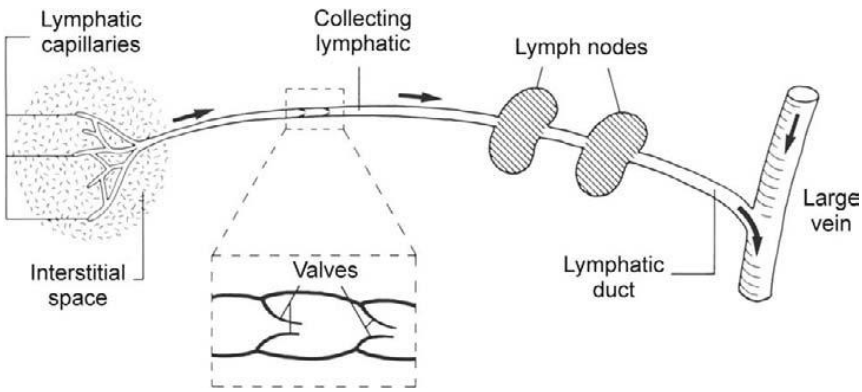

Fig. 1.3 Schematic representation of the lymphatic vascular tree.

1.8 Lymphatic drainage mechanisms

Lymph formation requires filtration from capillaries or post-capillary venules. A common characteristic of all organs is the fact that lymphatic fluid is compressible at the pressures encountered in blood vessels or in the tissue space.

Lymph formation is sustained by hydraulic pressure gradients ($P_{lymph} < P_{int}$) developing between the vessel lumen and the interstitium. Given that in the tissues P_{int} is minor of the atmospheric pressure, lymph formation requires mechanisms able to generate P_{lymph} values more negative with respect to P_{int}. When the lymph is in the lymphatic lumen, it must progresses to the collecting ducts and then to the veins, where hydraulic pressure is positive. There are mechanisms able to build either a negative pressure in the lymphatic lumen, to sustain lymph formation, followed by a positive pressure to permit the centripetal progression. These complex functions are possible because the hydraulic pressure in the lymphatic lumen is not constant, but it has a cyclic oscillatory behaviour, assuming values from ~ - 20 to ~ + 10 mmHg. There are two periods in the pump cycle, an expansion period and a compression period (Fig. 1.4): a) during lymphatic expansion, a P_{lymph} decrease with respect to P_{int} makes the initial lymphatic filled with interstitial fluid; during this period the primary lymphatic valves must be open and the secondary valves inside the lymphatics close, to prevent lymph backflow along the lymphatic duct; b) during lymphatic compression, the lymphatic channel is compressed, P_{lymph} increases, sometimes also with respect to P_{int} and the primary valves must be closed to prevent escape of fluid back into the interstitium, while the secondary valves in the lymphatic lumen are open. The lymph is transported along the initial lymphatic lumen to the collecting lymphatics through unidirectional secondary valves, and eventually to the lymph nodes.

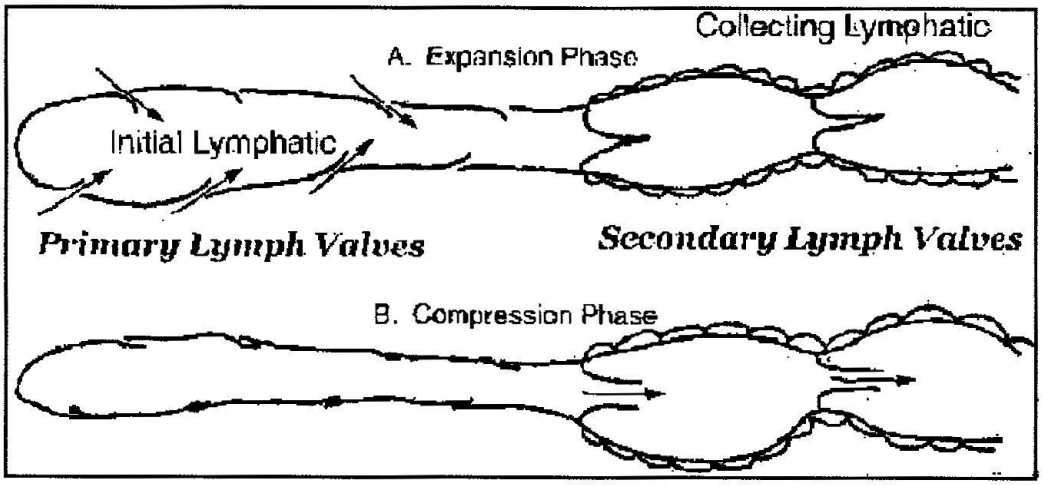

Fig. 1.4 Schematic image of opening and closing of primary and secondary lymph valves during expansion (**A**) and compression (**B**) cycle of the lymphangion. (**A**) During expansion, the primary valves are open to permit fluid entry from interstitium, while secondary valves are closed to prevent reflow inside the lymphatic lumen. (**B**) During compression, the primary valves are closed to prevent reflow into the interstitium, while the secondary valves are open for drainage toward the central lymphatics.

1.8.1 Intrinsic lymph pump

The intrinsic lymph pump mechanism consists of the periodic compression of lymphatics by contraction of their own smooth muscle. This activity serves to empty the lymph into the subsequent collecting lymphatics and to expand the lymphatic during the filling phase. The expansion of the lymphatic is carried out by tissue tensile stresses, while at the same time fluid percolates between the solid tissue phase of the interstitial space into the lymphatic. Thus, as long as the resting shape of a lymphatic ending has an open lumen, the smooth muscle contraction leads to expansion of the connective tissue in its vicinity and elastic recoil restores the lumen to its resting shape (Schmid-Schonbein, 1990).

In the active lymph pump, flow through a lymphatic bed is generated by the coordinated contractions of the lymphatic muscle cells (Mislin, 1976; Zweifach and Prather, 1975). The brisk contraction of these cells leads to a rapid reduction of the lymphatic diameter,

an increase in the local lymph pressure, a closure of the upstream lymph valve, opening the downstream lymph valve, and an ejection of some fraction of the lymph within that vessel. This contraction propagates along the lymphatic, producing a pulse in lymph flow. Phasic contractions of the lymphatics are the result of action potentials initiated by pacemakers that propagate along the vessel, coordinating the pumping activity. Pacemaker seems to be located in each lymphangion immediately downstream to each valve (Ohhashi et al., 1980), probably in the circular muscle layer (McHale and Roddie, 1976). As in heart muscle, each contraction is preceded by a single action potential (Allen et al., 1983). Action potentials in the lymphatic muscle cell produce changes in the intracellular calcium that are somewhat similar to those seen in cardiac muscle cells (Zawieja et al., 1999). The depolarization and the action potential spread from cell to cell along the lymphatic induces an increase in intracellular calcium (Van Helden, 2000; Zawieja et al., 1999), leading to the contraction of the muscle cells. Within a given lymphangion the contraction spreads at a velocity of 4-5 mm/s (Ohhashi et al., 1980), suggesting a cell-to-cell propagation as in cardiac or visceral smooth muscle. The contractile cycle of these vessels can be divided into periods of lymphatic systole and diastole (Granger, 1979). The contractions can be modulated by transmural pressure, luminal flow, neural input. Acute and chronic changes in many of these factors can affect the efficiency of the lymph pump and alter its normal pressure-flow relationship. Many inflammatory mediators may inhibit the lymph pump leading to the development of tissue oedema. Humoral agents, such as α and β adrenergic agonists and prostaglandins, can also affect both the tone of lymphatics as well as alter the active pump activity (Bridenbaugh et al., 2003). The phasic contractile activity is pressure-stretch sensitive (Hargens and Zweifach, 1977). Increases in vessel wall stretch can

produce large increases in the lymphatic contraction frequency and in the strength of the contractions. The ionic mechanisms involved in the initiation of lymphatic contractions are not completely understood, however pacemaker is know to be pressure-stretch sensitive (Mislin, 1976) and it is likely to be influenced by other mechanisms of control. The contractions rely on the energy-driven, calcium controlled, regulated interaction of the actin (thin filament) and myosin (thick filament) molecules. Tonic contractions are generally slow, low-amplitude, energy-efficient muscle contractions that modulate cell tension, lymphatic diameter and resistance to flow.

1.8.2 Extrinsic lymph pump

There are two mechanisms to fill initial lymphatics without an intrinsic smooth muscle: 1) lymph pumping at steady-state volume, 2) lymph pumping at unsteady initial lymph volume.

In the first case, pump would operate without expansion or compression of the initial lymphatics and produce lymph fluid flux at constant volume. This mechanism depends on either a steady drop in fluid pressures from the interstitium into the lymphatic lumen, or an active lymphatic wall pump mechanism mediated possibly by a specialized cellular transport mechanism intrinsic to the lymphatic endothelium (Schmid-Schonbein, 1990).

In the second case the lymphatics are expanded and compressed periodically, and the mechanism responsible for the deformation of the initial lymphatic channels is an extrinsic pump since the tissue surrounding the lymphatic endothelium has to be deformed. The nature of the tissue stresses (compressive and extensive tissue stresses), since it requires a change of the initial lymphatic duct volume, depends on vessel initial

shape under tissue stress. If the resting shape of the initial lymphatics is associated with a closed lumen, then tensile solid tissue stresses will be required to open the lumen. If the resting shape of the initial lymphatics is associated with a completely open lumen, then compressive tissue stresses will be required to compress the initial lymphatics. A partially open lymphatic may be subject to either a compressive or a tensile tissue stress for the outflow of lymph fluid. Its expansion is associated with percolation of fluid toward the lymphatic, and its compression is associated with outflow of lymph fluid toward the collecting lymphatics. Several studies demonstrated that lymphatic expansion and compression depend on the adjacent tissue movements: in skeletal muscle, arteriolar vasomotion, pulsation, and skeletal muscle contraction adjacent to the lymphatics may serve to expand and compress the initial lymphatics. Contraction of the arterioles leads to expansion of the lymphatic lumen, and, conversely, expansion of the arterioles causes compression of the adjacent lymphatic (Skalak et al., 1984). The compression and expansion of the initial lymphatics can be demonstrated after active skeletal muscle contraction and passive stretch (Mazzoni et al., 1987). Data from skeletal muscle experiments support this hypotesis (Bach and Lewis, 1973), since both passive and actively stimulated muscle contractions lead to elevated lymph flow, whereas in the resting muscle a reduced flow of lymph is present. In the extrinsic pump of initial lymphatics several different mechanisms can be operative at the same time: arteriolar vasomotion, pressure pulsation, skeletal muscle contraction, respiration, walking, skin tension and external tissue compression. Each of these mechanisms can be modulated according to physiological activity, and each can be superimposed onto the others so as to make an additive contribution to the resultant lymph flow. Numerous studies have shown that limb motion enhances lymph flow (Calnan et al., 1970).

Passive limb movement or gentle skin massage increase peripheral lymphatic pressure in lymphatics (Calnan et al, 1970, Brace et al., 1977; Ohhashi et al., 1991). In human, daily activity, such as walking and running, greatly increases lymph flow rates from the foot (Olszewski and Engeset, 1979; White et al., 1933), whereas lack of the tissue compression during sleeping leads to minimum lymph output during a daily cycle (Olszewski et al., 1977). Rhythmic tissue deformations, such as arterial pulse and vasomotion (Intaglietta and Gross, 1982; Skalak et al., 1984), intestinal peristalsis (Simmonds 1957; Womack et al., 1988), and muscle contractions (Mazzoni et al., 1990), augment lymph flow. Respiration is an important factor in pulmonary lymph flow (Abeld et al., 1986; Patterson et al., 1985): hyperventilation enhances lymph flow, whereas a pneumothorax reduces thoracic lymph flow (Schad et al., 1978). Thus lymph fluid formation is dependent on rhythmic tissue expansion and compression. External compression functions best when the compression is applied to the initial lymphatics rather than to the collecting lymphatics because interstitial fluid is largely absorbed into the initial lymphatics, with only limited absorption into collecting lymphatics (Schmid-Schonbein, 1990).

1.9 Lymphatic system regulation of the interstitial volume

The interstitial fluid volume is a very tightly controlled variable, averaging in the adult near to 12 litres under normal conditions. The diffusion of substances from the capillaries to distant cells, requiring that the substances diffuse through tightly packed tissues, becomes restricted. When the interstitial fluid volume is too great, the distance from the capillaries to outlying cells becomes correspondingly increased. Therefore,

transfer of substances between the capillaries and the cells becomes compromised. There is an optimal interstitial fluid volume for maximum transfer of nutrients, such as oxygen, from the capillaries to the cells or of cellular excreta, such as carbon dioxide, back to capillaries (Reed at al. 1995).

Two specific relationships have proved to have the most important effects on overall control of the interstitial fluids: 1) the relationship between interstitial fluid volume and interstitial fluid pressure, and 2) the relationship between interstitial fluid pressure and lymph flow. Figure 1.5 illustrates the effect on interstitial fluid pressure when the interstitial fluid volume increases (Guyton, 1965).

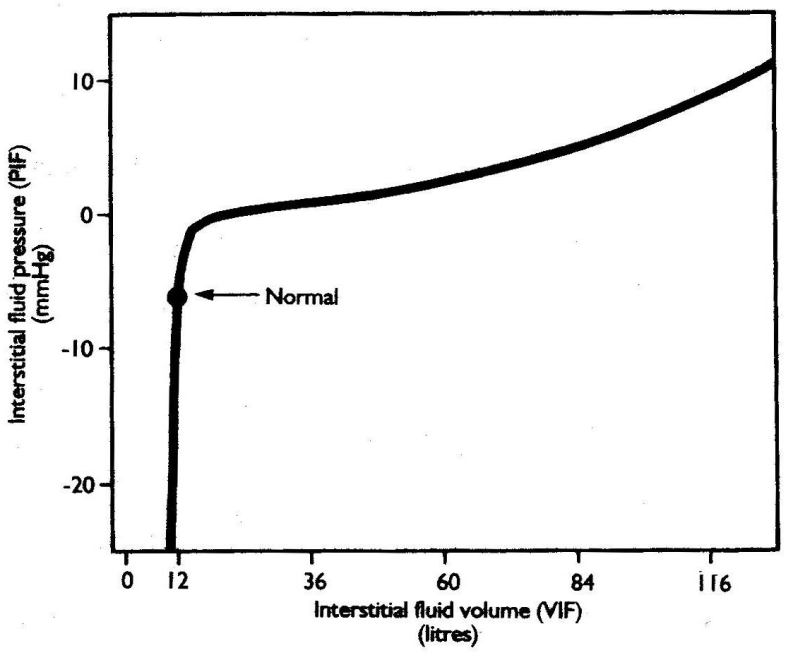

Fig. 1.5 Relation between the interstitial fluid volume and the interstitial fluid pressure.

The curve in this figure is made up of two separate segments. The first segment, corresponding to physiological condition (interstitial liquid volume is minimum), is very steep and vertical, and it lies entirely in the negative interstitial fluid pressure range

(less than atmospheric pressure). The second segment is quite flat and lies horizontal in the positive pressure range (above atmospheric pressure). It is on the steep portion of the curve in figure 1.5 that the interstitial fluid control system normally operates. Because of this steepness, even an extremely slight decrease in interstitial fluid volume below normal will cause the interstitial fluid pressure to fall drastically towards extremely negative values. Conversely, a very small increase in interstitial fluid volume will cause the interstitial fluid pressure to rise from its normal negative value up towards atmospheric pressure (0 mmHg). Compaction of the tissues is the cause of the steep portion of the curve in figure 1.5. In the normal state, the interstitial fluid volume is small enough that cells, intracellular fibrils and tissue gel are all compacted against each other. Therefore, it is difficult for additional amounts of fluid to be removed from the interstitial fluid spaces. For this reason, the interstitial fluid pressure can vary widely from negative values as low as -30 to -50 mmHg, up to atmospheric pressure (0 mmHg) with very little change in interstitial fluid volume. The horizontal portion of the curve in figure 1.5 demonstrates that in most tissues even a slight rise of the interstitial fluid pressure into the positive pressure range (that is above atmospheric pressure) can cause extreme expansion of the interstitial fluid spaces. In this portion of the curve, very slight further increases in interstitial fluid pressure push the cells apart, and excess fluid accumulates extremely rapidly. This is the state known as “extracellular fluid oedema”. This extreme expansion of the interstitial fluid spaces is caused by the fact that in most tissues, especially the subcutaneous tissues, the fibrils holding the cells together are very weak. Therefore, even the slightest increase in interstitial fluid pressure above 0 (atmospheric pressure) can push the cells and other tissue elements apart. Once this occurs, the limiting factor against developing still more oedema is not tensional

elements within the tissues themselves but instead it's the tensional strength of the outer covering of each respective tissue (for example, for subcutaneous tissues of the body, the limit becomes the tensional elements of the skin). Therefore, from a functional point of view, it is important for the interstitial fluid control system to operate on the steep portion of the curve in figure 1.5. The curve slope depends on the mechanical characteristics of each tissue. In normal conditions, the tissue behaves as a rigid structure, so that a small increase of the interstitial liquid volume causes a great interstitial pressure increase. The tissue is thus characterized by a low mechanical compliance. This phenomenon is very important for the control of the interstitial volume. Indeed, in physiological conditions, a capillary filtration increase and, in turn, an interstitial volume increase determine a P_{int} increase. The P_{int} increase (Eq. 1.1) causes a rapid decrease of the filtration, and a contemporary increase of the local lymphatic flow (Eq. 1.3). In fact, as illustrated in figure 1.6, in normal condition the lymphatic flow is very low. Moreover, a P_{int} increase over the normal level causes a great flow increase.

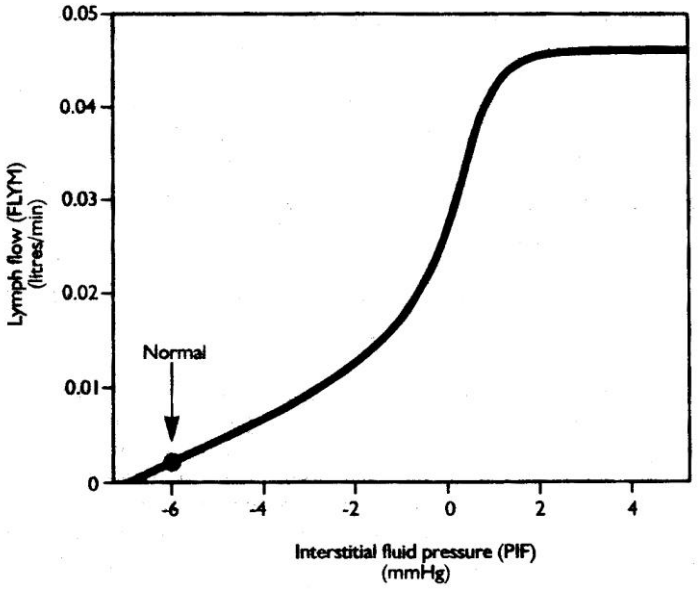

Fig. 1.6 Relation between the interstitial fluid pressure and the lymph flow.

Figure 1.6 illustrates the second crucial relationship in controlling the interstitial fluid (Taylor at al., 1973). This is the effect on lymph flow caused by increasing interstitial fluid pressure. Lymph flow is normally very small. However, an increase in interstitial fluid pressure above the normal level causes a drastic increase in the flow. The relationship between interstitial fluid pressure and lymph flow differs in different organs of the body. The curve in figure 1.6 shows a 20 to 25 fold increase in lymph flow, as the interstitial fluid pressure rises from the normal negative value of about -6 mmHg up to 1-2 mmHg above atmospheric pressure. During the phase of rapidly rising interstitial fluid pressure, the lymphatics become progressively more filled with fluid, thereby stretching the walls of the lymphatics and also increasing the activity of the lymphatic pump. However, once the interstitial fluid pressure rises above atmospheric pressure (horizontal portion of the curve), oedema fluid collecting in the interstitial spaces also begins to compress the outer walls of the lymphatic vessels, and this compression generally prevents further increases in lymph flow. Therefore, the important increase in lymph flow occurs mainly in negative or very slightly positive interstitial fluid pressure range before clinical oedema occurs, thus helping to stop the development of oedema. Moreover, above an atmospheric P_{int} value, there is the saturation of the lymphatic flow, which doesn't increase although the interstitial volume increases.

These two relationships (Fig 1.5 and 1.6) show: 1) a very slight increase in interstitial fluid volume above the normal level of 12 litres causes a very rapid increase in interstitial fluid pressure over the normal negative value of -6 mmHg; 2) the increase in interstitial fluid pressure causes a marked increase in lymph flow; 3) the increase in lymph flow causes rapid drainage of fluid from the interstitial spaces through the lymphatics into the circulating blood; 4) this drainage of fluid from the interstitial

spaces returns the interstitial fluid volume back towards normal. These steps demonstrate a negative feedback control system. If ever the interstitial fluid volume rises even slightly above normal, rapid change occurs in both interstitial fluid pressure and lymph flow until the interstitial fluid volume is returned very nearly back to normal, hopefully to prevent the oedema state from being reached (Reed et al. 1995). Some mechanisms might explain the lymphatic ability flow to adapt to a filtration change of the microvascular flow: 1) the fluid entering in the tissues increases the P_{int}, which increases the pressure gradient causing the lymphatic vessels filling; 2) the intra-lymphatic pressure increase might induce the contraction of the vessels which permits the lymph progression, the valve opening and the consequently intra-lymphatic pressure decrease; 3) the tissutal movements speed up the lymph flow; 4) when liquids enter in the interstitium, the tissutal spaces expand to permit the interstitial fluid movement. However, the tissues can't distend significantly themselves but there is an increase of the P_{int} that causes a drainage increase and so a lymphatic flow increase; 5) the substances release from the damage endothelial cells or from other cells, as neutrophils and macrophages, can increase the pumping of the lymphatic system.

1.10 Lymphatic endothelium

The lymphatic endothelial cells lack the inter-endothelial junctions (Schmelz et al., 1994) seen in vascular endothelium (Dejana, 1997) and they have a discontinuous endothelial basement membrane (O'Morchoe, 1987) with incomplete junction protein components (Nerlich and Schleicher, 1991). Their cytoplasm contains an assortment of organelles, caveolae, mitochondria and typical cytoskeletal proteins, including actin,

intermediate filaments, and microtubules with the ability to form stress fibers. The cytoskeletal proteins facilitate active changes in cell shape, such as pseudopod projection and formation of adhesion sites or cell migration, as in lymphangiogenesis, and they are able to undertake amoeboid migration (Ryan and Mayfield, 1988) and even phagocytosis (Ryan, 1988). The deformation process by endothelial cells is quite slow, and the actual cell shape during motility is complex and not associated with a unidirectional strain field, as in sarcomere direction of smooth or skeletal muscle (Schmid-Schonbein, 1990). The endothelial cells are attached to the surrounding extracellular matrix via a set of anchoring filaments (Leak and Burke, 1968), so that the two neighbouring endothelial cells are firmly attached via the basement membrane to the interstitial tissue matrix. One cell has a cytoplasmic extension without anchoring filaments or endothelial adhesion molecules, so that it is free to bend into the lymphatic lumen. In general, endothelial cells of initial lymphatics are highly attenuated and form a thin lining with a thickness of ~ 0.25 μm. Direct microscopy or tissue cultures with lymphatic endothelium have provided no conclusive record to indicate that initial lymphatics are contractile. Lymphatic endothelial cells, like vascular endothelial cells, have cytoskeletal proteins, which permit a variety of active cell shape changes (as pseudopod projection, phagocytosis or formation of adhesion sites), but there is no evidence that such cytoplasmatic motions translate into a contraction mechanism for an entire lymphatic channel, as in collecting lymphatics with smooth muscle. The compression and expansion depends on periodic motion of tissue structures positioned in immediate proximity to the initial lymphatics. For example, the arterioles serve an effective role in this respect (Skalak et al., 1984).

1.11 Filtration and lymph formation

Mechanical propulsion of lymph fluid can not be maintained unless additional fluid is filtered from the blood vessels into the interstitium. For persistent elevation of lymph flow, all "segments" of the transport pathways (filtration, interstitial transport, lymph formation and lymph transport) must operate synchronously. Lymph flow is interrupted when the contribution of any of the four segments is reduced, a situation that inevitably leads to interstitial and lymphatic oedema if transvascular filtration continues. There is a reserve in the existing lymph pump mechanisms to drain elevated fluid levels from the interstitium. Both elevation of venous pressure and reduction of the plasma colloidosmotic pressure lead to an elevation of lymph flow rate (Kramer et al., 1981). Although both procedures may cause alterations in pulse pressure, heart rate, or other intrinsic lymph pump mechanisms, they are accompanied by elevated filtration rates and presumably reduced venular reabsorption with elevation of interstitial pressures and fluid volume.

1.12 Lymphatic protein concentrations

Lymph protein concentration is lower than in the plasma. The protein output from the lymphatics is an inverse function of the lymphatic flow rate (Joyner et al., 1973) but also depends on the past histories of filtration and lymph flow rates. If lymph flow rates are not reduced, there is no elevation of the tissue protein concentrations (Brace et al., 1977). The lymph protein concentrations in afferent and efferent lymph are different across lymphatic nodes (Adair and Guyton, 1985): in lymph nodes a water equilibration takes place and it's determined by the hydrostatic and colloidosmotic pressures in the

nodal vascular and lymphatic compartment. High protein concentrations in the afferent lymph are diluted by fluid absorption in the node to an equilibrium concentration (at a lymph colloidosmotic pressure that balances the hydrostatic and osmotic forces acting across the nodal blood-lymph barrier); low afferent protein concentrations, in turn, are elevated by fluid removal to the equilibrium concentration (Adair and Guyton, 1983).

1.13 Pressure in lymphatics

In normal condition the lymphatic system has a relatively low pressure. These levels may be dramatically elevated during oedema, a situation where lymph flow often ceases. Generally, the pressures in any tissue compartment are determined by the boundary stresses applied to this compartment and the viscous dissipation during flow. Without flow, the pressures are only determined by the boundary pressures. For example, in a lymphatic region with initial lymphatics draining into a collecting lymphatic, if the collecting lymphatic is occluded and lymph fluid outflow is prevented, the lymphatic pressure in this region is uniform and determined by the fluid pressures and also by the tissue stress applied by the structures that surround the lymphatic vessel. Compression of such an isolated occluded lymph region at any point raises the pressure everywhere within the lymphatic lumen.

One of the common characteristics of the lymphatic system in different organs is the low intralymphatic resistance (Clough and Smaje, 1978). The pressure in the initial lymphatics is determined by two separate events. During filling of the initial lymphatics it is determined by the fluid pressure drop from the interstitium into the lymphatic lumen. During compression it is determined by the pressure gradient necessary to drive

the fluid along the length of the lymph duct. The fluid pressure drop along the lymphatic ducts is largely determined by the viscous resistance in those ducts, which in turn depends on the compliance of the lymphatic ducts and the flow resistance through the lymph nodes. Flow in the lymph ducts and in the lymph nodes is very low because of the relatively small channel dimensions. Thus the pressure drop is entirely determined by viscous forces, which in turn largely depend on the geometry of the lymphatic ducts, the lymph fluid viscosity and the flow rate. The presence of the valves permits stepwise changes in pressure from one lymphangion to the next. There is indication that much of the fluid resistance resides in the lymph nodes and possibly in the funnel-shaped narrowing of the lymph valves (Browse et al., 1984), and it was observed a pressure rise during the emptying phase of the lymphatics (Hargens and Zweifach, 1977). The lymph nodes have narrow fluid crevices and are made up of a soft tissue with a vascular compartment opposing the lymph compartment. The fluid resistance in the nodes depends on the size of the node and on flow rate (10 to >150 $mmHg \cdot ml^{-1}$, Browse et al., 1984). These values appear to be two orders of magnitude higher than the lymph fluid resistance in the afferent and efferent lymphatic ducts. The nodal resistance is higher at lower flows and decreases with higher flows. This effect is typical for distensible channels in soft organs, since an increased flow with its associated increased upstream pressure causes distension of the fluid channels and a reduction of the fluid resistance. In the immediate proximity of the contracting lymphatic endings it is possible to record a fall in tissue fluid pressure during contraction, which thereby causes movement of fluid from the surrounding interstitium toward the lymphatics. Each contraction is associated with a corresponding pressure pulse (Nicoll and Hogan, 1978). The lymphatic pressure also depends on the location in

the lymphatic system (before or after a lymph node) and the lymph flow rate depends on body position and body activity (Laine et al., 1987).

1.14 The diaphragm

The diaphragm is a dome-shaped structure, consisting of a central tendon not muscolarized region surrounded by a ring of radially oriented striated muscle fibres. There are openings in the diaphragm for the oesophagus, the phrenic nerve (which controls the movements of the diaphragm to control breathing), and the aorta and vena cava blood vessels, which lead to and from the heart. The diaphragm separates the thoracic and abdominal cavities. It is attached to the spine, the ribs and sternum and plays a very important role in the breathing process. The lungs are enclosed in a kind of cage in which the ribs form the sides and the diaphragm forms the floor. The physiology of the diaphragm is primarily considered from its respiratory activity. However it has additional roles as "a separator" between the thoracic and the abdominal cavities, and it is also a prominent agent of activities that are "expulsive" in nature and require building up high intra-abdominal pressures (Perry et al., 2010).

During inspiration, the diaphragm is drawn downward until it is flat, the chest cavity becomes larger and the abdominal pressure is driven up. This increase in pressure drives the abdominal contents down and out, which in turn increases the transverse size of the chest cavity. Because the diaphragm is covered by the inferior surface of the parietal pleura, when it contracts it pulls the pleura with it. This lowers the pleural pressure, which causes the alveolar pressure to drop, which, in turn, causes air to flow into the lungs. During quiet expiration, the diaphragm passively relaxes and returns to its

equilibrium position. However, during exercise, expiration becomes an active process, the abdominal muscles contract to raise abdominal pressure, which pushes the diaphragm upward and forces air out of the lungs. Thus contraction of the diaphragm has two different functions in the respiration activity: 1) decreasing intrapleural pressure, and 2) expanding the rib cage generating positive intra-abdominal pressure. The diaphragm is rich of lymphatic vessels: in particular the diaphragmatic lymphatic system removes fluid and solutes from the diaphragmatic interstitium and from the pleural and peritoneal cavities.

1.15 Diaphragmatic lymphatics system

The recognized role of diaphragm lymphatics is to remove fluid, solutes and cells from the thin diaphragmatic muscular tissue as well as from the pleural (Negrini et al., 1985; Wang, 1975) and peritoneal (Miserocchi et al., 1989; Ohtani Y and Ohtani O, 1997) serous cavities. This function is achieved through an extended network of initial lymphatic vessels, organized in planar submesothelial pleural and peritoneal lacunae and transverse lymphatic capillaries, which depart perpendicularly from the lacunae and empty in a deeper network of larger collecting lymphatics (Grimaldi et al., 2006; Negrini et al., 1992; Ohtani et al., 1993; Wang, 1975). One of the most typical features of the diaphragmatic lymphatic vessels is their organization into complex loops, formed at the confluence of long linear vessels (Negrini and Del Fabbro, 1999; Negrini et al., 2004).

1.16 The pleural space and pleural lymphatic system

The pleural space may be considered as an enlarged tissue space whose free liquid volume largely exceeds that of the solid elements, mainly consisting of a complex mesh of microvilli of the mesothelial cells. The ability of the serous spaces to remove fluid and particulates at high flow rate was already known in 1799 (Hewson, 1846). In 1863 Recklinghausen demonstrated that mesothelial cells are flat and very similar to the capillary endothelial cells in which he identified the presence of fenestrae (Reed et al., 1995). In 1895 Heidenhain proposed that fluid leaves the peritoneal space mainly through absorption into the blood capillaries (Heindenhain, 1895). At about the same time the studies of Starling (Starling, 1896; Starling and Tubby, 1894) showed that osmotic gradients are important to sustain fluid exchanges across mesothelial membranes (Recklinghausen, 1863), and that after "the establishment of osmotic equilibrium the absorption of fluid from the pleural cavity is extremely slow, so that it might perhaps be affected by the lymphatics alone" (Starling and Tubby, 1894). Furthermore, Leathes and Starling introduced the important concept that the mesothelial layer acts as a size-selective barrier for solute exchange (Leathes and Starling, 1895). In 1927, Florey pointed out the importance of rhythmic contractions of the large collecting lymphatics to propel lymph (Florey, 1927). Based on the Starling osmotic hypothesis, in 1923 Neergard reasoned that the negative pleural liquid pressure could result from fluid reabsorption through the visceral pleura because plasma colloid osmotic pressure largely exceeds the hydraulic pressure in the pulmonary capillaries (Neergard, 1923). According to this hypothesis, the pleural fluid drainage would be through the pulmonary capillaries.

The main function of pleural fluid is to guarantee a close apposition of lung and chest wall, allowing frictionless sliding of visceral and parietal pleurae during respiratory movements. The pleural fluid displays some specific features: 1) its volume is very small (from 0.4 to 2.5 ml for kg of body weight from both pleural spaces), depending upon the species considered (Miserocchi and Agostoni, 1971; Miserocchi et al., 1984), because only a thin layer of fluid separates the opposing pleural layers (about 10-20 μm) (Wang, 1985; Lai-Fook and Kaplowitz, 1985; Agostoni at al., 1969); 2) its hydraulic pressure is subatmospheric in physiological conditions; therefore, the pleural cavity may be considered as a relatively dehydrated interstitium; 3) its total protein concentration is low compared with other interstitial spaces, ranging between 1 and 2,5 g/dl and decreasing with increasing mammal size (Miserocchi and Agostoni, 1971; Miserocchi et al., 1984); 4) it contains surfactant phospholipids that act as lubricants (Hills, 1992; Hills et al., 1982); 5) its viscosity is essentially equal to that of water; 6) its ionic content is similar to that other extracellular fluids and plasma (Zocchi et al., 1991); 7) it contains about 2200-2400 cells per mm^3, including mesothelial cells, monocytes and lymphocytes (Miserocchi and Agostoni, 1971).

The pleural space, as all serous cavities, derived from the embryological development of the primitive coelomatic body space. The pleural cavity is delimited by parietal and visceral mesothelia covering the inner thoracic cavity and the lung, respectively. The maximum thickness of a mesothelial cell is about 4 μm (Wang, 1974). The Golgi apparatus and the rough endoplasmatic reticulum are barely developed, and few mitochondria are dispersed in a scant cytoplasm; adjacent cells are connected by tight junctions on the luminal side, and by desmosomes on the basal portion of the intracellular junction (Wang, 1985; Wang 1974; Bernaudin et al., 1991). These features

are common to mesothelia and vascular and lymphatic endothelia (Wang, 1985). Mesothelial cells are covered by 1-3 μm long microvilli, whose density varies from 2 to 30 per μm^2 (Wang, 1974; Mariassy and Wheeldon, 1983). High concentrations of glycoproteins and hyaluronic acid are trapped by microvilli on the most mobile lung caudal surface (Wang, 1985; Mariassy and Wheeldon, 1983). The cells contain the enzymic chains for production and assembly of macromolecules (as collagens I, III and IV) of the subpleural interstitial space; mesothelial cells also synthesize elastin, laminin, fibronectin, glycoproteins and proteoglycans (Bernaudin et al., 1991; Arai et al., 1975).

The mesothelia lie on a continuous basal lamina connected to the subpleural interstitium; the latter extends up to the alveolar and septal pulmonary interstitial space on the visceral side and to the endothoracic fascia on the parietal side. In mammals with thin pleurae (dogs, rabbits and cats; Bernaudin and Fleury, 1985), the thickness of the parietal subpleural interstitium (about 20 μm) is similar to that of the visceral side, whereas in mammals with thick pleurae (sheep, pigs, horses and humans), the parietal interstitium is about four times thinner than in visceral one (Mariassy and Wheeldon, 1983; Albertine et al., 1982 and 1984). In all mammals, blood supply to the parietal pleura is provided by a systemic microvascular network; the visceral pleural microvasculature derives from the pulmonary circulation in mammals with thin pleurae and from the branching of the systemic bronchial artery in mammals with thick pleurae. The average distance between mesothelial cells and the subpleural microvascular network is from two to five times smaller in the parietal than in the visceral pleura (Albertine et al., 1982 and 1984).

The visceral pleural lymphatic plexus runs parallel to the mesothelium, with no connection between the lymphatic lumen and the pleural space (Albertine et al., 1984).

The parietal pleura and the parietal peritoneum are supplied by a peculiar network of lymphatic (Fig. 1.7) (Bettendorf, 1978), characterized by the existence of the so-called "stomata", which establish a direct patent link between the pleural cavity and an extensive mesh of submesothelial lymphatic lacunae (Wang, 1985; Thomas and Ramwell, 1991; Wang, 1975). Lacunae consists of wide lymphatic vessels running parallel to the mesothelium, from which they are separated by a thin stratum of submesothelial interstitial space (Wang, 1985; Thomas and Ramwell, 1991; wang, 1975); stomata are delimited by adjacent mesothelial cells where they make contact with the endothelium of the lymphatic lacunae. Stomata may be isolated, grouped in clusters (Negrini et al., 1991), or organized to form a membrane made of a net-like arrangement of collagen fibres irregularly covering the roof of the underlying lacunae (Wang, 1985). Their density ranges from $100/cm^2$ on the intercostals surface to $8000/cm^2$ on the diaphragm where it displays the highest stomata/lacuna ratio (Negrini et al., 1991 and 1992), the diameter ranges from 0.5 to 20 μm. The cytoplasm of the endothelial cells delimiting the lumen of the lacunae contains actin filaments (Thomas and Ramwell, 1991), suggesting that the very initial portion of the pleural lymphatics may actively contract; furthermore, the endothelium of lacunae may differentiate to form unidirectional flap-like valves (Wang, 1985; Leak and Rahil, 1978; Tsilibary and Wissing, 1983).

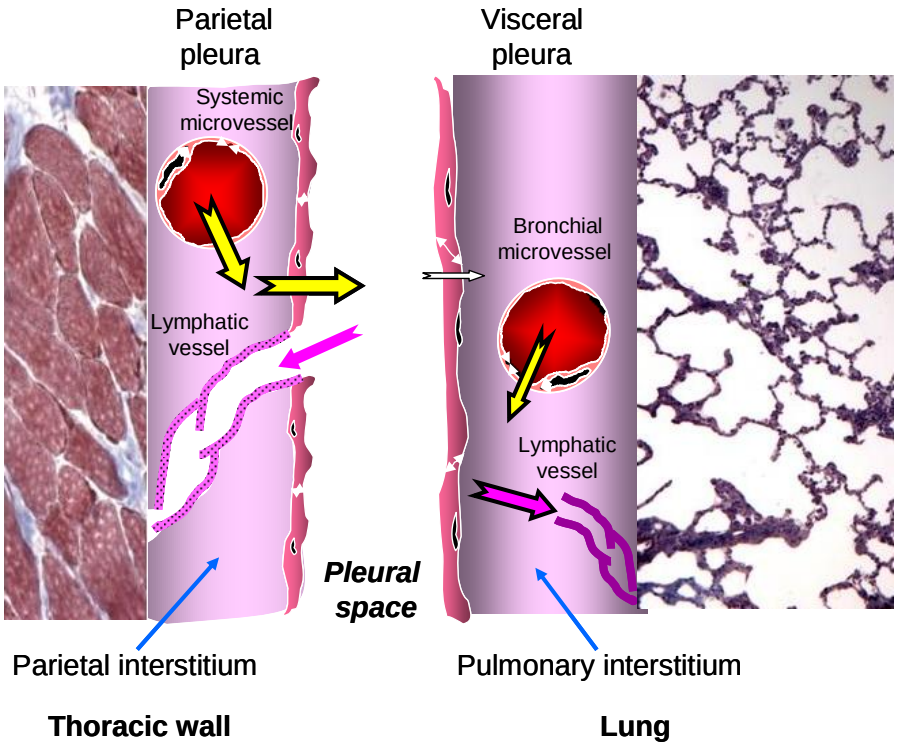

Fig. 1.7 Morpho-functional arrangement of the pleura structures.

1.17 Aim of the research

In spite of its importance in the control of tissue fluid volume and composition, several functional aspects of the initial lymphatic system in thoracic tissues have not yet been described. An important role of the lymphatic system is to maintain tissue fluid homeostasis. The diaphragmatic initial lymphatics are organized in long linear vessels and complex loops. In particular the diaphragmatic lymphatic system removes fluid and solutes from the diaphragmatic interstitium and from the pleural and peritoneal cavities. Lymph formation is sustained by transmural pressure gradients ($\Delta P_{TM} = P_{lymph} - P_{int}$) developing between the vessel lumen and the interstitium; while lymph progression is sustained by pressure gradients ($\Delta P_l = P_{lymph2} - P_{lymph1}$) developing between adjacent lymphatic segment (Fig. 1.4). In highly moving tissues, as the diaphragm, ΔP depends

upon cyclic lymphatic lumen compressions and expansions developing during the cardiac cycle and the respiratory cycle. However, the mechanisms by which tissue displacements may enhance lymph formation and progression are very complex and not completely unveiled.

The present study is aimed at providing a contribution to this issue examining the pattern of fluid kinetics in the submesothelial lymphatic lacunae and at clarifying whether the organization of the diaphragmatic lymphatic network in loops and/or linear vessels might be a tool to optimize either the lymphatic absorption of fluid from serous cavities and/or lymph progression towards deeper collecting ducts.

2 Organization of the study

The present study was organized in three different steps: in part I we measured lymph flow velocity and its value. In part II we measured the compliance of the lymphatic vessel wall *in vivo* and performed *ex vivo* mechanical tests on diaphragmatic tissue strips; in part III we studied the kinetics of fluid flux *in vivo* in complex diaphragmatic lymphatic loops and by developing a mathematical model built on the real vessel dimensions, flow and pressure gradients measured values, in order to clarify the function of the organization of the lymphatic network. In part IV, the possible presence of muscular fibers around the lymphatic vessel wall of contracting lymphatics was investigated in order to justify the lumen contraction phenomena described in part III.

3 Materials and methods

3.1 Anaesthesia and surgical procedures

Experiments were performed on adult pathogen-free male Wistar rats (Charles River; Laboratories Italy, Calco, (LC)). Rats were housed in ventilated cages with sawdust and fed *ad libitum* with rodent pellets (standard diet for rats and mice, Charles River Laboratories Italia Calco, (LC)) and water. All experimental procedures and protocols were approved by the Institutional Animal Care Committee at the University of Insubria, Varese, Italy in accordance with the Health Research Extension Act.

In part I of the present study the animals (mean body weight: 400 ± 18 g, n = 7) were anaesthetised with an intraperitoneal injection of a cocktail composed of 75 mg/kg of ketamine (Sigma Aldrich, Milan, Italy) in saline solution and 0.5 mg/kg medetomidine (Domitor, Pfizer). Successive ketamine half-boluses were administered every hour until the end of the experiments, when animals were euthanized via an anaesthesia overdose. Before the surgical procedure was started, and at regular time intervals during the experiment the attainment of a deep surgical anaesthesia level was assessed on the basis of the disappearance of the corneal reflex. Once deeply anaesthetized, the rats were turned supine on a warmed (37°C) blanket to maintain the body temperature; they were then tracheotomised, and a T-shaped cannula (outside diameter ~ 2.5 mm) was inserted into the trachea and connected to a heated Fleish pneumotachograph (model 8420, Hans Rudolph Inc.) equipped with a dedicated pneumotach amplifier (model 1110A, Hans Rudolph Inc.) to continuously record respiratory flow ($\dot{V}_E$). The flow signal was then digitized with a National Instruments BNC-2090 analog-to-digital board (sampling rate: 100 Hz) and integrated through dedicated LabView software (National Instruments) to obtain respiratory tidal volume (V_T); both flow and tidal volume signals were then displayed on a monitor. The femoral vein was exposed, and animals were paralyzed with a single bolus of 0.2 ml pancuronium bromide (Sigma Aldrich, Milan, Italy) solution (2 mg/ml in saline) administered in the femoral vein through a 27-gauge needle. Immediately after paralysis, the tracheal cannula was connected to a mechanical ventilator (ventilator model SPIRA, Harvard Instruments), and rats were ventilated in room air with a tidal volume of 4 ml and a respiratory rate of of 60 breaths/min. Then, the skin and the external intercostal muscles on the right side of the thorax were cleared to expose the ribs and the internal intercostals muscles, the chest was opened with a

little incision, and the caudal four to five ribs were unilaterally removed to expose the whole pleural surface of the diaphragm, with care taken not to pierce the diaphragmatic surface and proximal abdominal wall. The pleural diaphragmatic lymphatic network was explored with the aid of a stereomicroscope (SV11 Carl Zeiss, Milan, Italy). The diaphragmatic surface was frequently rinsed with a gentle flush of saline solution to avoid dehydration.

PART I

3.2 Lymph flow velocity

To detect the lymph flow velocity, lymphatic vessels were microinjected with a fluorescent dye (FITC-conjugated dextran, a high molecular weights polysaccharide conjugated with fluorescein-isothiocyanate (FITC)).

With the use of a vertical puller (PP30, Narishige, Tokyo, Japan), glass pipettes for microinjection were pulled from borosilicate glass capillaries (1B100-4, 1.0 mm outer diameter, 0.58 mm inner diameter, WPI Europe, Berlin, Germany) to tip diameters of ~20 µm. Pipettes were filled with mineral oil and mounted onto a mechanical micro-injector (WPI Europe) set to deliver 4.6 nl/injection. Under the stereomicroscope, pipettes were front filled with 1 µl of 0.2 µm filtered 2% FITC-dextran (282 kDa)-conjugated solution in saline (0.9% NaCl in distilled water).

Then with the use of a mechanical coarse/fine micromanipulator (Narishige, Tokyo, Japan), the injection pipette was longitudinally aligned over the lymphatic vessel to be injected with the shallowest possible angle with respect to the diaphragmatic surface. Careful positioning of the pipette tip with respect to the lymphatic vessel proved to be a

key point for an almost-complete injection success rate into the vessel itself. After being positioned, the pipette tip was gently advanced through the pleural diaphragmatic surface until it was inserted into the lymphatic vessel lumen. A single injection of 4.6-nl volume was then triggered, and the pipette tip was immediately withdrawn from the vessel. All these phases (pipette positioning, fluorescent dye injection, and distribution of the dye into the lymphatic vessel lumen) were recorded by the stereomicroscope which was equipped with a cooled black-and-white charge-couple device camera (ORCA ER, Hamamatsu, Milan, Italy) connected with a personal computer running SimplePCI software (Hamamatsu) to control all the aspects of image acquisition and analysis. FITC-dextran conjugate was excited with an optic fiber epi-illuminator equipped with a 425 ± 65nm bandpass filter (Carl Zeiss Italy). Fluorescence emission was collected by the stereomicroscope fitted with a two-bandpass filter (FITC/TRITC, catalog no. 56918, Chroma Technology, Rockingham, VT). Images were collected both in real time, to better follow the time course of the injection, and in time lapse (interframe interval: 10–30 s) a few minutes after the injection. The exposure time was routinely set to 1 s or lower to allow the detection of the faintest fluorescence signals without a significant increase in background noise. Images were directly stored in the hard disk of the computer and subsequently analyzed. Typical recordings of a single-vessel injection lasted ~25 min. To obtain the most clear and still images of lymphatic vessels during time-lapse recording, the diaphragmatic movements were temporarily (2–3 s) arrested by occluding the inspiratory line of the mechanical ventilator during image exposure and immediately reopening the inspiratory line after image acquisition; while during real-time recording, the inspiratory line was kept closed for time periods no longer than 10 s during a period of no more than 3 min, allowing several breaths in

between. Several measurements were made in each segment for each vessel. Direct measurements of vessel diameter and fluorescence progression velocity were performed on original images with SimplePCI software. Flow velocity was computed by dividing the distance travelled by the fluorescence front along the path of the lymphatic vessel by the interpicture time interval.

3.3 Recording of intraluminal lymphatic pressure

The measured lymph flow velocity might have been affected by changes in intraluminal lymphatic pressure (P_{lymph}) induced by the injection manoeuvre. To exclude the occurrence of this possible artefact, P_{lymph} was measured during and after the injection manoeuvre with the use of the micropuncture technique. P_{lymph} recordings were obtained through glass micropipettes bevelled down to 2-4 µm tip diameter, filled with 1M NaCl solution, and secured to a pipette holder filled with the same solution. The pipette holder was connected to a mineral oil-filled pressure transducer (Gould Instruments System, Inc), motor driven by an electrohydraulic system (Dual Servonull Pressure-Measuring System, Vista Electronics, Ramona, CA, USA). The pressure signal was relayed to an amplifier and a signal conditioner (model 6600, Gould Electronics), digitized with an analogue-to-digital board, and displayed on the monitor using dedicated LabView software (National Instruments). Prior to its use, each micropipette was calibrated in a modified Lucite box by imposing step changes of ± 5 mmHg in the box chamber; and pipettes displaying a nonlinear calibration in the pressure range of ± 30 mmHg were discarded. Once calibrated, the micropipette was mounted in a three-dimensional hydraulic micromanipulators (Joystick Micromanipulator MO-188 or MO-

109, Narishighe, Tokyo, Japan) equipped with a fourth micromanipulator movement to drive the tip of the micropipette into the tissue.

Electrical zeroing of the recording system was performed before and immediately after each measurement by dipping the micropipette tip in a saline pool positioned at the same height of the pipette insertion point. The criteria for acceptance of the micropipette pressure recordings were: 1) an unchanged electrical zero of the system on withdrawal from the tissue compared with the pre-insertion value, 2) a stable pressure reading for at least 2 min, and 3) repeated measurements from the same area were within 1 mmHg of each other.

P_{lymph} measurements might have been affected by some artefacts: a) once in the tissue, the intraluminal tip position could not be checked by dye injection through the pipette, as the injection manoeuvre would have disturbed the electrical zero of the servonulling pressure measuring circuit, invalidating the pressure reading; b) P_{lymph} might be affected by the micropipette tip position inside the vessel and by possible distortions of the tip against the vessel wall. To exclude these artefacts the pipette was driven into the vessel along its major axis to avoid distortion against the wall and at a depth of 20-30 μm, judging from the micromanipulator cursor. With these precautions, we believe that the micropipettes were recorded from inside the lymphatic vessel, with minimal distortion of the wall.

3.4 The lymphatic vessel thickness and lymph flow

To calculate lymph flow ($\dot{V}_{\text{lymph}}$) it was necessary to know the lymph flow velocity (v) and the vessel cross-sectional area because $\dot{V}_{\text{lymph}}$ is the product of lymph flow velocity (v) by vessel cross-sectional area (S) as follows (Eq. 3.1):

$$\dot{V}_{lymph} = v \times S = v \times (\pi \times \frac{d}{2} \times \frac{t}{2}) \qquad \textit{(Eq. 3.1)}$$

The lymphatic vessel cross-sectional area can be considered an ellipse where d is the diameter of the vessel on the diaphragmatic plane and t is the diameter on the axis perpendicular to the diaphragmatic surface (vessel thickness). The parameter d was directly measured on recorded stereomicroscope images of the vessel through SimplePCI software, whereas t could be only indirectly measured with the following procedure: three anaesthetized rats had undergone the same surgical preparation to expose the diaphragm as previously described; then they were placed under the stereomicroscope to explore the pleural diaphragmatic lymphatic network. When a linear or loop lymphatic vessel was detected, with the aid of a pipette micromanipulator, a bolus of mineral oil of known volume (injected oil volume V_{inj}: 2.3 nl) was injected in the vessel while images were recorded by the cooled black-and-white charge-coupled device camera before the injection and throughout the whole injection manoeuvre. We injected mineral oil, instead of the fluorescent dye which immediately distributed away from the injection site, because the oil didn't mix with the fluid present in the lymphatic vessel before the injection; it didn't rapidly flow into the vessel away from the injection point but it remained confined in a single and well-defined droplet and it displaced the fluid previously flowing in the lymphatic vessel, completely filling and occluding a short segment close to the injection site, as shown in Fig. 3.1.

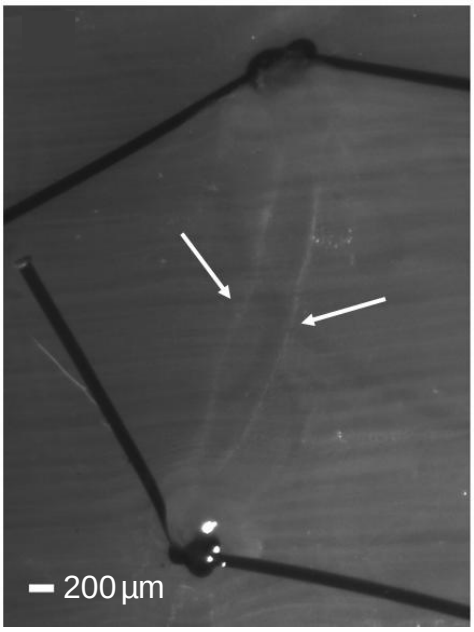

Fig. 3.1 Stereomicroscope image of a linear lymphatic segment delimited by two occluding silk knots. The diaphragmatic muscular fibres can be distinguished crossing the vessel perpendicularly.

Therefore the oil injection could be used to indirectly estimate *t*: the pre-injection (*d*) and post-injection vessel diameter (d_{inj}) and the area occupied by the oil drop (A_{inj}) within the vessel were measured by SimplePCI image analysis software. In an elliptical vessel cross-sectional area, the volume injected (V_{inj}) filled the vessel for a length (*l*), so we could calculate t_{inj} as post-injection vessel diameter perpendicular to the diaphragmatic surface (Eq. 3.2):

$$V_{inj} = (\pi \times \frac{d_{inj}}{2} \times \frac{t_{inj}}{2}) \times l \qquad \textit{(Eq.3.2)}$$

On bidimensional images, we could assume that the oil drop filled an almost rectangular area, so that one may approximate *l* as: $l = A_{inj}/d_{inj}$. Therefore, t_{inj} can be calculated from Eq. 3.3 as follows:

$$t_{inj} = \frac{4 \times V_{inj}}{\pi \times A_{inj}} \qquad \textit{(Eq. 3.3)}$$

3.5 Statistical analysis

Data are presented as means ± SE. Statistical significance of the differences between mean values was computed using Student's *t*-test providing the variance of the group was equal. In the case of failure of the equal variance test, differences were tested through the Mann-Whitney rank sum test. When required, a Kolmorogorov- Smirnov normality test was performed to verify the Gaussian distribution of a given parameter. Absolute values were compared with one-way ANOVA. Whenever one-way ANOVA detected a significant difference between mean values, all pairwise multiplecomparison procedures were performed (Holm-Sidak test). Differences between means were considered significant at $p < 0.05$.

PART II

In part II of the present study the animals (mean body weight: 374.3 ± 15.7 g, $n = 6$) were anaesthetised, paralyzed, mechanical ventilated and their chest wall was opened with the same procedures described in paragraph 3.1.

3.6 Measurement in vivo of the compliance of the lymphatic vessel wall

Once the diaphragmatic initial lymphatic network was visualized on the pleural diaphragm surface through a stereomicroscope (SV11 Carl Zeiss, Milan, Italy) equipped with a cooled B/W CCD camera (ORCA ER, Hamamatsu, Milan, Italy) and connected with a PC running SimplePCI software (Hamamatsu, Milan, Italy) to control all aspects of image acquisition and analysis, we proceeded in the measurements of the mechanical compliance of the lymphatic vessel wall *(*C_{wall}).

C_{wall} was measured *in vivo* and *in situ* in vessels identified on the pleural surface of the diaphragm. We preferred to investigate long and wide vessels (~ 200 μm diameter) where it was possible to simultaneously insert two micropipette tips in their lumen and we avoided lymphatic segments with detectable intraluminar valves. Leaving the vessel in place, two silk surgical threads (8/0 Viacryl) were secured around the vessel at a distance of ~2.5 mm; then the vessel segment was occluded at both ends to insulate the vessel segment from the remaining lymphatic network. Subsequently, two glass micropipettes were inserted in the segment lumen (Fig. 3.2): the first (tip diameter ~ 30 μm) was used to deliver multiple sequential injections of 2% lissamine green-coloured saline solution into the lymphatic segment lumen, while the second (tip diameter ~ 2-4 μm) was used to record intraluminal hydraulic lymphatic pressure (P_{lymph}) before, during and after sequential dye injections.

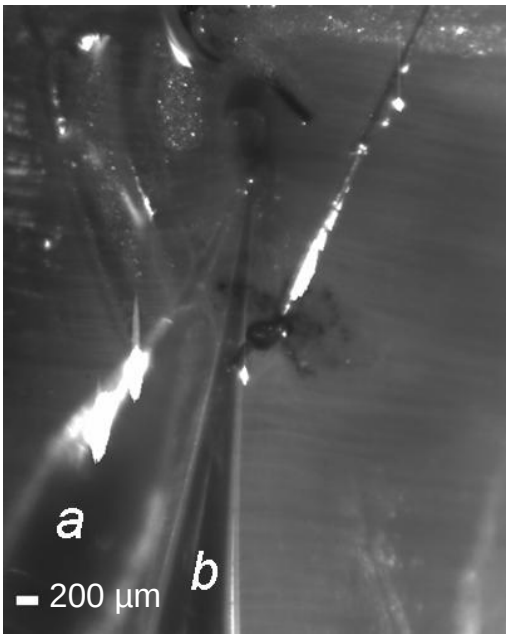

Fig. 3.2 Stereomicroscope image showing the insertion of the two micropipette into the lumen of a linear lymphatic segment. Pipette for P_{lymph} recording (a) and pipette for bolus injection (b) of 2% lissamine green-coloured saline solution.

The pressure measurement and injection system are the same already described in part I methods section. Multiple 4.6 nL dye boluses were injected in each lymphatic segment while simultaneously measuring P_{lymph} in proximity of the injection site. Generally, up to 30 sequential injections were performed in the same vessel. During the recording period (usually less than 5 minutes for each vessel), rats were temporarily disconnected from the ventilator and were oxygenated with a continuous intratracheal flux of 50% O_2 in nitrogen at a continuous positive airway pressure of 7 mmHg, in order to avoid artefactual oscillations of P_{lymph} due to the ventilator-induced inflation/deflation lung movements. Images of the injected segment vessel were acquired immediately before and at the end of each injection series. In the experiments in which extraluminal distribution of the dye during the injection occurred as a result of either an erroneous extraluminal positioning of the pipette tip or lymphatic wall damage due to insertion of the pipettes, the data were discarded. At the end of the experiments, the animals were suppressed with an intravenous anaesthesia overdose.

3.7 In vitro mechanical tests on diaphragmatic tissue strips

The *ex vivo* experiments and measurements on excised rat diaphragm tissue strips were performed in collaboration with the Laboratory of the Department of Structural Engineering, Politecnico of Milan.

Another group of rats (n = 7) were euthanized with an intraperitoneal overdose of the previously described anaesthetic cocktail (paragraph 3.1). The thorax was immediately opened through a wide mid-sternal thoracotomy to expose the whole diaphragm which was then excised by carefully micro-dissecting the tendineous fibres around the phrenic

centre and the muscular fibres along the external peripheral costal and vertebral margins. The pleural surface of the diaphragm was marked with a little thread knotted around the phrenic nerve-oesophagus-vena cava bundle. The excised diaphragm was first rinsed with saline solution and then maintained in 4°C PBS, then tissue strips were cut from fresh diaphragm within 2-3 hours from rat suppression. Four tissue strips (~ 8 mm long and ~ 3 mm wide, total strips = 28) were excised from different diaphragmatic regions, the strips were distinguished both for the diaphragmatic region of origin (ventral or dorsal) and the direction of excision (parallel or perpendicular) in respect to diaphragmatic fibres direction as schematically shown in figure 3.3:

1) the ventral emi-diaphragm, dissected in the direction parallel to diaphragmatic fibres axis
2) the ventral emi-diaphragm, dissected in the direction perpendicular to fibres axis
3) the dorsal emi-diaphragm, dissected in the direction parallel to diaphragmatic fibres axis
4) the dorsal emi-diaphragm, dissected in the direction perpendicular to fibres axis

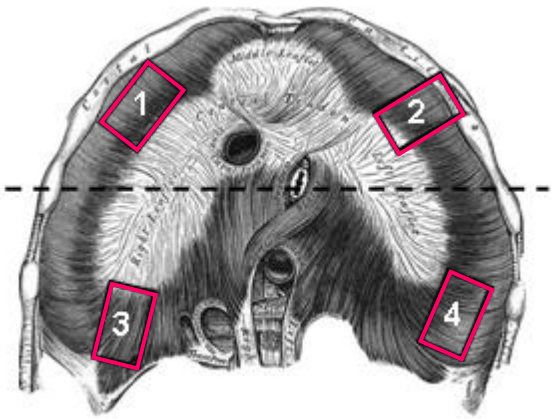

Fig. 3.3 Schematic image of the diaphragm with indicated the site of excision of the tissue strips: 1. ventral zone, trasversal to fibres axis; 2. ventral zone, longitudinal to fibres axis; 3. dorsal zone, longitudinal to fibres axis; 4. dorsal zone, trasversal to fibres axis.

The width and the thickness of each strip were measured with a calliper, then each sample was gripped at a testing machine (Fig. 3.4; Enduratec ELF3200, Bose Corporation, Eden Prairie, MN, USA, equipped with a load cell of 22 N) and underwent a series of tension tests.

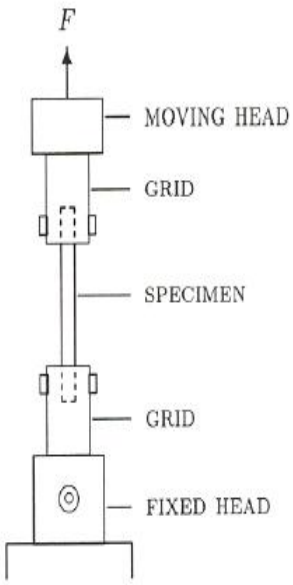

Fig. 3.4 Image of the apparatus used for tension test on diaphragmatic tissue strips. F indicated the force measured by the machine.

The length between the grips was measured by a calliper after imposing a preload of 0.05 N and defined as the initial sample length, and then 20 preconditioning cycles, up to 20% strain of their initial length, were imposed on tissue strips to stretch the fibres uniformly before starting the stress-relaxation cycles. Subsequently the specimens were exposed to increasing strain stress-relaxation test. Each relaxation test was performed by applying a fixed elongation corresponding to the desired strain and measuring the resulting force. The step-wise tension was defined as a series of 4 strain ramps, each 5% of the sample initial length, at a velocity of 10%/s, followed by stress relaxation to

equilibrium. After the last ramp, the samples were returned to the initial length and a constant velocity elongation of 10%/s was applied until specimen failure. The samples were immersed in physiologic solution during the test to avoid dehydration. From the stress-relaxation data we calculated the tissue elastic moduli *E* and the time relaxation constants (τ) for all the tested strain levels. *E* is the mathematical description of a material to be deformed elastically when a force is applied to it. The elastic modulus of an object is defined as the slope of its stress-strain curve in the elastic deformation region, and it is proper to each material. *E* was calculated as (Eq. 3.4):

$$E = \frac{\Delta\sigma}{\Delta\varepsilon} \qquad \textit{(Eq. 3.4)}$$

where $\Delta\sigma$ and $\Delta\varepsilon$ are variation of equilibrium stress and variation of strain between successive ramps, respectively. Stress (σ) is the force causing the deformation divided by the area to which the force is applied (measured in pascal) (Eq. 3.5):

$$\sigma = \frac{F}{A} = \frac{F}{\omega \cdot T} \qquad \textit{(Eq. 3.5)}$$

where F is the measured force returned by the machine, A is the specimen resistant area given by the product of specimen width (ω) times thickness (T).

The strain is the ratio of the change caused by the stress to the original state of the object (unitless), the units of *E* are pascals. Δε is the deformation related to the strain (Eq. 3.6):

$$\Delta\varepsilon = \frac{li - lo}{lo} \qquad \textit{(Eq. 3.6)}$$

where *lo* is the initial length of the tissue strip, *li* is the length *lo* after the stress imposition.

From the stress-strain curves we calculated the elastic modulus before failure ($E_{t,f}$), as slope of the linear portion of the curve before failure, the latter being the value of σ where the stress-strain curve bends before failure. In our experiments such linear portion ranged between 80% and 90% of the maximum stress. Calculation of stress, which is the ratio of the measured force by the resistant area, required the measurement of the specimen width and thickness. The width was measured by a calliper, whereas the thickness was measured, before the test sequence, by placing the sample between the machine grips and applying a small compressive load (5mN) in the direction of the sample thickness. The time relaxation constants (τ) were evaluated by fitting the relaxation curve to the following function (Eq. 3.7):

$$\frac{\sigma(\varepsilon_0,t)}{\sigma(\varepsilon_0,0)} = A_0 + A_1 \exp(-t/\tau_1) + A_2 \exp(-t/\tau_2) \qquad \textit{(Eq. 3.7)}$$

3.8 Statistical analysis

Data are presented as mean ± standard error of the mean (SE). Statistical significance of the differences between mean values was computed using Student's *t-test* provided the variance of the group was equal. In case of failure of the equal variance test, the differences were tested through the Mann –Whitney rank sum test. When required, a Kolmorogorov-Smirnov normality test was performed to verify the Gaussian distribution of a given parameter. Absolute values were compared by one–way ANOVA. Whenever one way ANOVA detected a significant difference between mean values, all pairwise multiple comparison procedures were performed (Holm-Sidak-test). Differences between means were considered significant at $p < 0.05$.

PART III

3.9 The kinetics of fluid flux

Lymph formation and progression in initial lymphatics toward deeper collecting ducts depends upon transmural pressure gradients (ΔP_{TM}) developing between the interstitial space and the lymphatic lumen. This is a very complex and not completely unveiled mechanism; therefore, we studied the fluid flux kinetics to clarify the function of the lymphatic network organization.

In part III of the study the animals (mean body weight: 294.37 ± 24.08g) were anaesthetised, paralyzed, mechanical ventilated and the chest wall was opened with the same procedures described in paragraph 3.1.

3.9.1 Recording of interstitial and intraluminal lymphatic pressures

We visualized the diaphragmatic initial lymphatic network on the pleural diaphragm surface through a stereomicroscope (SV11 Carl Zeiss, Milan, Italy) equipped with a cooled B/W CCD camera (ORCA ER, Hamamatsu, Milan, Italy) and connected with a PC running SimplePCI software (Hamamatsu, Milan, Italy) to image acquisition and analysis. Then we proceded with the pressures measurements: the pressures in the lymphatic vessel lumen (P_{lymph}) and in the adjacent interstitial space (P_{int}) were measured with the use of the micropuncture technique. Pressure recordings were obtained through glass micropipettes bevelled down to 2-4 µm tip diameter, filled with 1M NaCl solution, and secured to a pipette holder filled with the same solution. The pipette holder was connected to a mineral oil-filled pressure transducer (Gould

Instruments System, Inc), motor driven by an electrohydraulic system (Dual Servonull Pressure-Measuring System, Vista Electronics, Ramona, CA, USA). The pressure signal was relayed to an amplifier and a signal conditioner (model 6600, Gould Electronics), digitized with an analogue-to-digital board, and displayed on the monitor using dedicated LabView software (National Instruments) (Fig. 3.5). Prior to its use, each micropipette was calibrated in a modified Lucite box and mounted in two three-dimensional hydraulic micromanipulators; the electrical zeroing of the recording system and the criteria for acceptance of the micropipette pressure recordings were described in part I. All phases of pipette positioning and pressures measurements were recorded to calculate the net transmural pressure gradient as $\Delta P_{TM} = P_{lymph} - P_{int}$ for each micropuncture point.

3.9.2 Lymph flow and lymph direction in the lymphatic vessel

The same diaphragmatic initial lymphatic network visualized previously on the pleural diaphragm surface was used to study the direction of lymph flux. Glass micropipette (tip diameter ~ 30 μm) for microinjection, pulled with a vertical puller (PP30, Narishige, Tokyo, Japan) from borosilicate glass capillary (WPI Europe, Berlin, Germany, 1B100-4, 1.0 mm OD, 0.58 mm ID), was filled with mineral oil and mounted onto a mechanical microinjector (WPI Europe, Berlin, Germany); then, under the stereomicroscope, the tip of micropipette was front-filled with 1 μl of FITC-dextran conjugate, longitudinally aligned over the lymphatic vessel with the lowest possible angle with respect to the diaphragmatic surface and gently advanced through mesothelium until it was clearly inside the lymphatic vessel lumen. Injections of 4.6-nl volume were then triggered, and the pipette tip was immediately withdrawn from the

vessel. The phases of pipette positioning, fluorescent dye injection, and distribution of the dye into the lymphatic vessel lumen were recorded by the stereomicroscope which was equipped with a cooled black-and-white charge-couple device camera (ORCA ER, Hamamatsu, Milan, Italy) connected with a personal computer running SimplePCI software (Hamamatsu) (Fig. 3.5).

Injected FITC-dextran conjugate was excited with an optic fiber epi-illuminator equipped with a 425 ± 65 nm bandpass filter (Carl Zeiss Italy). Fluorescence emission was collected by the stereomicroscope fitted with a two-bandpass filter (FITC/TRITC, catalog no. 56918, Chroma Technology, Rockingham, VT). Images were collected both in real time, to better follow the time course of the injection, and in time lapse (interframe interval: 10–30 s) a few minutes after the injection. The exposure time was routinely set to 1 s to allow the detection of the faintest fluorescence signals without a significant increase in background noise. Images were directly stored in the hard disk of the computer and subsequently analyzed offline. Typical recordings of a single-vessel injection lasted ~20 min. To obtain the most clear and still images of lymphatic vessels during time-lapse recording, the diaphragmatic movements were arrested for 2–3 s by occluding the inspiratory line of the mechanical ventilator during image exposure and immediately reopening the inspiratory line after image acquisition during the recording.

The data of the experiments in which extraluminal distribution of the dye during the injection occurs as a result of either an erroneous extraluminal positioning of the pipette tip or lymphatic wall damage due to insertion of the pipettes were discarded. At the end of the experiments, the animals were suppressed with an intravenous anaesthesia overdose.

Direct measurements of the fluorescence progression velocity were performed on original images. Vessel thickness, flow velocity (v) and lymph flow ($\dot{V}_{lymph}$) was detected as described in paragraph 3.2 and 3.4.

With the flow information and the interstitial and intraluminal lymphatic pressures, we developed a mathematical model in order to describe the lymph mechanism of formation and progression. We analyzed all lymphatic networks and used acquired data to feed the model and to derive the most significant parameters affecting lymph flow.

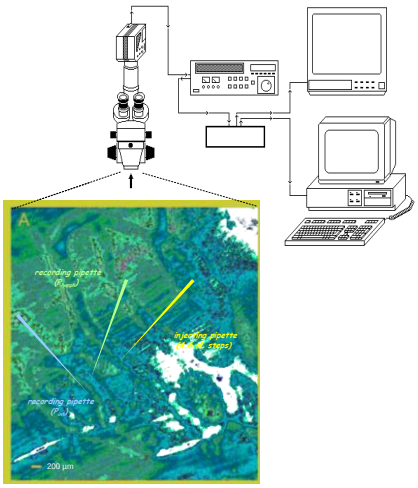

Fig. 3.5 Experimental set-up.

PART IV

3.10 Visualization of muscular fibers around lymphatic vessels

3.10.1 Samples collection

In part IV of the study 5 healthy adult Wistar rats (mean body weight: 284.00 ± 16.35g) were anaesthetised and tracheotomised and 1ml of 2% FITC-dextran (FD 250S – Sigma

Aldrich) solution with 10% of 0.1 µm diameter green fluo-spheres (FluoSpheres carboxylate-modified microspheres, 0.1µm, yellow-green fluorescent (505/515), Invitrogen) was injected intraperitoneally through a little cannula. Then the animal was placed prone over a warmed (37°C) blanket to maintain the body temperature for 30 minutes. After 30 minutes the animal was connected to a mechanical ventilator, turned supine, and the chest wall was opened with the same procedures described in paragraph 3.1. The pleural diaphragmatic initial lymphatic network was visualized by stereomicroscopy to verify that the fluorescent solution arrived in lymphatics of the pleural side. Then the animal was euthanized via an anaesthesia overdose, and the specimens with the dye into the lymphatic vessel lumen were isolated and fixed in 4% paraformaldehyde in PBS for 30 minutes at room temperature for indirect immunofluorescence analysis. All these phases were conducted in the darkness to better visualize the fluorescent signals and to prevent bleaching of the dye.

3.10.2 Immunostaining

After fixation with paraformaldehyde, each sample was washed three times with PBS for 5 minutes. Pretreatment with cold (-20°C) methanol 100% for 5 minutes resulted in considerably enhanced immunofluorescence. The tissue specimens were then permeabilized by incubation in 0.5% TRITON-X100 in PBS at room temperature (RT) three times for 5 minutes each. Samples were incubated with blocking solution (1% BSA (bovine serum albumin) and 5% goat serum in PBS) for 1 hour at RT to block unspecific binding of the antibodies, then they were cut into two pieces.

One section was incubated with primary antibody mouse anti SMC actin (Actin Alpha 2 Smooth Muscle Antibody (1A4) – Novus Biologicals; 1:25 dilution), in blocking

solution and stored at 4°C overnight. The second section was treated for the same amount of time with blocking solution and used as a negative control. Both sections were rinsed three times for 10 minutes each in PBS, followed by an incubation with the secondary antibody, goat anti-mouse antibody conjugated to Alexa Fluor 647 (goat anti-mouse IgG2a – Molecular Probes, Carlsbad, CA; 1:100 dilution) for 1 hour at RT. The tissues were finally washed with PBS, three times for 10 minutes. Then the samples where mounted on a coverslip with a drop of mounting medium (citifluor, citifluor Ltd., London UK) with the pleural side up. The stained vessels were confocally scanned throughout the entire vessel diameter in 0.5 μm z-axis steps with a Leica SP-5 confocal miscroscope, collecting images separately. Vessels were imaged with a 20X objective (dry) and a pinhole value matched to 1 Airy Unit. An image reconstruction of the image stacks was performed using the Leica Confocal Software package. The negative controls for the experiments were produced and analyzed via identical procedures, except that the control samples were incubated with no primary antibody. For the experiment aorta specimens were used as positive controls and they were produced and analyzed with the same procedures. The corresponding negative and positive controls were scanned at the same instrument settings as the unknowns for a valid comparison of relative fluorescence intensities.

3.10.3 Data analysis

The analysis of confocal images was performed using Image J and Adobe Photoshop software. The pleural lymphatic network overview was obtained *in silico* by capturing a large amount of consecutive image tiles and aligning them into a continuous panorama using Adobe Photoshop software. 3D reconstruction of the lymphatic vessel was

performed using VolumeJ plugin of Image J software, with cine-mode renderer and a complete rotation around the y axis of each single channel z-stack separately. Finally the cross section of the lymphatic vessel was obtained using Reslice function of Image J software on the merged z-stack.

4 Results

4.1 PART I

By using semi-tangential epi-illumination it has been possible to investigate the pleural diaphragmatic surface in order to distinguish lymphatic vessels from the surrounding tissue, blood vessels, and nerves, because lymphatics are characterized by a darker-than-surrounding lumen lined by whitish translucent borders (Fig. 4.1A and 4.1B). Moreover these vessels could be grouped into two populations: one ran in a more or less tortuous, but approximately linear way (Fig. 4.1A), while the second population comprised vessels organized into singular loops or series of loops (Fig. 4.1B). Short ducts often sprouted from linear vessels. These branches were placed in parallel or in series with each other; while singular loops had one to four ducts connecting them to another loop or linear vessel. The presence of interconnected linear vessels and loops creates a very complex network whose physiological properties are difficult to study.

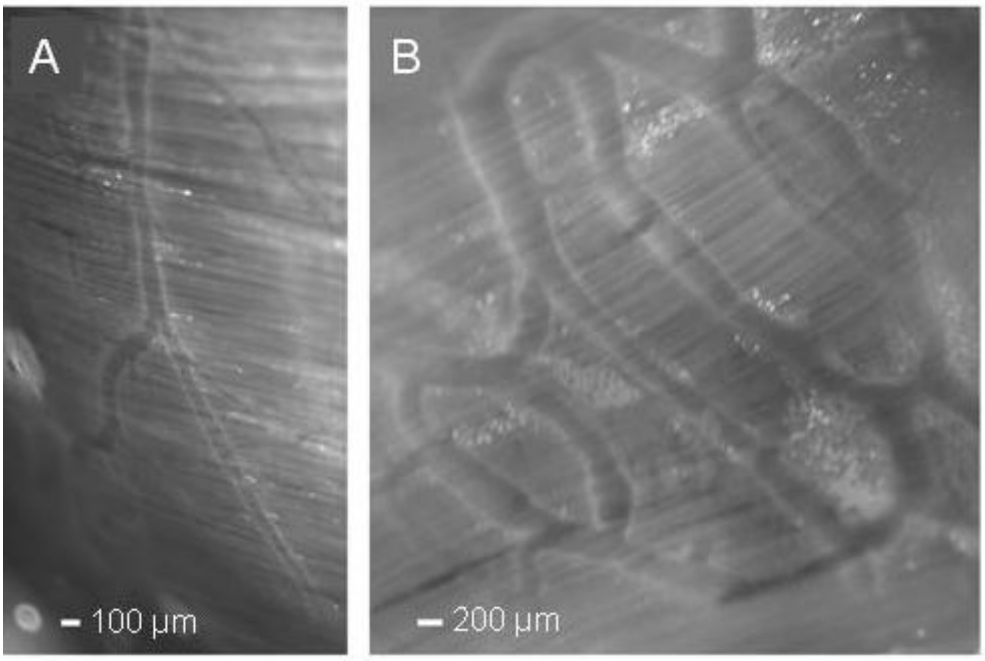

Fig. 4.1 A and B Stereomicroscope images of lymphatic vessels under white light epi-illumination. Lymphatic vessels appeared transparent over a dark background (diaphragm) delimited by white borders. Moreover, under the lymphatics diaphragmatic muscular fibers run almost perpendiculary with respect to lymphatic vessels. A: Principal and linear vessel branched in smaller lymphatics,. B: Lymphatic loop on the pleural surface of the diaphragm under white light epi-illumination. From a single linear vessel the loop branched into shorter ducts placed in parallel and in series with each other.

A great length variability has been found: linear vessels were significantly longer (8106.5 ± 3137.7µm, n = 18) than loops (2492.9 ± 1954µm, n = 21, $p < 0.05$) as shown in Tab. 4.1.

Moreover, the two vessel populations are localized in different diaphragmatic regions: loops were preferentially located in the peripheral ventrolateral regions of the diaphragm, whereas linear lymphatics were dispersed over the whole surface, apparently connecting different regions (Fig. 3.3). Loops in the medial tendineous portion of the diaphragm were never detected.

Lymphatic vessels		
	LINEAR	LOOP
Length (μm)	8106.5 ± 3137.7 *	2492.9 ± 1954
Diameter (μm)	103.4 ± 8.5 **	54.6 ± 3.3
Thickness (μm)	48.8 ± 4.7	
Mean velocity (μm/s)	26.3 ± 1.4 **	51.3 ± 3.2
Mean lymph flow (nl/min)	10.6 ± 3.2	6.9 ± 1.1
Distance between 2 valves (μm)	966.9 ± 128.8	840.5 ± 194.8

Table. 4.1 Student's t-test values: * $p < 0.05$, ** $p < 0.01$ linear with respect to loops.

Diameters of the two populations of lymphatic vessels were normally distributed and significantly greater in linear vessels (103.4 ± 8.5 µm, n = 18, range: 54.6 to 170.5 µm) than in loops (54.6 ± 3.3 µm, n = 21, range: 38.3 to 98.1 µm) ($p < 0.01$), which also appeared to be more uniform in size.

There weren't differences in post-injection thickness, in the lymphatic vessels used for the evaluation of vessel thickness, between linear vessels and loops (average 48.8 ± 4.7 µm, n = 16). However, as it is possible to see in figure 4.1C, the injection locally deformed the vessels and the ratio between pre and post-injection diameter was 0.7 ± 0.05. Assuming the same ratio in thickness, the average pre-injection would be 36.1 ± 6 µm.

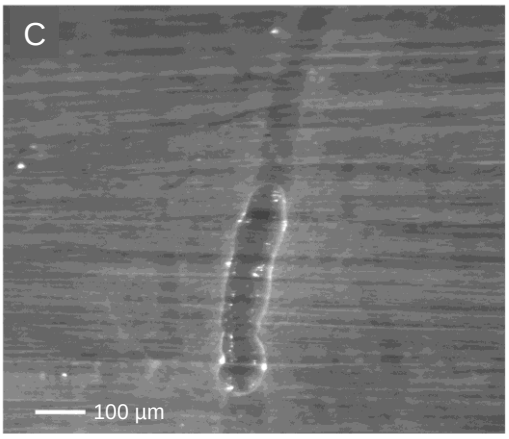

Fig. 4.1 C Mineral oil of a known volume injected in a linear lymphatic lumen through a micropipette, allowing the derivation of vessel thickness.

Flow velocity was computed by dividing the distance travelled by the fluorescence front along the path of the lymphatic vessel (Fig. 4.2A and 4.2B) by the interpicture time interval.

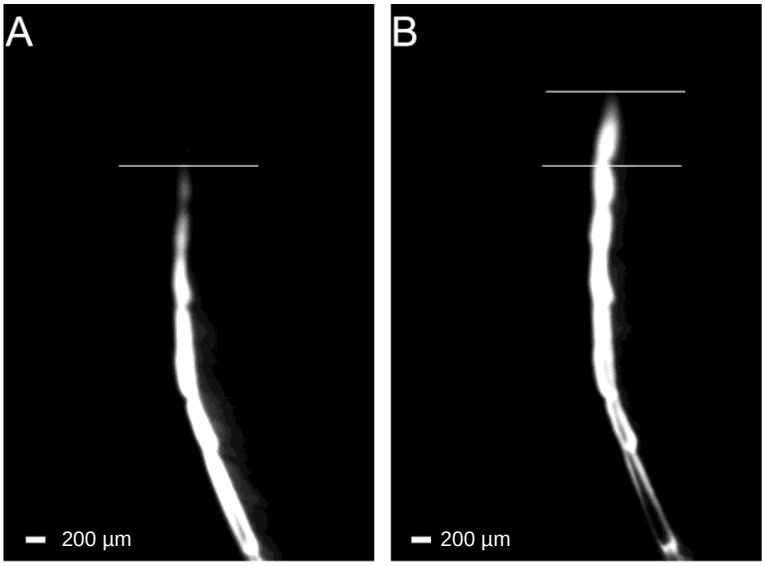

Fig. 4.2 A and B Stereomicroscope images of a linear vessel after a FITC-dextran injection. In the frame shown in figure 2B, which was taken 28.2 s after the frame shown in figure 2A, the fluorescent dye front, detected by the thin horizontal line against the black background, progressed by 627.3 µm at a velocity of 22.2 µm/sec, which was calculated by dividing the distance traveled by the dye within the vessel along the path of the vessel by the time interval.

To calculate the intraluminal flow velocity the spreading velocity of the fluorescent dye within the vessel was used. Before using this parameter, it has been verified that the FITC-dextran freely moves within the vessel without escaping from the wall, and that this dextran has density and properties similar to the lymph. Testing the fluorescent behaviour, thirty minutes after FITC-dextran injection (longer than our longest recording time of ~ 22 min) the fluorescence signal was confined in the lumen and it did not leak out of the vessel even after image processing to amplify the fluorescent signal (Fig. 4.3 and inset).

Fig. 4.3 and inset Stereomicroscope images of FITC-dextrans at 30 min from the injection in a linear lumen vessel. The fluorescence invaded the vessel and its smaller collaterals (inset) without going out from the lumen.

Through the micro-injection techniques, it has been possible to observe the P_{lymph} behaviour after the fluorescent injection: immediately after the injection, P_{lymph} recorded in proximity to the injection pipette tip increased from a baseline value of 1.5 ± 0.4 mmHg to 5.6 ± 2.8 mmHg (n = 7), then it decayed to baseline value with a time course well fitted by a double-exponential decay with a fast time constant of 151 ± 12.3 ms and a slow time constant of 7.4 ± 1.2 s (Fig. 4.4).

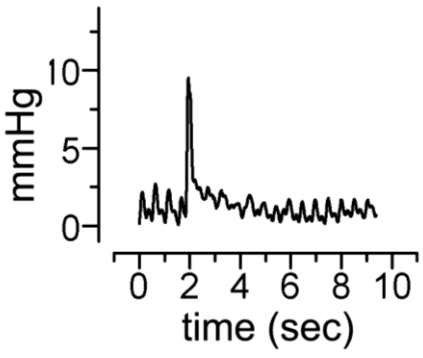

Fig. 4.4 Intraluminal P_{lymph} in mmHg before and after the injection of a singular FITC-dextran bolus. The pressure raised from the control value to a maximum value and then dropped quickly to control values. It is possible to see the cardiogenic oscillations, like a smaller track, as a results of the cardiac contraction.

The mean and median velocity distribution of the dye were 81.7 ± 28.9 µm/s (n = 18) and 20.9 µm/s (range: 2.9 to 346.6 µm/s) in linear vessels, and 83.2 ± 16.4 µm/s (n = 21) and 62.5 µm/s (range: 5.4 to 303.2 µm/s) in loops, respectively, as shown in table 4.2.

Lymphatic vessels		
	LINEAR	LOOP
Mean (µm/s)	81.7 ± 28.9	83.2 ± 16.4
Median (µm/s)	20.9 (2.9 to 346.6 µm/s)	62.5 (5.4 to 303.2 µm/s)

Table. 4.2 Mean and median of the fluorescence velocity distribution in linear and loop vessels.

However, the frequency distribution of flow velocities was asymmetrical, significantly departing from normality in both linear vessels ($p < 0.01$) and loops ($p < 0.05$). Therefore, to statistically compare the two data distributions, the original flow velocity values were first transformed into their corresponding base 10 logarithms ($\log_{10}$) and then transformed back to obtain the geometrical means of the two populations, calculated as the antilogarithm of the mean of the $\log_{10}$ distributions. The mean $\log_{10}$ velocity was respectively 1.4 ± 0.2 µm/s in linear vessels and 1.7 ± 0.1 µm/s in loops. When transformed back, the geometric means of the original velocity distributions were significantly lower ($p < 0.01$) in linear vessels (26.3 ± 1.4 µm/s) than in loops (51.3 ± 3.2 µm/s). It was moreover observed that, when plotted as a function of the corresponding vessel diameter, flow velocity data were quite dispersed (Fig. 4.5), although they tended to exponentially decrease with increasing diameter in both linear

vessels (solid circles; $v = 8630.3^{-0.058d}$, $n = 18$, $r^2 = 0.60$, $p < 0.01$) and loops (open circles, $v = 1526.4^{0.059d}$, $n = 21$, $r^2 = 0.43$, $p < 0.01$).

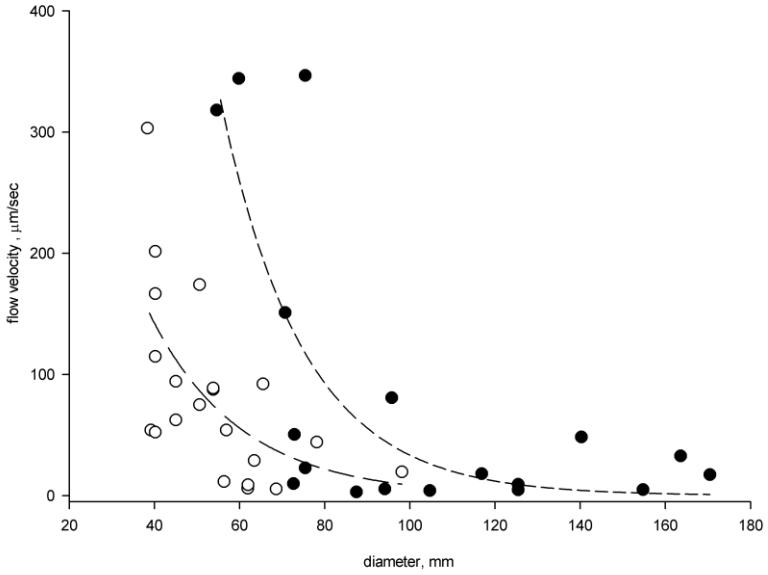

Fig. 4.5 Flow velocity (*v*) plotted as a function of the vessels diameter in linear vessels (•) and lymphatic loops (◦). The two populations did not differ significantly when transformed into the corresponding $\log_{10}$ vs diameter linear regressions.

To test whether the two populations might differ, despite the data variability, the original flow velocity values were transformed into the corresponding $\log_{10}$ flow velocity values and plotted against vessel diameter. The regression lines fitted through the linear vessel ($\log_{10} v = 2.3 - 0.084 \cdot d$, $n = 18$, $r^2 = 0.18$) and loop ($\log_{10} v = 2.4 - 0.0115 \cdot d$, $n = 21$, $r^2 = 0.15$) data points were significant, with no differences in either slope or elevation. The decay rate of flow velocity plotted as a function of the corresponding vessel cross-sectional area, calculated as $S = \pi \cdot (d/2) \cdot (t/2)$, was described by a translated hyperbola of the following type: $y(x + b) = a \cdot b$ (Fig. 4.6), in both linear vessels ($a = -65.6$, $b = -242.6$, $r^2 = 0.56$, $t = 5.9$, $n = 18$, $p < 0.001$) and loops

(a =-37.8, b = -168.1, r^2 = 0.42, t = 3.9, n = 21, p < 0.001). Although the higher variability, a hyperbolic decay seemed adequate to fit the data even when the data were pooled (a = -368.9, b = -60.9, r^2 = -0.19, t = 2.8, n = 39, p < 0.01).

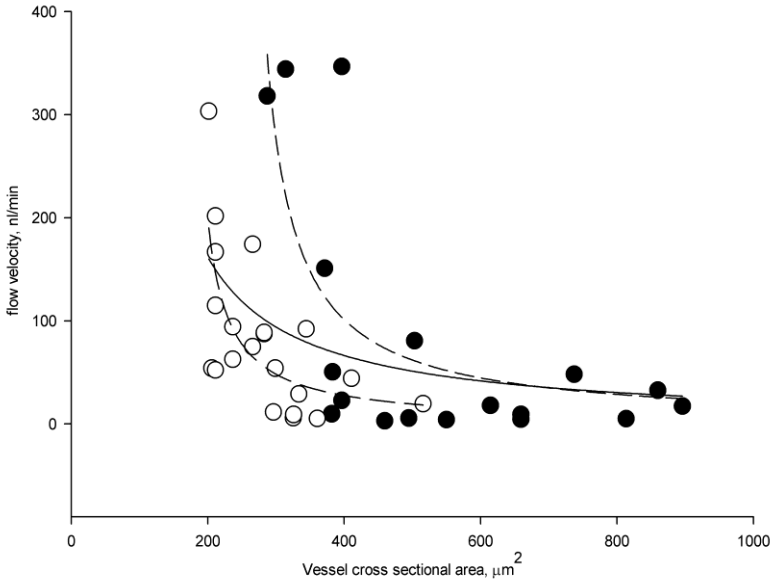

Fig. 4.6 Flow velocity plotted as a function of the vessel cross-sectional area in linear vessels (•) and in loops (◦). The two data populations and all data (solid line) were fitted by a translated hyperbole: $y(x + b) = a \cdot b$.

Lymph flow was calculated as the product of lymph flow velocity multiplied by cross-sectional area (Eq. 3.1), and was not significantly different in linear lymphatic vessels (10.6 ± 3.2 nl/min, n = 18) and single vessels belonging to complex loops (6.9 ± 1.1 nl/min, n = 21), with an average lymph flow value $\dot{V}_{lymph}$ = 8.6 ± 1.6 nl/min (n = 39). During the experiments the position of intraluminal valves was searched through white light epi-illumination of the diaphragmatic surface, but the presence and positioning of unidirectional valves were not easily detectable (Fig. 4.1A and B). However, the progression of the injected fluorescent dye bolus into a vessel was sometimes impeded by a closed intraluminal valve which obstructed the lumen, causing the accumulation of FITC-dextran at the site of the obstruction and indirectly revealing the presence of the

valve itself (Fig. 4.7). In other cases, the valve was seen as a vessel constriction brighter than the vessel wall. At time of injection, a faint profile of the convolute vessel was left after the fast initial distribution of the dye (Fig. 4.7A). As shown in Fig. 4.7A and inset at a greater magnification, vessel dilation on the right of the small inlet vessel (arrow) suggested the presence of a unidirectional valve closed by fluid backflow. Similarly, the accumulation of the dye shown in Fig. 4.7C (arrow) suggested the presence of another valve, which was at first closed and then opened, allowing further fluid progression into the vessel (Fig. 4.7, C–E).

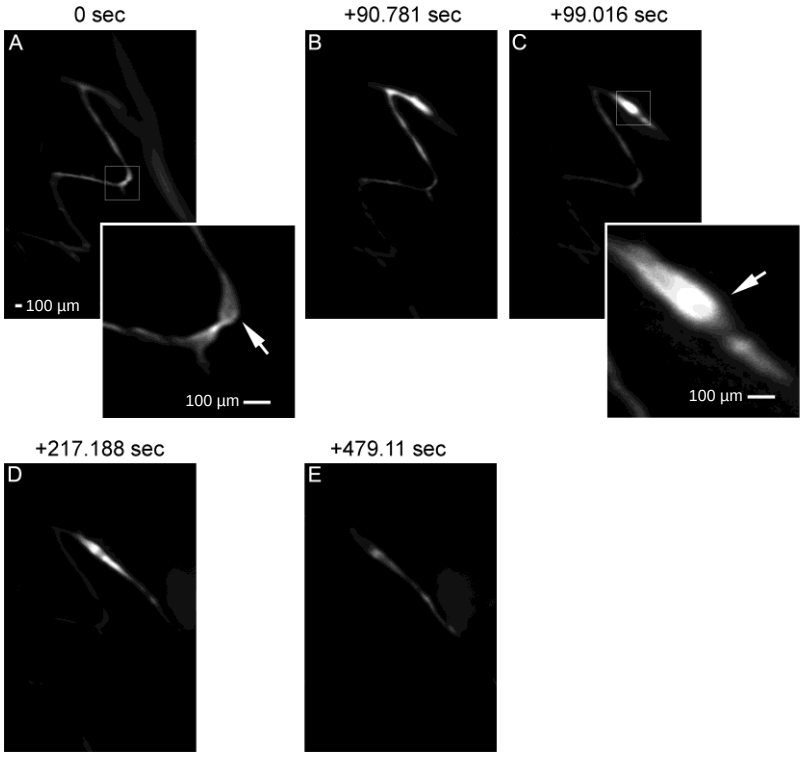

Fig. 4.7 A-E Stereomicroscope image sequence acquired after the fluorescence injection in a linear but tortuous vessel. In the top of the panels is shown the time elapsed between two consecutive frames. FITC-dextran was injected in the left side of the each image, the dye progressed towards right and through the valves (arrows) visible in inset A and C.

Intraluminal valves in linear vessels and also in loops (Fig. 4.8) seemed to control both flow direction and recirculation of fluid within the loop. As shown in figure 4.8, the dye

passed through a first valve (detectable in Fig. 4.8C), and the dye oscillated back and forth for ~ 4 min before being squeezed forward, filling the loop counter clockwise (Fig. 4.8F). In this example of lymph progression in a loop, dye passage was obstructed by a closed valve (Fig. 4.8G) and favoured in the counter clockwise direction (Fig. 4.8H and I). Moreover, distances between any two detectable intraluminal valves were similar in linear vessels (966.9 ± 128.8 µm, n = 25) and loops (840.5 ± 194.8 µm, n = 17). Differently, the geometric mean velocity of the dye in the segments with valves averaged 18.5 ± 1.05 µm/s (n = 6), which was significantly slower if compared with both linear vessels and loops ($p < 0.05$ by ANOVA) with no apparent valves. Therefore it seems that valves control the direction of lymph progression and slow down the velocity of the dye.

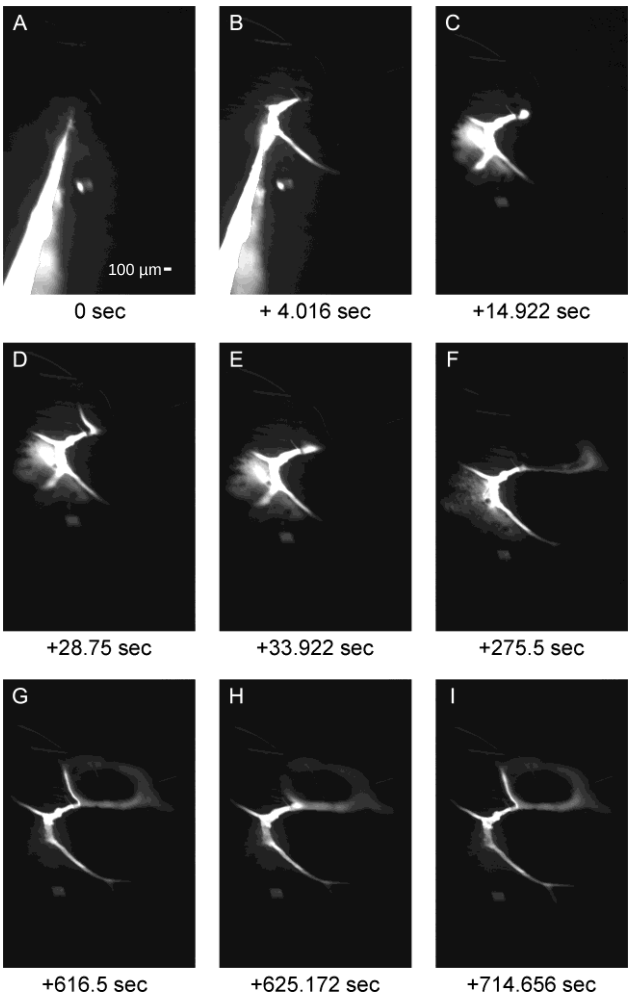

Fig. 4.8 A-I Stereomicroscope image sequence after fluorescence injection in a lymphatic loop. In bottom left of the panel A and B it is visible the microinjection pipette which was then withdrawn Initially, the dye filled a small segment of the vessel (B), then it oscillated back and forth without entering the loop because it was occluded by a closed valve (C-E). 4 minutes after the injection (F), the valve opened and the dye flowed counter clockwise through the loop (H and I).

4.2 PART II

4.2.1 Compliance of submesothelial lymphatics

In the *in vivo* experiments the pre-injection diameter (d_0) was 255 ± 13.5 µm and the length (l_0) between two occluding threads of the submesothelial lymphatic segments was 2516.9 ± 345.7 µm. Evidences from Part I revealed that the cross sectional area of

diaphragmatic superficial lymphatics was elliptical rather than cylindrical, the smaller radius in the plane perpendicular to the pleural surface ($r_{min\text{-}0}$) being ~ 35% of the larger radius in the plane parallel to the pleural surface ($r_{max\text{-}0}$). So for $r_{min\text{-}0} = 0.35\ r_{max\text{-}0}$ the pre-injection segment volume (V_0) was calculated as $V_0 = \pi \cdot r_{max\text{-}0} \cdot r_{min\text{-}0} \cdot l_0$, averaged 44.2 ± 11.1 nL. Therefore, each injected bolus amounted to ~ 10 % of V_0.

In figure 4.9 pre-injection P_{lymph} values (at t = 0) and P_{lymph} values during sequential injections of 4.6 nL lissamine-green saline boluses are shown. Each trace refers to a single experiment with injections in the same lymphatic network. A great variability of P_{lymph} values and response within the same lymphatic network was seen: pre-injection P_{lymph} was very variable among lymphatics, ranging from -6.5 to 5.5 mmHg (average value = 1.5 ± 1.6 mmHg). Moreover each P_{lymph} trace was characterized by regular pressure swings (amplitude ~ 1 mmHg), reflecting cardiogenic displacements of the diaphragmatic tissue. Each injection was followed by a pressure increase ($\Delta P_{lymph\text{-}peak}$) until attainment of a transient peak ($P_{lymph\text{-}peak}$) value, followed by a slower decay towards a post-injection plateau. The increase ($\Delta P_{lymph\text{-}peak}$) and the following P_{lymph} decrease with a quasi-exponential decay rate reflect a “stress relaxation” phenomenon, typical of elastic structures.

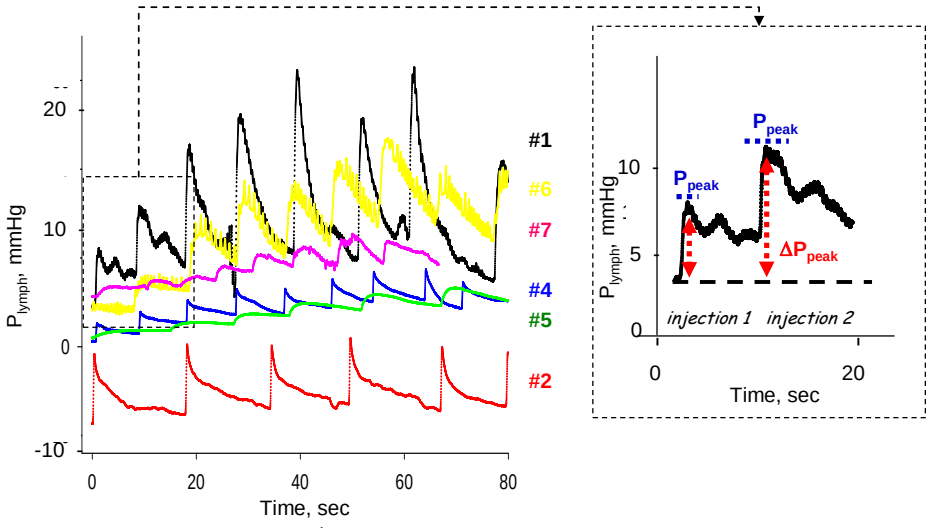

Fig. 4.9 and inset Lymphatic pressure (P_{lymph}) traces of different experiments during 4.6 nL sequential injections of lissamine-green saline solution. Detail of one P_{lymph} track after two sequential injections (inset): P_{lymph} increased quickly after the injection (ΔP_{peak}) and then decayed to a slower P_{lymph} with a typical exponential kinetic.

Through bolus injection technique, in one lymphatic it was possible to see the effect of the opening of an intraluminal valve on P_{lymph}: when P_{lymph} reached a value of about 6-7 mmHg during sequential injections, it suddenly dropped to the baseline pre-injection value (Fig. 4.10), suggesting the opening of the intraluminal valve.

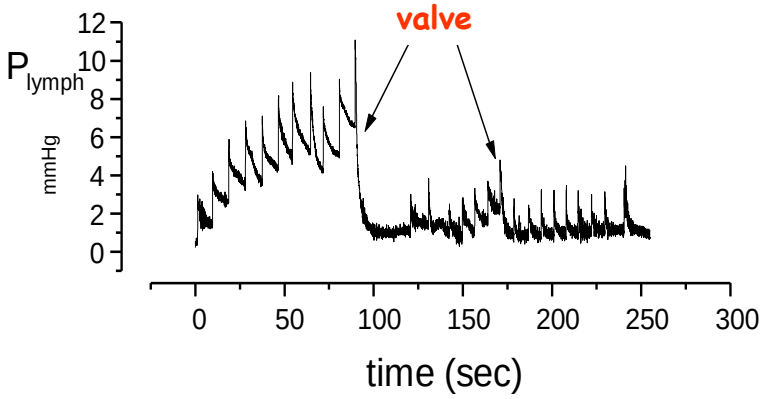

Fig. 4.10 P_{lymph} during sequential lumen injections. The opening of an intraluminal valve is suggested by the drop of P_{lymph} to the baseline pre-injection value.

Pooling all data, P_{lymph} decay rate following $P_{lymph\text{-}peak}$ attainment in response to a single injection was filled by an exponential function (mean time constant τ = 3.2 ± 0.4 sec, range 2.6 to 4.3 sec, n = 54), which was independent upon initial vessel volume, pre-injection P_{lymph} or $P_{lymph\text{-}peak}$. Through the pressure volume behaviour, it was possible to calculate the compliance of the submesothelial lymphatic (C_{lymph}) as the slope of the relationship obtained by plotting the cumulative injected volume ($V_{injected}$) as a function of the corresponding $P_{lymph\text{-}peak}$ (Fig. 4.11). Within each experimental set, only data relative to the first few injections were fitted through a statistically significant linear relationship. They describe a highly significant linear regression (elastic behaviour), while at higher cumulative injected volumes $P_{lymph\text{-}peak}$ tended to remain unchanged, vessel wall behaviour is very variable and not reproducible among vessel (plastic behaviour).

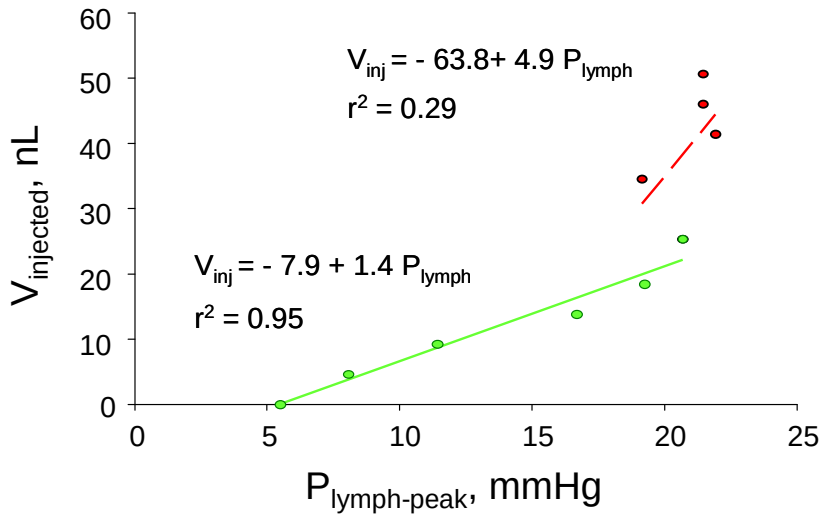

Fig. 4.11 Example of the relationship between sequential injections ($V_{injected}$) of 4.6 nL of lissamine-green saline solution and P_{peak} after each injection in a single vessel (the slope value represents the mechanical vessel compliance). At low volumes data described a significant linear regression (°), while at higher volumes (°) P_{peak} was unchanged suggesting fluid leakage through vessels in excessive mechanical stress condition.

Therefore, the analysis was limited to the linear phase of the $V_{injected}$ vs $P_{lymph\text{-}peak}$ plots attained at a volume increase not larger that 50 nL. When $V_{injected}$ was plotted as a function of $P_{lymph\text{-}peak}$ to account for the physiological variability of individual pre-injection P_{lymph}, all data were distributed in two populations (Fig. 4.12), characterized by a significantly different C_{lymph} ($p<0.001$) (Fig. 4.13) amounting to 6.7 ± 1.6 nL/mmHg (high-C_{lymph} population, H-C_{lymph}, t-student of the slope, $t_b = 3.9$, $n = 18$, $p<0.001$) and 1.5 ± 0.4 nl/mmHg (low-C_{lymph} population, L-C_{lymph}, $t_b = 4.2$, $n = 28$, $p<0.001$), while the dimensions of the vessel segments of the H-C_{lymph} data set ($r_{max\text{-}0}$ 121 ± 13 µm, l_0 = 2542 ± 446 µm; V_0 = 44.6 ± 15.6 nL) were similar to those of the L-C_{lymph} set ($r_{max\text{-}0}$ 130 ± 32 µm, l_0 = 2219 ± 693 µm; V_0 = 430007 ± 19.1 nL). Normalizing $V_{injected}$ by the individual V_0 and then plotting the normalized values as a function of $P_{lymph\text{-}peak}$, data still described two distinct populations with C_{lymph} amounting to 0.15 ± 0.041 $mmHg^{-1}$ (H-C_{lymph}, t-student of the slope, $t_b = 3.8$, $n = 18$, $p<0.01$) and 0.027 ± 0.009 $mmHg^{-1}$ (L-C_{lymph}, $t_b = 3.1$, $n = 28$, $p<0.01$). The H-C_{lymp}h and L-C_{lymph} populations were not distinguishable on the basis of their orientation over the diaphragmatic surface, because all vessels investigated were perpendicular to the underlying diaphragmatic muscular fibres. Since the compliance between the two populations of lymphatics does not depend on the vessels morphological characteristics (radius, length and volume before injections were similar), the mechanical characteristics of tissue surrounding the initial lymphatics vessels were investigated. Moreover, knowing that lymphatics run longitudinally and transversally to fibres axis and both in the dorsal zone and ventral zone, tissue strips were cut along different fibres directions and in different diaphragmatic regions.

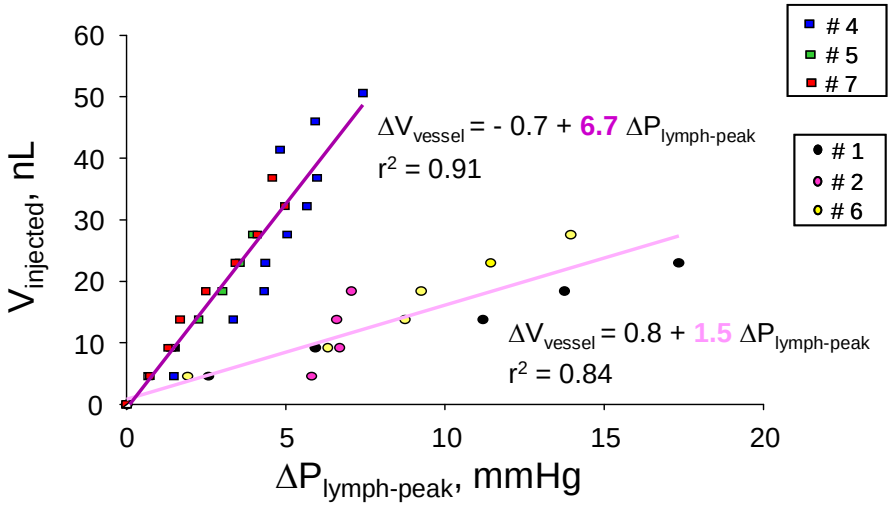

Fig. 4.12 All data from all lymphatic segments (different symbols) were plotted: V_{inj} is plotted as a function of ΔP_{peak}. Different colors identify data of different vessels. Data are distributed in two populations described by linear regressions with two compliance significantly different ($p < 0.05$): respectively high-compliance 6.7 nL/mmHg and low-compliance 1.5 nL/mmHg.

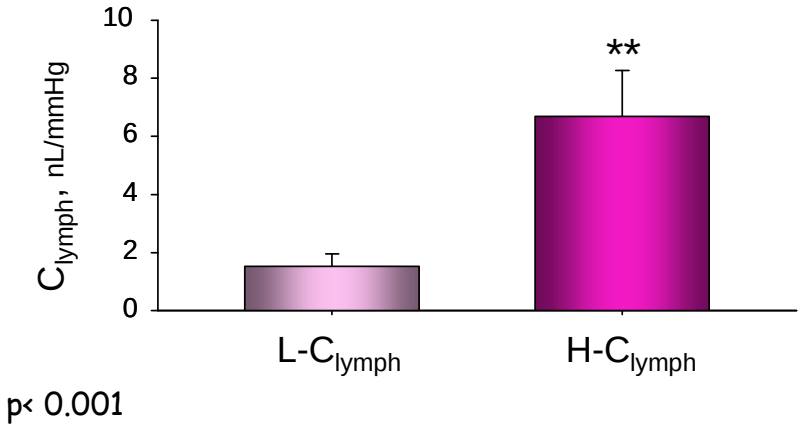

Fig. 4.13 Histogram showing the compliance values of the two populations, low compliance (L-Clymph) and high compliance (H-Clymph). Student's t-test values: ** significantly different ($p < 0.001$) from L-Clymph.

4.2.2 Diaphragmatic tissue elastic module

Coming from different rats and from different zones of the same diaphragm, diaphragmatic samples were not homogeneous. Therefore, to have similar initial conditions, the samples were exposed to 20 preconditioning cycles up to 20% strain (Fig. 4.14).

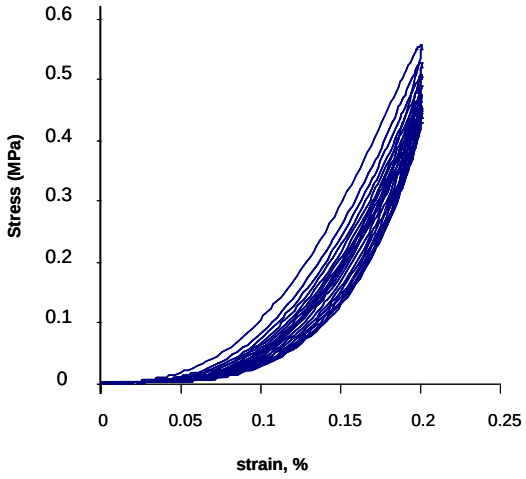

Fig. 4.14 Example of pre-conditioning curves (stress-strain) after the 20% elongation of the initial strips length.

Through the stress relaxation curves following stretch the diaphragmatic tissue elastic module (E_t), the stress (σ), the strain (ε) and the time relaxation constant (τ) were calculated (Fig. 4.15). The stress increased when the strain ramp was applied until attainment of the strain peak, then the tissue relaxed while the stress decreased to an equilibrium value during the constant strain phase. This behaviour reflects the P_{lymph} curves seen previously in the *in vivo* results, although the time scale was very different (higher in the *ex vivo* results because the extracted tissue was more stiff). The average elastic modulus, E_t, calculated (Eq. 3.4) from the curve equilibrium values of the tested diaphragmatic strips (n = 28), significantly increased at 15% and 20% strip elongation (Fig. 4.16) with respect to the 5% and 10% applied strain ($p<0.01$ from values at 5%

strain, $p<0.01$ from values at 10% strain), while average time constant τ was not affected by strain (Fig. 4.17).

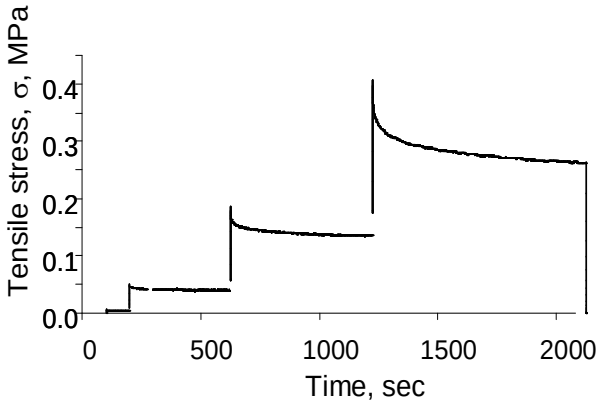

Fig. 4.15 Example of stress-relaxation curve following diaphragmatic strip stretch of 5%, 10%, 15%, 20% at a constant velocity elongation of 10%/s. Stress values increased when the strain ramp was applied until attainment of the strain peak; then the tissue relaxed and the stress decreased to an equilibrium value.

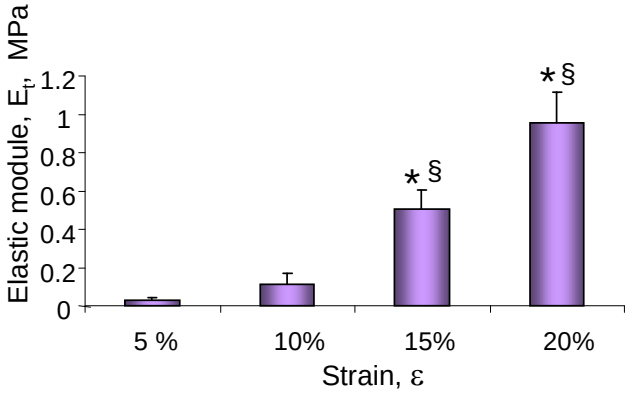

Fig. 4.16 Elastic modulus (E_t) for increasing strain (ε) level of 5%, 10%, 15%, 20% of initial strip length. Student's t-test values: * significantly different ($p < 0.01$) from values at 5% strain, § significantly different ($p < 0.01$) from values at 10% strain.

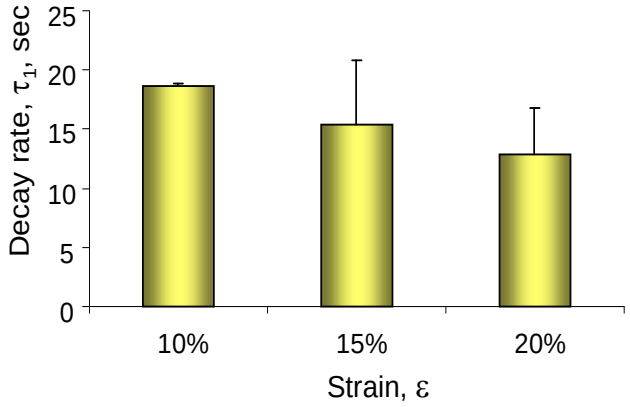

Fig. 4.17 Average values of the first relaxation (τ_1) constant.

E_t, obtained by stretching the tissue along different fibres directions and in different diaphragmatic regions, was higher (Fig. 4.18), but not significantly, when stress was applied in the transversal (T) rather than in the longitudinal (L) direction to the diaphragmatic fibers axis and in strips excised from the ventral (V) rather than the dorsal (D) diaphragmatic region. Similar results were provided by the elastic module at failure, $E_{t,f}$ (Fig. 4.19), although it was not seen significant differences in the different strips. $E_{t,f}$ was measured as the slope of the linear portion of the curve before failure (Fig. 4.20), mathematically it was obtained as: $Et, f = \frac{\Delta\sigma}{\Delta\varepsilon}$. The stress relaxation time constant after 10% strain was significantly higher ($p<0.01$) after elongation in the transversal than in the longitudinal fibers direction and in ventral than dorsal diaphragmatic tissue strips ($p<0.01$) (Fig. 4.21).

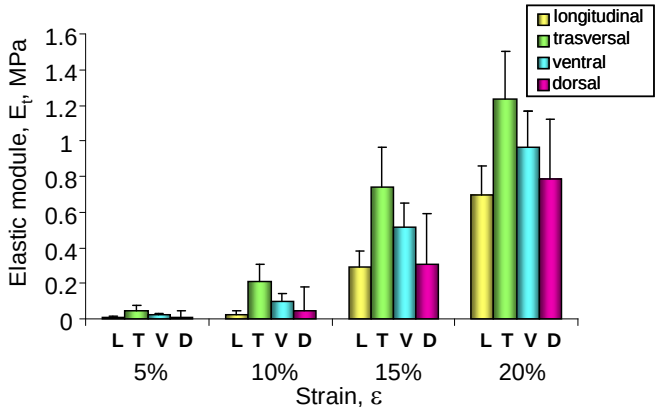

Fig. 4.18 Elastic module (E_t) for increased strain (ε) levels grouped by direction of fiber orientation (strain applied longitudinally to the fibers axis L and transversally to the fibers axis T) and by anatomical location (strips excised from the dorsal diaphragmatic zone D and from the ventral zone V).

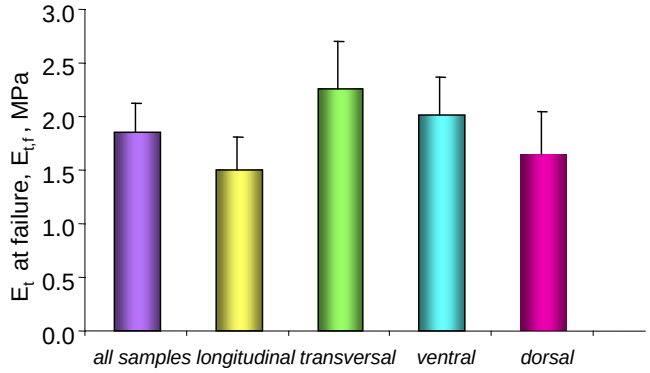

Fig. 4.19 Average elastic module before failure, $E_{t,f}$, of all strips excised in different fibers direction or location.

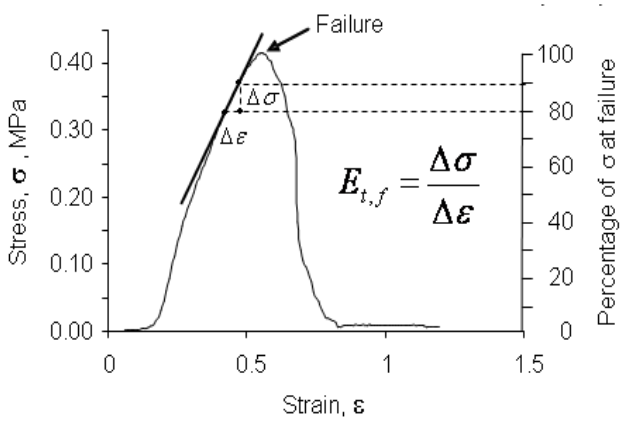

Fig. 4.20 Stress-strain plot until failure of a diaphragmatic tissue strip. The elastic module before failure $E_{t,f}$ was represented by the slope of the tangential line to the stress-strain curve at a stress of 80 to 90% of the failure stress.

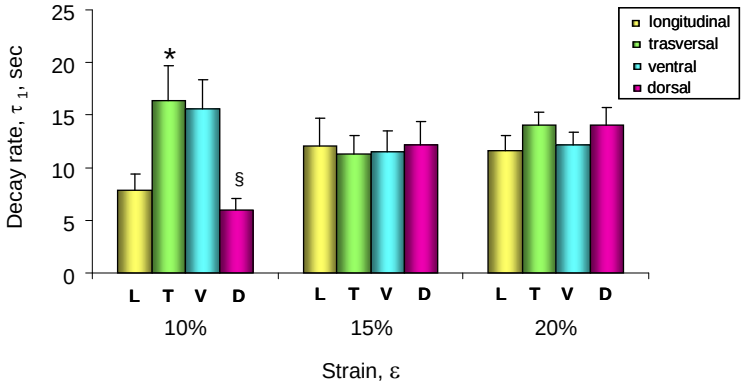

Fig. 4.21 Relaxation time constant (τ_1) for increasing strain (ε) levels (10%, 15%, 20%) grouped by direction of fibers orientation (longitudinally and transversally) and by anatomical location (dorsal and ventral zone).

4.3 PART III

In this part of the study, the kinetics of fluid flux was studied in order to clarify the function of the organization of the submesothelial lymphatic network. It was possible to distinguish two types of lymphatic vessels, loops and linear, characterized both by simple or complex structures with one or many branches arranged in parallel or in series. As previously reported (results part I), the localization of two vessel populations

in different diaphragmatic regions has been confirmed: loops were preferentially located in the peripheral ventro-lateral regions of the diaphragm, whereas linear lymphatics were dispersed over the whole surface, apparently connecting different regions. Diameters of the two populations of lymphatic vessels were similar in linear (137.93 ± 23.61 µm, range: 174.68 to 93.88 µm) and in loops (131.78 ± 20.14 µm, range: 77.92 to 199.94 µm). Flow velocity was computed by dividing the distance travelled by the fluorescence front along the path of the lymphatic vessel (Fig. 4.2 A and 4.2B) by the interpicture time interval.

To use this parameter, it has been verified that the FITC-dextran freely moved within the vessel lumen without escaping from the vessel wall (up to thirty minutes after FITC-dextran injection, longer than the longest recording time of ~ 24 min), and with a velocity similar to the lymph velocity because this dextran has density and viscosity similar to the lymph. The mean dye velocity was 163.04 ± 40.08 µm/s (range: 108.22 to 241.09 µm/s) in linear vessels, and 190.71 ± 103.69 µm/s (range: 11.42 to 533.71 µm/s) in loops, as shown in table 4.3. Lymph flow was calculated as the product of lymph flow velocity multiplied by cross-sectional area (Eq. 3.1), and was not significantly different in linear lymphatic vessels (77.38 ± 47.80 nl/min) and complex loops (113.94 ± 66.44 nl/min), with an average lymph flow value $\dot{V}_{\text{lymph}}$ = 100.23 ± 43.20 nl/min. The minimum lymph flow was similar in both populations (6.61 ± 4.76 nl/min in linear vessel and 6.33 ± 3.71 nl/min in loops), while the maximum lymph flow was very different but not significantly (220.40 ± 174.19 nl/min in linear and 510.60 ± 269.50 nl/min in loops). These results showed a great variability within all lymphatic vessels, however mean and maximum lymph flow in loops were higher albeit not significantly, compared to linear ones (Tab. 4.3).

Lymphatic vessels		
	LINEAR	LOOP
Diameter (μm)	137.93 ± 23.61	131.78 ± 20.14
Mean velocity (μm/s)	163.04 ± 40.08	190.71 ± 103.69
Mean lymph flow (nl/min)	77.38 ± 47.80	113.94 ± 66.44
Lymph flow min (nl/min)	6.61 ± 4.76	6.33 ± 3.71
Lymph flow max (nl/min)	220.40 ± 174.19	510.60 ± 269.50

Table. 4.3 Kinetics and morphological parameters of linear vessels and loops.

Moreover, it was found that in some loops the flow direction reverted multiple times with an average frequency of 0.07 ± 0.02 Hz. In these loops the lymph progressed in an oscillatory way simultaneously or in sequence in the same and/or different tracts of the loop. The diameters in loops with oscillatory flow and without this phenomena were similar (153.28 ± 38.21 nl/min in the former and 128.46 ± 18.0 nl/min in the latter), while the velocity of oscillatory flow was significantly different (458.79 ± 70.48 nl/min; $p < 0.05$) in comparison with not oscillatory flow (136.26 ± 60.05 nl/min), and the lymph flow was higher but not significantly in oscillatory flow (206.28 ± 119.41 nl/min) in comparison with not oscillatory flow (51.61 ± 26.52 nl/min), as shown in table 4.4.

Lymphatic loops		
	Oscillatory flow	Not oscillatory flow
Diameter (μm)	153.28 ± 38.21	128.46 ± 18.00
Mean velocity (μm/s)	458.79 ± 70.48 *	136.26 ± 60.05
Mean lymph flow (nl/min)	206.28 ± 119.41	51.61 ± 26.52
Lymph flow min (nl/min)	10.64 ± 8.58	12.28 ± 9.35
Lymph flow max (nl/min)	600.16 ± 192.91	177.79 ± 119.69
Frequency (1/sec, Hz)	0.07 ± 0.02	-

Table. 4.4 Student's t-test values: * $p < 0.05$ oscillatory flow with respect to not oscillatory flow.

In some loops the flow reverted multiple times with a variable frequency independent from both cardiac (161 ± 16 breaths/min) and ventilatory (77 ± 2 breaths/min) frequency (Fig. 4.22).

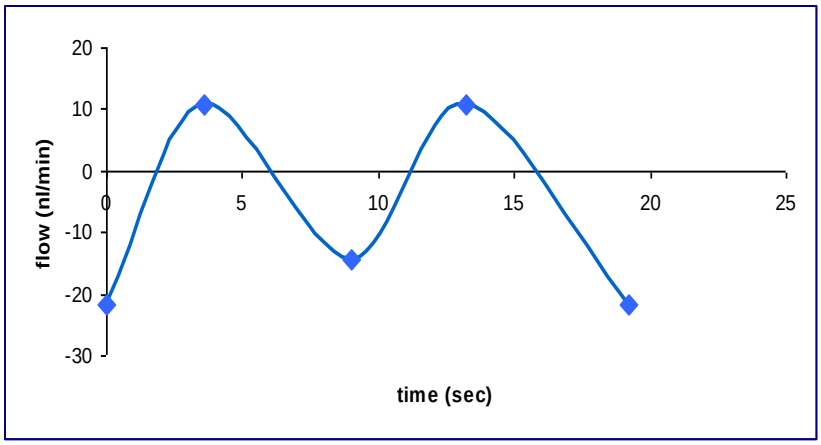

Fig. **4.22** Dependence of flow direction and amplitude on time in a lymphatic loop.

Two phenomena of flow oscillation were seen in loops: in the first, the oscillatory flow reverted in the same loop portion in sequential time. In this case the flow trend was very variable, suggesting the presence of valves and/or musculature involved in the forward/backward flow direction changes (Fig. 4.23).

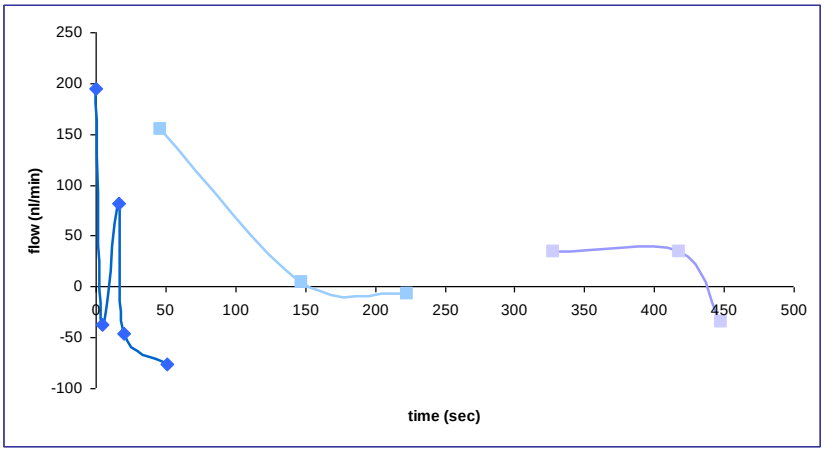

Fig. 4.23 Example of complex oscillatory flow in the same loop segment over time.

In the second, the oscillatory flow was seen in different loop tracts simultaneously: within the same loop there were different segments showing different behaviours, both oscillatory and not oscillatory flow over time (Fig. 4.24 and Fig. 4.25). As shown in

these figures, the flows described very different curves over time, suggesting the existence of a very complex pumping mechanism within the same loop with tracts having a specific contraction rhythm and activity.

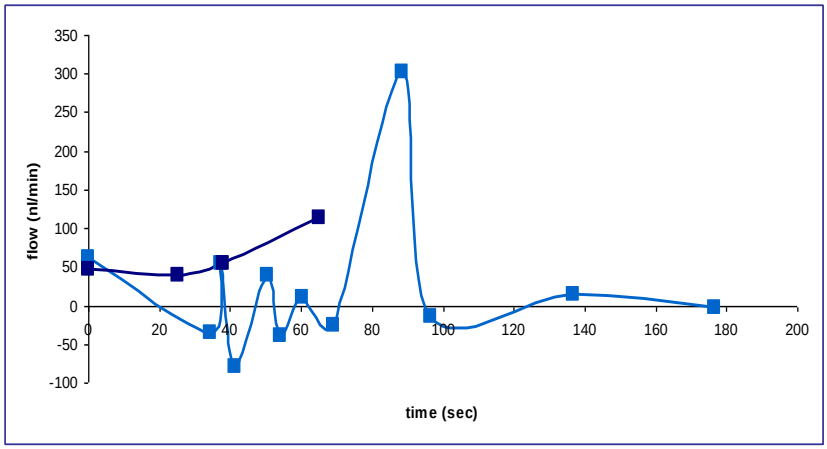

Fig. 4.24 Example of simultaneous activity of oscillatory flow in different loop tracts.

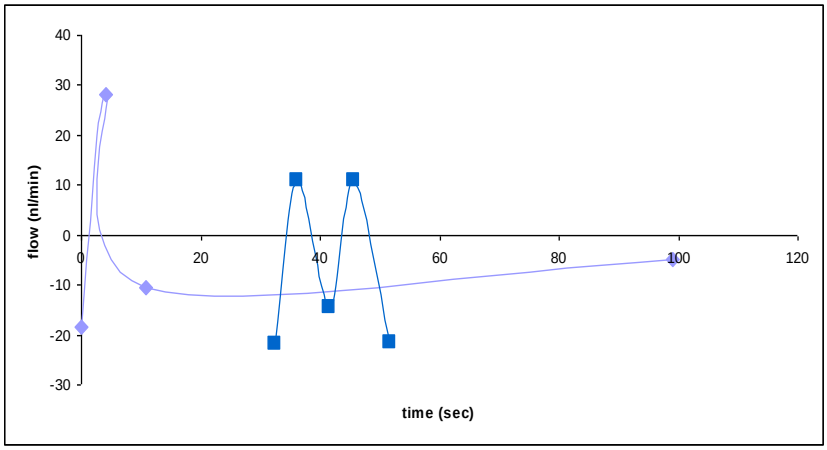

Fig. 4.25 Oscillatory flow in different loop tracts contemporaneously.

The lymph flow is fast and reverts frequently its direction within oscillatory loops, probably due to the presence of intraluminal valves. As a consequence, the valves structure has been investigated. The presence of unidirectional valves were not easily detectable however, it has sometimes been possible to identify the position of

intraluminal valves observing the progression of the injected fluorescent dye bolus into a vessel. Valves appeared as a vessel constriction brighter than the vessel wall (Fig. 4.26). Closed valves momentarily impeded the lymph flow, obstructing the pathway and causing the accumulation of FITC-dextran at the site of the obstruction: the valves seemed to control both flow direction and recirculation within the loop.

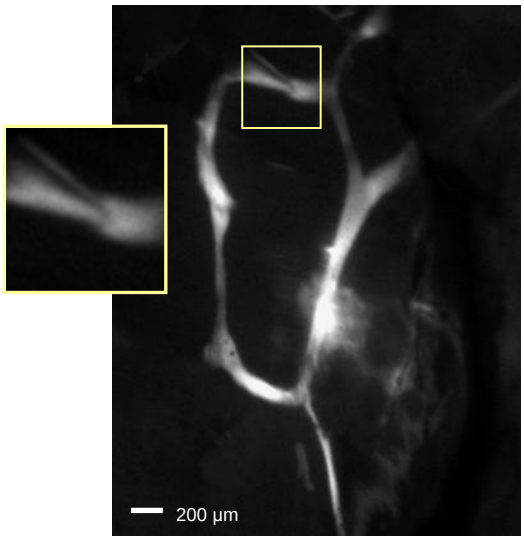

Fig. 4.26 Stereomicroscope images acquired after a FITC-dextran injection in a lymphatic loop. In the inset an intraluminal valve is visible.

Sometimes it has been possible to see the lymphatic contraction to favour the lymph progression. In these cases the diameter of the same lymphatic tract changed during lumen compressions and expansions (Fig. 4.27).

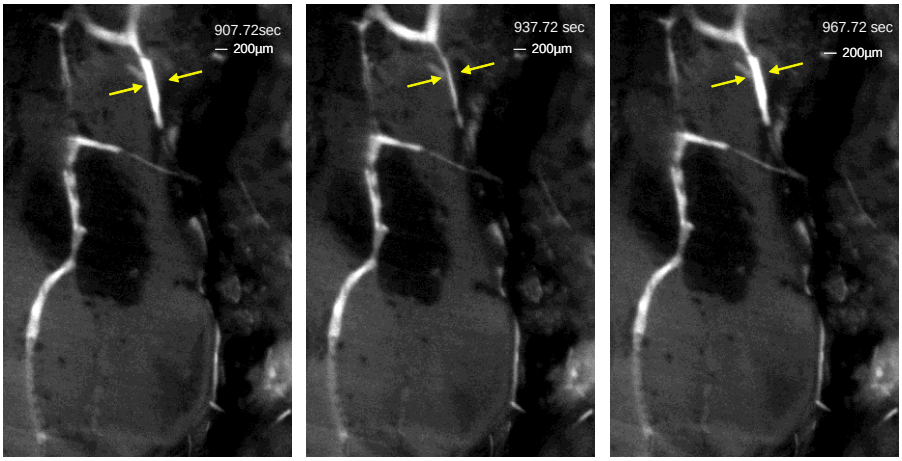

Fig. 4.27 Stereomicroscope image sequence of a loop acquired after a FITC-dextran injection showing the lymphatic contraction to promote lymph progression. In the first frame, which was taken 907.72 s after the injection, the segment of the vessel on the right side of the loop was expanded; in the second frame, taken 30 s after the first, the tract was contracted, while in the third frame, taken 30 s after the previously frame, the vessel was relaxed again.

Analyzing the diameter changes it has been possible to calculate the diameter variation between the relaxed phase and the contracted phase over time (Δ diameter = $diameter_1$ – $diameter_2$) in the same vessel tract. Mean diameter constriction (expressed as 1 - Δ diameter %) during "diastolic" periods was 6.66 ± 1.67 %, while diameter constriction during "systolic" periods attained a mean value of 49.6 ± 2.94 %, significantly different ($p<0.01$) from the diastolic value (Fig. 4.28).

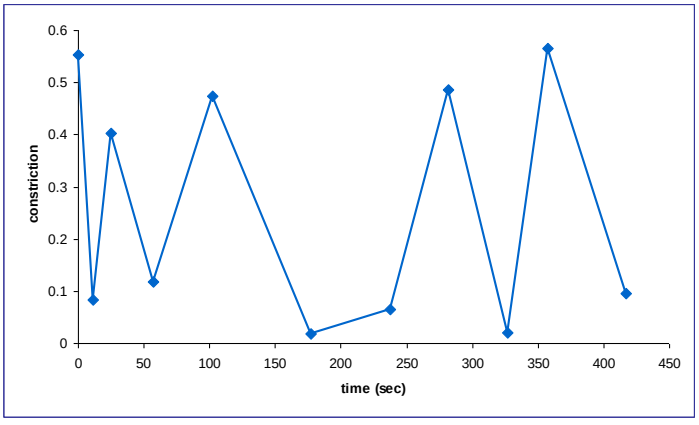

Fig. 4.28 Example of diameter change of the same lymphatic tract during lumen compressions and expansions.

These observations suggested that when the vessel was relaxed there wasn't propulsion activity, while vessel contraction was accompanied with lymph propulsion. Moreover, this observation points to the existence of an active muscular layer in some tracts of the superficial diaphragmatic lymphatic network.

The existence of an active pumping mechanism in these vessels is suggested by the changes measured in the vessel diameter due to the lumen contraction and by the observation that flow direction was independent upon the intraluminar P_{lymph} pressure gradient. Analyzing the intraluminar pressure curves, it was possible to see that the intraluminal gradients between adjacent lymphatic segments revert multiple times in adjacent vessel tracts (as shown in Fig. 4.29), thus suggesting the presence within the loop of numerous intraluminal valves able to control lymph flow direction and circulation.

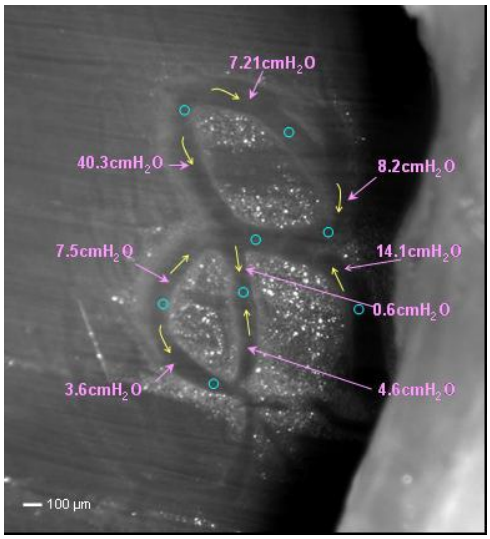

Fig. 4.29 Stereomicroscope image of a complex lymphatic loop with the pressure gradients (pink arrow) between adjacent lymphatic segments calculated as $\Delta P_{lymph} = (P_{lymph1} - P_{lymph2})$. Yellow arrows indicate the pressure gradients direction.

The net transmural pressure gradient developing between the lymphatic lumen and the adjacent interstitium was calculated as $\Delta P_{TM} = (P_{lymph} - P_{int})$. It gives information about

the lymph formation: this hydraulic pressure gradient sustains the entrance of the lymph in the lymphatic vessel when negative ($P_{int} > P_{lymph}$). The gradients measured in the different tracts of different linear lymphatic and loops were very variable but on average (-8.03 ± 2.7 cmH_2O) they showed negative values suggesting the lymph entrance in the vessel through the lymphatic wall (Fig. 4.30).

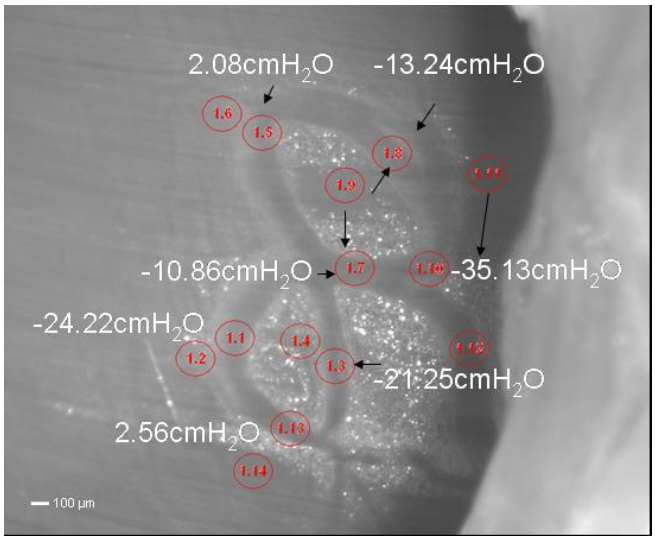

Fig. 4.30 Stereomicroscope image of a complex lymphatic loop with the net transmural gradient calculated between the lymphatic lumen and the adjacent interstitium (red circles with progressive number).

4.4 PART IV

4.4.1 Muscular fibres around lymphatic vessels

In this part of the work, the possible presence of muscular fibers around the lymphatic vessel wall of contracting lymphatics was investigated by indirect immunofluorescence assay in order to justify the lumen contraction phenomena described in part III. Lymphatic vessels in the diaphragm of adult rats were aspecifically labelled *in vivo* by an intraperitoneal injection of FITC-dextran (Fig. 4.31B), while samples cut from the diaphragm were immunohistoichemically stained in whole-mount using antibodies

against smooth muscle cells actin (α-SMA) and then acquired with confocal microscope as described in Material and Methods chapter 3.10.2.

It was observed that smooth muscle cells with α-SMC actin immunoreactivity formed a dense network around lymphatic vessels (Fig. 4.31A). Moreover, lymphatic vessels were generally much thicker than the blood capillaries and most of the lymphatic vessels ran independently of blood vessels and in the deeper layers of the diaphragm. The SM actin distribution around the vessels was not homogeneous: the smooth muscle was disposed both around the loop and the linear tracts, but the muscular fibers were more dense close to the loop in analogy with the contractile activity seen in the *in vivo* experiment described in part III (seen Fig. 4.31A). There was a clear correspondence between the contractile activity in specific lymphatic tracts seen *in vivo* and the results of *in vitro* experiments: in the lymphatic tracts the densest smooth muscle mesh was found in the same regions that presented a great contractility *in vivo*. Contractile activity was not detected in *in vivo* experiment in the regions where fewer muscular fibers were found (Fig. 4.32). Moreover, the cross section of the lymphatic vessel (Fig. 4.32C) showed that FITC-dextran fluorescence could be found inside the lymphatic lumen and the immunostained smooth muscle cells were detected around the vessel. In some regions the musculature was clearly not continuous and it was possible to see some tracts where the red fluorescence was interrupted (Fig. 4.32C). Very interesting to note was that the ratio between the diameter and thickness dimensions was maintained about 35%, as described in result part I, and the shape of the vessel was elliptical (Moriondo et al., 2010). In conclusion, these results can explain diameter changes of lymphatic tracts due to the contraction of muscular fibers around the vessel wall that promotes lymph propulsion.

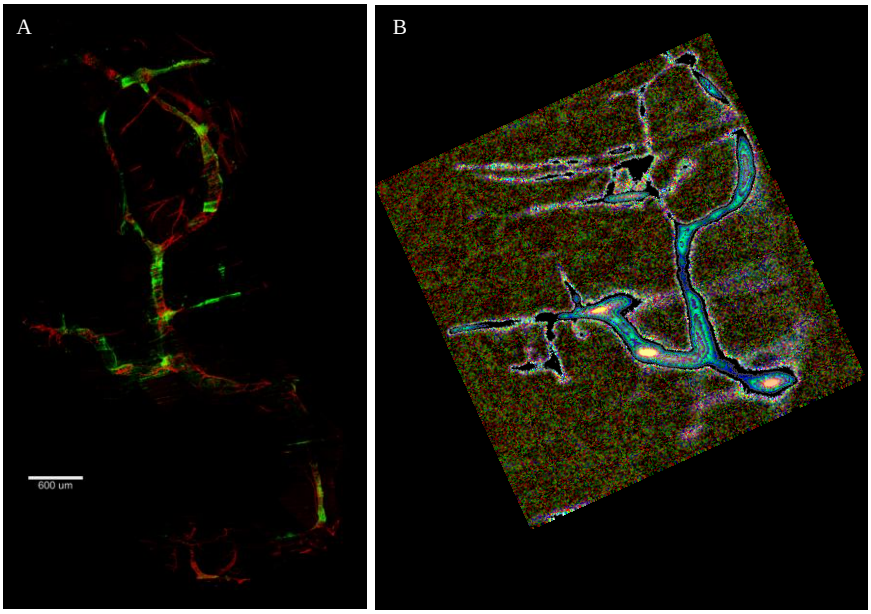

Fig. 4.31 Overview of complex lymphatic loop network. A. In green the FITC-dextran fluorescence inside the lumen vessel, in red the α-SMC-actin stained muscular fibres of the vessel wall. B. The same lymphatic network aspecifically labelled *in vivo* by an intraperitoneal injection of FITC-dextran.

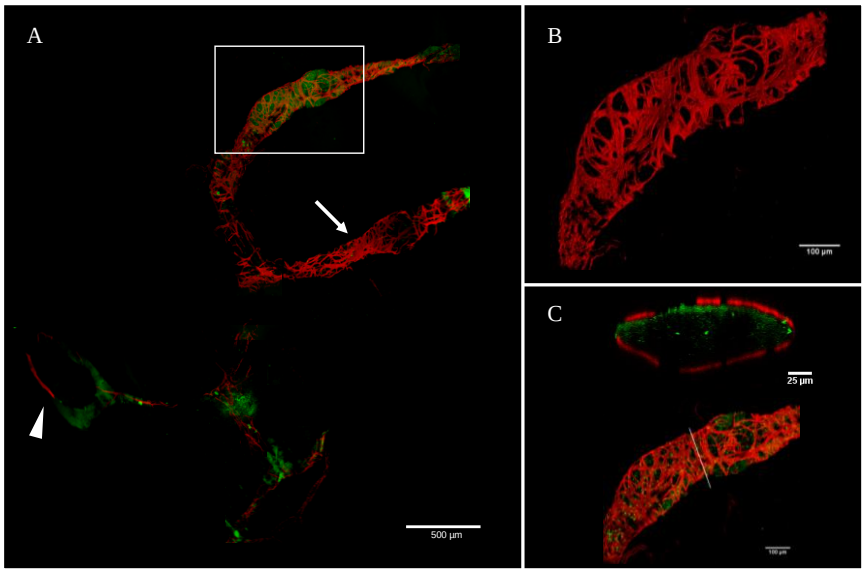

Fig. 4.32 Confocal immunostaining images of a complex diaphragmatic lymphatic network **A.** Lymphatic network, in green FITC-dextran aspecifically labelled lymphatic lumen, in red α-SMC-actin labelled muscular fibres. The arrow indicates the region where can be seen the densest muscular mesh around the vessel while the arrowhead indicates the one with scattered muscular fibers. **B. and C.** Magnification of a lymphatic vessel detail. **B.** 3D reconstruction of the smooth muscle around the vessel (VolumeJ plugin of ImageJ software). **C.** Cross-section of the lymphatic vessel in the side indicated by the white line. The specific immunostaining shows the muscle surrounding the lymphatic lumen labelled by FITC-dextran (Reslice function of Image J software on the merged z-stack).

5 Discussion

Limits and advantages of the experimental procedure. The "*in vivo*" experimental approach enables us to visualize the pleural diaphragmatic dome in order to micropuncture some lymphatic vessels. These manipulations cause few modifications of the normal pressure regimen: 1) when the chest is opened, pleural pressure becomes atmospheric; therefore, lung inflation needs to be supported by positive end-inspiratory alveolar pressure, which, in turn, is expected to increase pulmonary vascular resistances, reducing cardiac output; 2) since pleural pressure is raised to atmospheric value, the pressure difference between the peritoneal and pleural sides of the diaphragm is almost null, this in turn modifies the shape of the diaphragmatic dome by increasing its radius of curvature; 3) in order to apply the micropuncture technique on the lymphatic vessels present over the pleural diaphragmatic surface, the diaphragm must be paralyzed and the animals must be mechanical ventilated. This approach abolishes active inspiration and releases diaphragmatic skeletal muscle tone, therefore in the open chest the radial stress exerted by diaphragmatic muscular fibers on the wall of submesothelial lymphatics is expected to be smaller than in the closed chest.

These factors can influence the calliper of the lymphatic vessels that might be decreased as a consequence of the reduced radial tension and of the lack of the pulling action exerted by the subatmospheric intrapleural pressure. The decreased calliper increases viscous resistances to lymph flow with respect to the physiological values, so it is possible that lymphatic function is reduced in our open chest preparation, also because diaphragmatic lymphatic pressure is significantly more subatmospheric in the close than in the open chest (Negrini and Del Fabbro, 1990). Nevertheless, the diaphragmatic

lymphatics activity is maintained even in the open-chest by cyclic pressure gradients, developing into the lymphatic lumen as a consequence of the cardiogenic tissue displacement (Negrini et al., 2004), so that it is reasonable to assume that in our open chest preparation loops and linear segments maintain their properties in the network.

In the first part of our we have described some typical features of the submesothelial lacunae of the initial lymphatic network: 1) they can be easily observed under the transparent parietal pleura covering the diaphragmatic surface as darker-than-background vessels delimited by white borders 2) they form a bidimensional mesh laying on top of muscular or tendineous diaphragmatic fibers 3) their average thickness is compatible with the depth of pleural and peritoneal submesothelial interstitial space: ~35 μm.

To measure the intraluminal lymph flow velocity, dextran boluses of 4.6 nl were injected into the vessels. This volume was chosen in order to minimize the injected volume and the injection-associated physiological perturbation; moreover, the dextrans used had approximately the same molecular weight of plasma globulins at a concentration (~2 g/dl) similar to the total protein concentration of rat pleural fluid. These characteristics of the liquid injected did not alter the protein concentration and the viscosity of the lymph normally flowing in the submesothelial lacunae. As shown in Fig. 4.3, the injected fluorescence did not escape from vessel walls but the injected dextrans remained in the vessel during all the recording time (~ 30 minutes after dye injection), and they were homogenously mixed with the intraluminal fluid. The fluorescence remained in the injected lymphatics because the primary valves, observed in the diaphragm (Grimaldi et al., 2006), confined the dextrans in the vessel lumen preventing dye backflow through the vessel wall.

Since intraluminal lymph flow velocity was derived from the speed of progression of the fluorescent dye injected into the vessel, the pressure increase induced by the injection manoeuvres could cause an overestimation of the real lymph flow velocity. However, as shown in Fig. 4.4, upon injection, the lymphatic pressure raised from the resting value up to a maximum of 8.4 mmHg only for ~ 2 seconds and then dropped back to control values within 4 seconds. To get rid of this phenomenon, the flow velocity has been measured starting after 30 seconds from the injection time and up to 20–25 min after the injection.

Lymph flow velocity. Flow velocity measured in diaphragmatic lymphatics is much lower compared to that measured in mesenteric vessels (Dixon et al., 2006): lymph flow is about two order of magnitude higher in pre-nodal mesenteric lymphatics than in diaphragmatic lacunae. This difference may indicate that: a) total mesenteric lymph flow is much higher than diaphragmatic lymph flow, and/or b) pre-nodal mesenteric lymphatics receive and collect lymph from other smaller tributary vessels originating directly from the intestinal wall. Moreover, in mesenteric lymphatics the flow kinetics and velocity have the typical behaviour observed in contractile lymphatics; indeed, in soft tissues, like the mesentery or dermis, lymph formation and propulsion depend on synchronized contractions of smooth muscle cells in the wall of adjacent lymphangions. In thoracic tissues this mechanism of lymph propulsion exists, but only little morphological evidence of smooth muscle cells was found in the wall of the diaphragmatic submesothelial lacunae or in transverse lymphatics (Grimaldi et al., 2006). It is known that in thoracic tissues lymph formation and progression depend mostly on compression or expansion of the lymphatic vessel lumen caused by external forces developing across the vessel wall when the tissue is displaced by the beating

heart or by the contraction and relaxation of respiratory muscles (Negrini et al., 2004). Thus, these differences in flow velocity between diaphragmatic and mesenteric or dermal lymphatics might be related with the specific function in the lymphatic network: pre-nodal mesenteric lymphatics operate as propulsive ducts, while submesothelial lymphatic lacunae seem to serve as collecting reservoirs that receive fluid from stomata and drain lymph into deeper collecting ducts.

Linear vessels and loops. Through the different morphological aspects and the distribution of the lymphatic vessels, linear vessels and loops on the diaphragmatic surface can be distinguished although they belong to the same hierarchic order of lymphatics. Linear vessels were found over both the muscular and tendineous diaphragmatic regions, whereas complex loops were preferentially observed at the diaphragmatic muscular periphery.

Lymph flow was higher in loops than in linear vessels and flow kinetics were also very different: in linear vessels the injected fluorescent bolus progressed unidirectionally from the peripheral to the ventro-medial zone of the diaphragm, while in loops the flow progressed counter-clockwise inside the loop. All these considerations might suggest that loops receive lymph directly from the pleural stomata and they might serve as "fluid reservoirs" to subsequently redistribute the lymph to larger linear vessels running toward the tendineous portion of the diaphragm and to transverse and collecting ducts running deeper in diaphragmatic tissue. Thus, linear vessels might sustain fluid propulsion along the lymphatic network.

Lymph formation and propulsion in the lymphatics of the pleural diaphragmatic surface is influenced by the respiratory activity. During expiration the tone of diaphragmatic muscular fibers is low and pleural liquid pressure in the region facing the diaphragm,

although subatmospheric, is higher than at end inspiration. This condition might enhance lymph formation in loops in peripheral muscular diaphragmatic zones. On the other hand, during inspiration, muscular fibers contract and shorten while the medial tendineous fibers are stretched: this condition might favour squeezing of the lymph from loops into linear vessels present over all the diaphragmatic surface.

Lymph flow direction is set by the lymphatic vessels' intraluminal valves. Due to the presence of the parietal pleura and the subpleural interstitial space that covered valves, they are hardly detectable in the submesothelial lymphatics by conventional epi-tangential illumination when viewed at the stereomicroscope. However, their presence can be easily inferred: a) by observing the motion pattern of the injected fluorescence during its progression along both linear and loop vessels, b) by the intraluminal pressure measures, where sudden decreases in P_{lymph} are the effect of valve opening. They have a very important function in controlling the direction (especially in linear vessels) and the recirculation of fluid (especially in loops). Valves opening and closing impose to the fluid the direction and the eventual recirculation of the lymph into, within and out of the loops (Fig. 4.8); moreover, valves can modulate flow velocity, especially in loops, isolating the entire loop or connecting it to the inlet and outlet linear vessels.

Mechanical properties of the initial lymphatics. The second part of this work has been devoted to the study of the role of the mechanical properties of the initial lymphatic wall and of the surrounding tissue that eventually could support lymph formation and progression. In the past, some studies about the lymphatic vessels properties were conducted in isolated collecting ducts or in mesenteric lymphatics (Zawieja et al., 1993) that can be easy isolated from the surrounding tissue. On the contrary, the initial lymphatics are more difficult to study because of their tight

connection to the extracellular matrix tissue; in particular, in tissues like the pulmonary or muscular ones are not easily accessible "*in vivo*". Thus, in order to study the mechanical behaviour of initial lymphatics, we approached the initial lymphatics on the surface of the diaphragm, a tissue where they are relatively accessible: indeed, the diaphragmatic superficial vessels could be visualised "*in vivo*" and studied "*in situ*" without inducing a great perturbation of their physiological conditions.

Measurement of vessel compliance, obtained by recording P_{lymph} in a closed vessel segment after injections of boluses of known volumes of fluorescence, revealed the existence of two populations of diaphragmatic lymphatic vessels with different mechanical properties coexisting in the superficial diaphragmatic lymphatic network. All C_{wall} determinations were performed in straight vessels of rather homogeneous size oriented perpendicularly to the diaphragmatic muscle fibres in the peripheral muscular region of the right emi-diaphragm, indeed it was easier to isolate a segment and made double micropunctures in this kind of vessels, while the experimental procedure couldn't be performed in complex loops formed at the confluence of shorter vessels (Moriondo *et al.*, 2008). Despite this limit, one common characteristic of superficial linear vessels and loops was that, unlike deeper diaphragmatic lymphatics completely surrounded by muscular or tendineous diaphragmatic fibres, they were partially immersed in the diaphragmatic tissue and partially exposed to the pleural space and covered by the pleural membrane. Thus, their mechanical properties might reflect: a) their depth within the diaphragmatic tissue, b) the stiffness of the tissue and c) the compliance of the thin serosal wall constituted by the lymphatic endothelium and the pleural tissues. The similarity between the time constants of the P_{lymph} decay rate after

attainment of post-injection $P_{lymph\text{-}peak}$ (Fig.4.9) and of the tissue stress relaxation tests (Fig. 4.16) indicated the role of tissue cuff in defining the vessel mechanical response.

The compliance studies allowed us to identify two initial lymphatic populations with different mechanical properties and functions: 1) vessels delimited by a compliant wall (H-C_{lymph}) acted like reservoirs of drained interstitial lymph. These were likely the most superficial vessels, whose C_{wall} basically mirrored the distensibility of the mesothelial layer. The high tensile stress regimen in their superficial wall might favour the opening of mesothelial stomata, while their high compliance would allow to accommodate large fluid volumes drained from the pleural and peritoneal cavities; 2) vessels surrounded by a stiffer wall (L-C_{lymph}) propelled fluid along the network. This was the case of vessels that, although superficial, were deeper embebbed in the muscular or tendinous tissue. There was no evidence of significant differences in the behavior between the fibres directions and diaphragmatic regions. C_{wall} values, intermediate between those measured in the two population of diaphragmatic vessels, were reported in relaxed isolated mesenteric lymphatics (Zhang et al., 2007). This suggests that in lymphatic networks not surrounded by muscular/tendineous tissue environments, the well developed layer of smooth muscle cells in the vessel wall may not only sustain active lymphatic pumping, but also provide a relatively stiff mechanical support.

The present average diaphragmatic tissue elastance (Fig. 4.19) compares well with other estimates obtained on relaxed preconditioned rat tissue strips (Navajas *et al.*, 1992; Boriek *et al.*, 2001). It is worth noting that "*in vivo*" end-expiratory and, even more, end-inspiratory tissue stiffness is very likely higher than that measured in this study performed on excised tissue strips. As suggested by data of Fig. 4.18 and 4.21, tissue elastance was mildly higher in ventral compared to dorsal regions of the diaphragm, as

expected from the anatomically higher percentage of stiffer tendineous fibres in the ventral than in the dorsal diaphragm (Boriek *et al.*, 2005). These regional differences might be important in terms of lymphatic function. Lymph formation in pleural diaphragmatic lymphatic network depends upon the difference between pleural fluid pressure (P_{liq}) and P_{lymph}. While regional end-expiratory and end-inspiratory distribution of P_{liq} is well documented (Negrini and Del Fabbro, 1999), no systematic recording of regional diaphragmatic P_{lymph} has been performed yet. At end-expiration, the peripheral diaphragmatic muscular fibres are relaxed and passively stretched by the pulling action of the stiffer central tendon fibres. This condition and the sub-atmospheric diaphragmatic P_{liq} might distend the superficial lymphatics oriented transversally to the muscular fibres and reduce P_{lymph}, favouring end-expiratory lymphatic filling. It is worth noting that, given a relaxation time constant greater than 5 sec (Fig. 4.21), the distending effect is assured during the entire end-expiratory pause lasting in rat about ~ 600-700 msec. On inspiration, the muscular fibres contract and shorten and the central tendineous fibres are stretched while diaphragmatic P_{liq} decreases (Miserocchi *et al.*, 1984), a condition that, by limiting lymph formation, might instead favour deep lymphatics squeezing and lymph progression in the network.

Lymph flow kinetics. In order to complete the study about the organization and the mechanisms of lymph propulsion in the diaphragmatic lymphatic network, the kinetics of fluid flow were studied.

Through the analysis of acquired fluorescence images, a great variability has been found among all lymphatic vessels: in some loops lymph flow was fast and reverted multiple times its direction, the velocity of oscillatory flow was significantly different from not oscillatory flow, while the lymph flow was higher but not significantly. However, in the

loops where the flow direction reverted multiple times with a variable frequency it was seen that this direction change was independent from both cardiac (161 ± 16 breaths/min) and ventilatory (77 ± 2 breaths/min) frequencies. It was evident that other mechanisms favor this phenomenon, probably due to the presence of intraluminal valves and a muscular layer in the vessel wall. In addition, sometimes two different behaviors in the oscillatory flow were seen. Lymph progressed simultaneously or in sequence in the same and/or different tracts of the loop: 1) in the same loop segment the flow trend was very variable, suggesting the presence of valves and/or musculature involved in the forward/backward flow direction changes; 2) within the same loop there were different segments showing simultaneous activity, both oscillatory and not oscillatory flow over time. Another peculiar behavior was the diameter changes of the same lymphatic tract during lumen compressions and expansions. In fact, diaphragmatic lymphatic vessels showed different kinetic behaviours: "diastolic" periods, characterized by a larger diameter, were distinguished from "systolic" periods, with a smaller diameter. This observation pointed to the existence of an active muscular layer in some tracts of the superficial diaphragmatic lymphatic network, being these periodic contractions of the lymphatic vessel an additive mechanism to promote and modulate lymph progression.

The existence of an active pumping mechanism in these vessels was suggested by the observation that flow direction was sometimes independent upon the intraluminar P_{lymph} pressure gradient (pressure gradients between adjacent lymphatic segments reverted multiple times in adjacent vessel tracts without significant links with the flow direction) and by the appearance of "systolic" contractions in some tract of the lymphatic network, closely associated with lymphatic loops. In the past, works performed on the mesenteric

lymphatic vessels demonstrated that, in analogy to the cardiac cycle, when the upstream organ produces more lymph, the lymphatic vessels should respond with an increased amplitude and frequency of contractions (Bohlen et al., 2009; Benoit et al., 1989; Ohtani Y. and Ohtani O., 2001). However, in the diaphragmatic vessels the mechanism of contraction has never been previously described.

At the end of the work, to investigate the lumen contraction phenomenon with immuno-fluorescence assays the eventual presence of muscular fibers around the lymphatic vessel wall was studied. Surprisingly, smooth muscle cells with α-SMC actin immunoreactivity formed a more or less sparse network around lymphatic vessels (Fig. 4.32). These results can explain the diameter changes of lymphatic tracts due to the contraction of muscular fibers around the vessel wall which promotes lymph propulsion, albeit most if not all of these vessels do not belong to the most superficial ones which have been previously investigated by the micropuncture technique.

Conclusion. The pattern of fluid distribution within the diaphragmatic submesothelial lacunae suggestes that lymphatic loops might be the preferential sites of fluid entrance into the diaphragmatic lymphatic network. This role might be enhanced at end expiration when muscle fibers are relaxed, pleural liquid pressure is the least negative throughout the respiratory cycle, and a favorable pleural-to lacunae pressure gradient develops. Larger linear vessels encountered mainly in the medial diaphragmatic tendon seem, on the contrary, to be more specifically involved in conveying lymph out of the diaphragm on inspiration, when contraction of the peripheral muscular fibers squeezes the lymph from the loops. In addition, the geometrical arrangement of the submesothelial lymphatic network, the different mechanical properties of the two initial lymphatic populations identified (delimited by a compliant tissue or by a stiffer tissue)

and the presence around some lymphatic vessels of a network of smooth muscle cells permitte to exploit local tissue forces developing in the diaphragmatic tissue during cardiac and respiratory activity.

Therefore, the spatial organization and geometrical arrangement of the diaphragmatic submesothelial vessels seem to be finalized at exploiting the contraction and relaxation phases of diaphragmatic muscle fibers to alternatively enhance lymph formation or progression into the lymphatic network, thus contributing to optimize fluid and solute removal from the pleural and peritoneal cavities throughout the entire respiratory cycle.

6 References

Abelda S.M., Hansen-Flaschen J.H., Lanken P.N. and Fishman A.P. Effects of increased ventilation on lung lymph flow in unanesthetized sheep. *J. Appl. Physiol*. **60**: 2063-2070, 1986

Adair T.H. and Guyton A.C. Modification of lymph by lymph nodes. II. Effect of increased lymph node venous blood pressure. Am. J. Physiol. **245** (*Heart Circ. Physiol*. 14): H616-H622, 1983

Adair T.H. and Guyton A.C. Lymph formation and its modification in the lymphatic system. In: Experimental Biology of the Lymphatic Circulation, edited by M.G. Johnston. Amsterdam: Elsevier, 1985, **2**: 13-44

Agostoni E., Miserocchi G. and Bonanni M.V. Thickness and pressure of the pleural liquid in some mammals. *Resir. Physiol*. **6**: 245-256. 1969

Albertine K. H., Wiener-Kronish J. P., Roos P. J. and Staub N. C. Structure, blood supply and lymphatic vessels of the sheep's visceral pleura. *Am. J. Anat*. **165**: 277-294. 1982

Albertine K.H., Fox L.M. and O'Morchoe C:C:C: the morphology of canine lymphatic valves. *Anat. Rec*. **202**: 453-461, 1982

Albertine K. H., Wiener-Kronish J. P. and Staub N. C. The structure of the parietal pleura and its relationship to pleural liquid dynamics in sheep. *Anat.Rec*. **208**: 401-409. 1984

Allen J. M., McHale N.G. and Rooney B. M. Effect of norepinephrine on contractility of isolated mesenteric lymphatoics. *Am. J. Physiol*. **244**: H479-H486, 1983

Allen J.M. and McHale N.G. Neuromuscular transmission in bovine mesenteric lymphatics. *Microvasc. Res*. **31**: 77-83, 1986

Aria H., Endo M., Sasai Y., Yokosawa A. Sato H., Motomiya M. and Konno K.

Histochemical demonstration of hyaluronic acid in a case of pleura mesothelioma. *Am. Rev. Respire*. Dis. **111**: 699-702. 1975

Aukland K. and Nicolaysen G. Interstitial fluid volume: local regulating mechanisms. *Physiol. Rev.* **61**: 556-583, 1981

Aukland K. and Reed R. K. Interstitial-Lymphatic Mechanisms in the Control of Extracellular Fluid Volume. *The American Physiological Society*. **73**: 1-78, 1993

Azuma T. Ohhashi T. and Sakaguchi M. Electrical activity of lymphatic smooth muscles. *Proc. Soc. Exp. Biol. Med.* **155**: 270-273, 1977

Bach C. and Lewis G.P. Lymph flow and lymph protein concentration in the skin and muscle of the rabbit hind limb. *J. Physiol. Lond*. **235**: 477-492, 1973

Benoit JN, Zawieja DC, Goodman AH and Granger HJ. Characterization of intact mesenteric lymphatic pump and its responsiveness to acute edemagenic stress. *Am J Physiol Heart Circ Physiol.* **257**: 2059-2069, 1989

Bernaudin J.F. and Fleury J. In the pleura health and desease 8Cretien J., Bignon J. and Hirsh A. eds) 101-124, *Marcel Dekker Inc*. New York, 1985

Bernaudin J. F., Jaurand M. C., Fleury J. and Bignon D. J. Mesothelial cells. *The lung Scientific Foundation* (Crystal R. G. and West J. B., eds.) 631-638, Raven Press, New York. 1991

Bettendorf U. Lymph flow mechanism of the subperitoneal diaphragmatic lymphatics. *Lymphology.* **11**: 111-116. 1978

Bohlen H.G., Wang W., Gashev A., Gasheva O. and Zawieja. Phasic contractions of rat mesenteric lymphatics increase basal and phasic nitric oxide generation in vivo. *Am J Physiol Heart Circ Physiol*. **297**: 1319-1328, 2009

Brace R.A., Taylor A.E. and Guyton A.C. Time course of lymph protein concentration in the dog. *Microvasc. Res*. **14**: 243-249, 1977

Bridenbaugh E.A., Anatoly A., Gashev M.D. and Zawieja D. Lymphatic muscle: a

review of contractile function. Lympohatic *Research and Biology*. Vol. 1, **2**: 147-158, 2003

Browse N.L., Doig. R.L. and Sizeland D. The resistance of a lymph node to lymph flow. Br. J. Surg. 71; 192-196, 1984

Calnan J. S., Pflug J.J., Reis N. D. and Taylor L.M. Lymphatic pressures and the flow of lymph. *Br. J. Plast. Surg*. **23**: 305-315, 1970

Casley-Smith J. R. The identification of chylomicra and lipoproteins in tissue secretion and their passage into jejunal lacteals. *Journal of Cell Biology*. **15**: 259-277, 1962

Casley-Smith J. R. The role of the endothelial intercellular junctions in the functioning of the initial lymphatics. *Angiologica*. **9**: 106-131, 1972

Casley-Smith J.R. Lymph and lymphatics. In: Kaley G., Altura B.M. eds. *Microcirculation.* Baltimore, M.D.: University Park.423-502, 1977

Casley-Smith J.R. Varying total tissue pressure and the concentration of initial lymphatic lymph. *Microvasc. Res*. **25**: 369-379, 1983

Castenholz A. Morphological characteristics of initial lymphatics in the tongue as shown by scanning electron microscopy. *Scanning Electron Microscopy* **1984**: 1343-1352, 1984

Chen H. I., Granger H. J. and Taylor A. E. Lymph flow transients following elevation of venous pressure in the dog hindpaw. *Lymphology* **24**: 155-160, 1991

Courtice F. C. and simmonds W. J. Physiological significance of lymph drainage of the serous cavities and lungs. *Physiol. Rev*. **34**: 419-448. 1954

Daroczy J. New structural details of dermal lymphatic valves and its functional interpretation. *Lymphology* **17**: 54-60, 1984

Dejana E. Endothelial adherens junctions: implications in the control of vascular permeability and angiogenesis. *J. Clin. Invest*. **100**: S7-S10, 1997

Dixon JB, Greiner ST, Gashev AA, Cote GL, Moore JE and Zawieja DC. Lymph flow,

shear stress, and lymphocyte velocity in rat mesenteric prenodal lymphatics. *Microcirculation*. **13**: 597-610, 2006

Florey H. W. Observations on the contractility of lacteals. Part I. *J. Physiol*. (London) **62**: 267-272, 1927

Florey H. W. Observations on the contractility of lacteals. Part II. *J. Physiol*. (London) **63**: 1-18, 1927

Foster R.S. Jr. General anatomy of the lymphatic system. *Surg Oncol Clin N Am*. **5**: 1-13, 1996

Fung Y.C. Biodynamics: Circulation. New York: Springer-Verlag, 39-47, 1984

Granger H. Role of the interstitial matrix and lymphatic pump in regulation of transcapillary fluid bilance. *Microvasc Res*. **18**: 209-216, 1979

Grimaldi A, Moriondo A, Sciacca L, Guidali ML, Tettamanti G. Negrini D. Functional arrangement of rat diaphragmatic initial lymphatic network. *Am J Physiol Heart Circ Physiol* **291**: H876-H885, 2006

Guyton A. C. Interstitial fluid pressure. II. Pressure-volume curves of interstitial space. *Circ. Res.* **16**: 452-460, 1965

Guyton A. C. and Coleman T. G. Regulation of interstitial fluid volume and pressure. *Ann. N. Y. Acad. Sci.* **150**: 537-547, 1968

Guyton A. C., Taylor A. E. and Granger H. J. *Circulatory Physiology II. Dynamics and Control of Body Fluids*. W. B. Saunders, Philadelphia, PA, 1975

Hall J. G., Morris B. and Wooley G. Intrisnsic rhythmic propulsion of lymph in the unanesthetized sheep. *J. Physiol. (London)* **180**: 336-349, 1965

Hargens A.R. and Zweifach B.W. Transport between blood and peripheral lymph in intestine. *Microvasc. Res*. **11**: 89-101, 1976

Hargens A.R. and Zweifach B.W. Contractile stimuli in collecting lymph vessels. *Am. J.*

Physiol. **233** (Heart Circ. Physiol. 2):H57-H65, 1977

Heidenhain R. Bemerkungen und versuche betreffs der resorption in der bauchohole. *Pfleuger's Arch*. **72**:320, 1895

Hewson, W. The works of William Hewson (Syndenham Soc., ed.), *Gullieur*, London, 1846

Hills B. A., Bitler B. D. and Barrow R. R. Boundary lubrication imparted by pleural surfactants and their identification. *J. Appl. Physiol*. **53**: 463-469. 1982

Hills B. A. Graphite-like lubrication of mesothelium by oligolamellar pleural surfactant. *J. Appl. Physiol*. **73**: 1034-1039. 1992

Horstmann E. Uber die funktionelle Struktur der mesenterialen Lymphgefasse. *Morphologisches Jahrbuch*. **91**: 483-510, 1952

Ikomi F. and Scnmid_Schonbein G.W. Lymph pump mechanics in the rabbit hind leg. *Am. J. Physiol*. **271**: H173-H183, 1996

Ikomi F., Hunt J., Hanna G. and Schmid-Schonbein G.W. Interstitial fluid, protein, colloid and leukocyte uptake into interstitiallymphatics. *J. Appl. Physiol*. **81**: 2060-2067, 1996

Ikomi F., Zweifach B.W., Schmid-Schonbein G.W. Fluid pressures in the rabbit tissue motion. *Lymphology*. **30**: 13-23, 1997

Intaglietta M. and gross J.F. Vasomotion, tissue fluid flow and formation of lymph. *Int. J. Microcirc. Clin. Exp*. **1**: 55-65, 1982

Jetsch M., Tammela T., Alitalo K. and Wilting J. Genesis and pathogenesis of lymphatic vessels. *Cell Tissue Res*. **314**: 69-84, 2003

Johnston M.G. Involvement of lymphatic collecting ducts in the physiology and patophysiology of lymph flow. In: Research Monographs in Cell and Tissue Physiology. Experimental Biology of the Lymphatic Circulation, edited by M.G. Johnston. Amsterdam: Elsevier, 1985, vol. **9**: 81-120

Joyner W.L., Carter R.D. and Renkin E.M. Influence of lymph flow rate on concentrations of proteins and dextran in dog leg lymph. *Lymphology* **6**: 181-186, 1973

Kalima T.V. Ultrastructure of the intestinal lymphatics in regards to absorption. *Scand. J. Gastroenterol*. **8**: 193-196, 1973

Klein J. Immunology. *Blackwell*, Oxford. (1990)

Kramer G.C., Harms B.A., Gunther R.A., Renkin E.M. and Demling R.H. The effect of hypoproteinemian on blood to lymph fluid transport in sheep lung. *Circ. Res*. **49**: 1173-1180, 1981

Lai-Fook S. J. and Kaplowitz M. R. Pleural space thickness in situ by light microscopy in five mammalian species. *J. Appl. Physiol*. **59**: 603-610. 1985

Laine G.A., Allen S.J., Kats J., Gabel J.C. and Drake R.E. Outflow pressure reduces lymph flow rate from various tissues. *Microvasc. Res*. **33**: 135-142, 1987

Leak L. and Burke J.F. Fine structure of the lymphatic capillary and the adjoining connective tissue area. *Am. J. Anat*. **118**: 785-810, 1966

Leak L. and Burke J.F. Ultrastructural studies on the lymphatic anchoring filaments. *J. Cell. Biol*. **36**: 129-149,1968

Leak L. V. and Rahil K. Permeability of the diaphragmatic mesothelium: the ultrastructural basis for "stomata". *Am. J. Anat*. **151**: 557-594. 1978

Leathes J. B. and Starling E. H. The absorption of salt solution from the pleural cavities. *J. Physiol*. (London) **18**: 106-116, 1895

Mariassy A. T. and wheeldon E. B. The pleura: a combined light microscopy, scanning and transmission electron microscopic study in the sheep. *Exp. Lung Res*. **4**:293-313. 1983

Mazzoni M.C., Skalak T.C. and Schmid-Schonbein G.W. The structure of lymphatic valves in the spinotrapezius muscle pf the rat. *Blood Vessels*. **24**: 304-312, 1987

Mazzoni M.C., Skalak T.C. and Schmid-Schonbein G.W. The effect of skeletal muscle

fiber deformation on lymphatic volume. *Am. J. Physiol*. **259**: H1860-H1868, 1990

McHale N.G and Roddie I.C. The effect of transmural pressure on pumping activity in isolated bovine lymphatic vessels. *J. Physiol. Lond*. **261**: 255-269, 1976

McHale N.G and Allen J.M. The effect of external Ca^{2+} concentration on the contractility of bovine mesenteric lymphatics. *Microvasc. Res*. **26**: 182-192, 1983

Mendoza E. and Schimid-Schonbein G.W. A model for mechanics of primary lymphatic valves. *J. Biomech. Eng*. **125**: 407-414, 2003

Miserocchi G. and Agostoni E. Contents of the pleural space. *J. Appl. Physiol*. **30**: 208-218. 1971

Miserocchi G., Negrini D. and Mortola J. Comparative features of Starling-lymphatic interaction at the pleural level in mammals. *J. Appl. Physiol*. **56**: 1151-1156. 1984

Miserocchi G. and Negrini D. Contribution of starling and lymphatic flow to pleural liquid exchange in anesthetized rabbits. *J. Appl. Physiol*. **61**: 325-330. 1986

Miserocchi g., Negrini D., Mukenge S., Turconi P. and Del Fabbro M. Liquid drainage through the peritoneal diaphragmatic surface. *J. Appl. Physiol*. **66**: 1579-1585. 1989

Mislin H. Active contractility of the lymphangion and coordination of lymphangion chains. *Experientia Basel*. **32**: 820-822, 1976

Morris B. The effect of diaphragmatic movement on the absorption of protein and of red cells from the peritoneal cavity. *Aust. J. Exp. Biol. Med. Sci*. **31**: 227-238, 1953

Neergard K. Zur Frage des Drukes in Pleuraspalt. *Beitr. Klin. Erforsch. Tuberk. Lungenkr*. **65**: 476-485, 1923

Negrini D, Pistolesi M., Miniati M., Bellina R., Giuntini C. and Miserocchi G. Regional protein absorption rates from the pleural cavity in dogs. *J Appl Physiol* **58**: 2062-2067, 1985

Negrini D., Mukenge S., Del Fabbro M., Gonanao C. and Miserocchi G. Distribution of

diaphragmatic lymphatic stomata. *J. Appl. Physiol*. **70**: 1544-1549. 1991

Negrini D., Del Fabbro M., Gonano C., Mukenge S. and Miserocchi G. Distribution of diaphragmatic lymphatic stomata. *J. Appl. Physiol*. **72**: 1166-1172. 1992

Negrini D. and Del Fabbro M. Subatmospheric pressure in the rabbit pleural lymphatic network. *J Physiol* **520**: 761-769, 1999

Negrini D., Moriondo A. and Mukenge S. Transmural pressure during cardiogenic oscillations in rodent diaphragmatic lymphatic vessels. *Lymphat Res Biol* **2**: 69-81, 2004

Nerlich A.G. and Schleicher E. Identification of lymph and blood capillaries by immunohistochemical staining for various basement membrane components. *Histochemistry*. **96**: 449-453, 1991

Nicoll P.A. and Hogan R.D. Pressures associated withlymphatic capillary contraction. *Microvasc. Res*. **15**: 257-258, 1978

Ohhashi T., Azuma T. and Sakaguchi M. Active and passive mechanical characteristics of bovine mesenteric lymphatics. *Am. J. Phisiol*. **239**: H88-H95, 1980

Ohhashi T., Yokoyama S. and Ikomi F. Effects of vibratory, stimulation and mechanical massage on micro- and lymph-circulation in the acupuncture points between the paw pads of anesthetized dogs. In: Niimi H., Zhuang F.Y. eds. *Recent Advances in Cardiovascular diseases*. Osaka, japan: Natl Cardiovasc Ctr; 1991:125-133

Ohtani Y., Ohtani O. and Nakatani T. Microanatomy of the rat diaphragm: a scanning and confocal laser scanning microscopic study. *Arch Histol Cytol* **56**: 317-328, 1993

Ohtani Y. and Ohtani O. Obliteration of the lymphatic trunks draining diaphragmatic lymph peritoneal fluid to enter the pleural cavity. *Arch Histol Cytol* **60**: 503-510, 1997

Ohtani Y. and Ohtani O. Postnatal Development of Lymphatic Vessels and Their Smooth Muscle Cells in the Rat Diaphragm: a Confocal Microscopic Study. *Arch Histol Cytol*. **64** n.5: 513-522, 2001

Olszewski W.L, Engeset A., Jaeger P.M., Sokolowski J. and Theodorsen L. Flow and

composition of leg lymph in normal men during venous stasis, muscular activity and local hyperthermia. *Acta Physiol. Scand.* **99**: 149-155, 1977

Olszewski W.L. and Engeset A. Intrinsic contractility of leg lymphatics in man. Preliminary communication. *Lymphology*. **12**: 81-84, 1979

O'Morchoe C.C. and O'Morchoe P.J. Differences in lymphatics and blood capillary permeability: ultrastructural-functional correlations. *Lymphology*. **20**: 205-209, 1987

Patterson G.S. Mitzner W,.A. and Sylvester J.T. Assessment of fluid balance in isolated sheep lungs. *J. Appl. Physiol*. **58**: 882-891, 1985

Pepper M. The Lymphatic System. *Microvascular Research*. Elsevier Academic Press. Vol 1, Chapter 81: 523-527, 2006

Perry S.F., Similowski T., Klein W. and Codd J.R. The evolutionary origin of the mammalian diaphragm. *Respiratory Physiology & Neurobiology*. **171**: 1-16, 2010

Ragen D.M.S., Schmidt E.E., Macdonald I.C. and Groom A.C. Spontaneous cyclic contraction of the capillary wall in vivo, impeding red cell flow: a quantitative analysis. Evidence for endothelial contractility. *Microvasc. Res.* **36**: 31-39, 1988

Recklinghausen F.T., von. Zur Fittresorption. *Virkow's Arch*. **26**: 172-208, 1863

Reed R.K., McHale N. G., Bert J. L., Winlove C.P. and Laine G. A. Interstitium, Connective Tissue and Lymphatics. *Portland Press Proceedings*, **1995**

Ryan U.S. Macrofage-like properties of endothelial cells. News Physiol. Sci. 3: 93-96, 1988

Ryan U.S. and Mayfield L.J. Computer tracking of endothelial activation responses. In: *Vascular Endothelium in Health and Disease*, edited by S. Chien. New York: Plenum, p. 185-193, 1988

Roddie I. C. Lymph transport mechanisms in peripheral lymphatics. *News Physiol. Sci*. **5**: 85-89. 1990

Schad H., Flowaczny H., Brechtelsbauer H. and Birkenfeld G. The significance of

respiration for thoracic duct flow in relation to other driving forces of lymph flow. *Pfluegers Arch*. **378**: 121-125, 1978

Schmeltz M., Moll R., Kuhn C. and Franke W.W. Complexus adhaerentes, a new group of desmoplakin-containing junctions in endothelial cells: II. Different types of lymphatic vessels. *Differentiation*. **57**: 97-117, 1994

Schmid-Schonbein G.W. Microlymphatics and lymph flow. *Physiol Rev*. **70**: 987-1028, 1990

Schmid-Schonbein G.W. The Second Valve System in Lymphatics. *Lymphatic Research and Biology*. **1**: 25-31, 2003

Schmid-Schonbein. Foundations of Microlymphatic Function. *Microvascular Research*. Elsevier Academic Press. Vol 1, Chapter 82: 529-534, 2006

Shepro D. *Microvascular Research*. Elsevier Academic Press. Vol 1, 2006

Shinohara H. Lymphatic System of the Mouse Diaphragm: Morphology and Function of the Lymphatic Sieve. *The anatomichal Record*. **249**: 6-15, 1997

Simmonds W.J.Q. The relationship between intestinal motility and the flow and rate of fat output in thoracic duct lymph in unanaesthetized rats. *J. Exp. Physiol*. **42**: 205-221, 1957

Skalak T.C., Schimid-Schonbein G.W. and Zweifach B.W. New morphological evidence for a mechanism of lymph formation in skeletal muscle. *Microvasc. Res*. **28**: 95-112, 1984

Smith C.S. and Taylor A. E. Increased initial lymphatic uptake in high-flow high-protein oedema: an additional safety factor against tissue oedema. *Lymphology* **24**: 2-6, 1991

Straling E. H. and Tubby A. H. On absorption from and secretion into the serous cavities. *J. Physiol*. (London) **16**:140-155, 1894

Straling E. H. On the absorption of fluids from the connective tissue space. *J. Physiol*.

(London) **19**:312-326, 1896

Swartz M.A. The physiology of the lymphatic system. *Adv Drug Deliv Rev*. **50**: 3-20, 2001

Swarts M.A., Kaipainen A., Netti P.A., Brekken C., Boucher Y., Grodzinsky A.J. and Jain R.K. Mechanics of interstitial-lymphatic fluid transport: Theoretical foundation and experimental ventilation. *J. Biomech*. **32**: 1297-1307, 1999

Taylor A.E., Gibson H., Granger H.J. and Guyton A. C. The interaction between intracapillary forces in the overall regulation of the interstitial volume. *Lymphology* **6:** 192-208, 1973

Taylor A.E. The lymphatic edema safety factor: the role of edema dependent lymphatic factors (EDLF). *Lymphology* **23:** 155-160, 1991

Thomas G. and Ramwell P. W. Interaction of non-arginine compounds with the endothelium derived relaxing factor inhibitor N^G-monomethyl-arginine. *J. Pharmacol. Exp. Ther*. **260**: 676-679. 1991

Trzewik J., Mallipattu S.R., Artmann G.M., DeLano F.A. and Achmid-Schonbein G.W. Evidence for a second valve system in lymphatics endothelial microvalves. *FASEB J*. **15**: 1711-1717, 2001

Tsilibary e. C. and wising S. L. Lymphatic absorption from peritoneal cavity: regulation of patency of mesothelial stoma. *Microvasc. Res.* **25**: 22-39. 1983

Unthank J.L. and Bohlen H.G. Lymphatic pathways and role of valves in lymph propulsion from small intestine. *Am. J. Physiol*. **254** (Gastrointest., Liver Physiol 17): G389-G398, 1988

Van Helden D.F., Zhaoj. Lymphatic vasomotion. *Clin Exp Pharmacol Physiol*. **27**: 1014-1018, 2000

von der Weid P.Y. and Zawieja D.C. Lymphatic smooth muscle: the motor unit of lymph drainage. *Int J Biochem Cell Biol*. **36**: 1147-1153, 2004

Yoffey J.M. and Courtice F.C. *Lymphatic, lymph and the lymphomyeloid complex*. London: Academic Press. 1970

Wang N. S. The regional differences of pleural mesothelial cells in rabbits. *Am. Rev. Respir. Dis*. **110**: 623-633. 1974

Wang N. S. The preformed stomata connecting the pleural cavity and the lymphatics in the parietal pleura. *Am. Rev. Respir. Dis*. **111**: 12-20. 1975

Wang N. S. Mesothelial cells in situ. In The Pleura in Health and Disease (Chretien J., Bignon J. and Hirsh A., eds.) 23-42, *Marcel Dekker*, Inc, New York, 1985

Wenzel J. Normale Anatomie des Lymphgefass-Systems. *Handbuch der Allgemeinen Pathologie*, edited by H. Meessen Berlin: Springer vol.**3**, pt. 6: 89-148, 1972

White J. C., Field M. E. and Drinker C. K. On the protein content and normal flow of lymph from the foot of the dog. *Am. J. Physiol*. **103**: 34-44, 1933

Wigle J. T. and Oliver G. Prox1 function is required for the development of the murine lymphatic system. *Cell*. **98:** 769–778, 1999.

Wilting J., Papoutsi M., Othman-Hassan K., Rodriguez-Niedenfuhr M., Prols F., Tomarev S. I., and Eichmann A. Development of the avian lymphatic system. *Microscopy Research and Technique*. **55:** 81–91, 2001.

Womack W.A., Tygart P.K., Mailman D., Kvietys P.R. and Granger D.N. Villous motility: relationship to lymph flow and blood flow in the dog jejunum. *Gastroenterol*. **94**: 977-983, 1988

Zawieja D.C. Kossman E. and Pullin J. Dynamic of the microlymphatic system. *J Prog Appl Microcirc*. **23**: 100-109, 1999

Zocchi l., Agostoni. E and Cremaschi D. Electrolyte transport across the pleura of rabbits. *Respir. Physiol*. **86**: 125-138. 1991

Zweifach B.W. and Prather J.W. Micromanipulation of pressure in terminal lymphatics in the mesentery. *Am. J. Physiol*. **228**: 1326-1335, 1975

7 Acknowledgements

I would like to thank everyone helped me during my PhD period at the Department of Experimental and Clinical Biomedical Sciences, University of Insubria, Varese.

I'm very grateful to my Professor Daniela Negrini who consented me to work in her laboratory giving me continuous advice, support, trust and for the precious scientific discussions during these years.

A particular acknowledgement to Dr. Andrea Moriondo for the precious suggestions and the great patience, for the brilliant and genial ideas and his friendly approach teaching me the Physiology.

A special thanks to Dr.ssa Marcozzi Cristiana for precious support and advices, for sharing the "hard and enjoyable working days", for her constant friendship.

A thanks to Dr.ssa Eleonora Solari for her valuable help in different fields and for her friendship, and to Ing. Simone Lattanzio and Ing. Federica Boschetti for their engineering contributions.

8 Contributions

The results obtained in the present research project, have contributed to the publication of the following scientific manuscripts:

1. Moriondo A, Bianchin F, Marcozzi, Negrini D. "Kinetics of fluid flux in the rat diaphragmatic submesothelial lymphatic lacunae." *Am J Physiol Hearth Circ Physiol*. **295** (3): H1182-H1190, 2008

2. Moriondo A, Boschetti F, Bianchin F, Lattanzio S, Marcozzi C, Negrini D "Tissue contribution to the mechanical features of diaphragmatic initial lymphatics" *J Physiol*. **588**: 3957-3969, 2010

In addition the data of this research have been presented in national and international scientific meetings:

1. Moriondo A, Bianchin F, Marcozzi C, Negrini D. Kinetics of fluid flux in the rat diaphragmatic submesothelial lymphatic lacunae. *Acta Physiologica 2008*; Volume 194, Supplement 665 :P99. The 59th National Congress of the Italian Physiological Society 17/09/2008-19/09/2008 Cagliari, Italy

2. Bianchin F, Marcozzi C, Moriondo A, Boschetti F, Lattanzio S, Negrini D. In vivo mechanical properties of diaphragmatic initial lymphatic vessels and adjacent intersitium. Riunione annuale dei Dottorandi della Società Italiana di Fisiologia, Pisa, 22-25 Giugno 2009

3. Bianchin F, Marcozzi C, Moriondo A, Boschetti F, Lattanzio S, Negrini D. In vivo mechanical properties of diaphragmatic initial lymphatic vessels and adjacent

interstitium. Riunione annuale dei Dottorandi della Società Italiana di Fisiologia, Pisa, 16-18 Giugno 2010

4. Bianchin F, Moriondo A, Marcozzi C, Solari E, Lattanzio S, Negrini D. Dynamic recruitment of diaphragmatic submesothelial lymphatics. The 61th National Congress of the Italian Physiological Society 15/09/2010-17/09/2010 Varese, Italy

5. Lattanzio S, Boschetti F, Moriondo A, Marcozzi C, Bianchin F, Negrini D. Tissue contribution to the mechanical features of diaphragmatic lymphatic vessels. The 61th National Congress of the Italian Physiological Society 15/09/2010-17/09/2010 Varese, Italy